Quark Mass Dependence of Nucleon Observables and Lattice QCD

Ph.D. thesis by

Massimiliano Procura

Physik-Department

Technische Universität München

Technische Universität München
Physik-Department
Institut für Theoretische Physik T39
Univ.-Prof. Dr. W. Weise

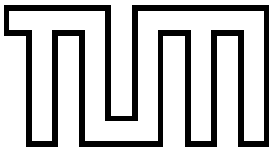

Quark mass dependence of nucleon observables and lattice QCD

Massimiliano Procura

Vollständiger Abdruck der von der Fakultät für Physik der Technischen Universität München zur Erlangung des akademischen Grades eines

Doktors der Naturwissenschaften (Dr. rer. nat.)

genehmigten Dissertation.

Vorsitzender: Univ.-Prof. Dr. Stephan Paul

Prüfer der Dissertation:

1. Univ.-Prof. Dr. Wolfram Weise
2. Univ.-Prof. Dr. Andrzej J. Buras

Die Dissertation wurde am 16.11.2005 bei der Technischen Universität München eingereicht und durch die Fakultät für Physik am 15.12.2005 angenommen.

Summary

Understanding hadron structure from first principles is one of the great unsolved problems in physics. Lattice QCD on one side and chiral effective field theory on the other are progressively developing as important tools to deal with the non-perturbative nature of low-energy QCD and the structure of the nucleon. At present, however, there is a gap between the relatively large quark masses accessible in fully-dynamical lattice simulations and the small quark masses relevant for comparison with physical quantities. We combine Chiral Perturbation Theory, which predicts the quark mass dependence of nucleon observables, with lattice computations where the quark mass is a tunable parameter. We explore the feasibility of a systematic approach, based on the chiral effective Lagrangian, for the chiral extrapolation of lattice QCD data. In the framework of baryon chiral effective field theories with and without explicit $\Delta\,(1232)$ degrees of freedom, we work out the quark mass dependence of the nucleon mass M_N and the axial-vector coupling constant g_A at one-loop order and perform a numerical analysis of the relevant formulae using as input the most recent lattice QCD results.

Zusammenfassung

Es ist eines der großen ungelösten Probleme in der Physik, die hadronische Struktur von Anfang an zu verstehen. Gitter-QCD auf der einen Seite und chirale effektive Feldtheorie auf der anderen entwickeln sich schrittweise zu wichtigen Werkzeugen, mit der nicht-perturbativen Natur der Niederenergie-QCD und der Nukleonstruktur umzugehen. Momentan besteht jedoch eine Lücke zwischen den relativ großen Quarkmassen, die in voll-dynamischen Gittersimulationen verwendet werden müssen, und den kleinen Quarkmassen, die für den Vergleich mit physikalischen Größen relevant sind. Wir kombinieren Chirale Störungstheorie, die die Quarkmassenabhängigkeit von Nukleon-Observablen vorhersagt, mit Gitterrechnungen, in denen die Quarkmasse ein veränderbarer Parameter ist. Wir untersuchen, ob ein systematischer Zugang zur chiralen Extrapolation von Gitter-QCD-Daten, basierend auf der chiralen effektiven Lagrangedichte, möglich ist. Im Rahmen von baryonischen chiralen effektiven Feldtheorien mit und ohne explizitem $\Delta\,(1232)$-Freiheitsgrad berechnen wir die Quarkmassenabhängigkeit der Nukleonmasse M_N und der Axialvektor-Kopplungskonstante g_A in führender Ein-Schleifen-Ordnung und führen eine numerische Analyse der relevanten Formeln mit den neuesten Gitter-QCD-Ergebnissen als Input durch.

Contents

Chapter 1

Introduction

According to present understanding, the observed diversity of the strong interaction phenomena is described by Quantum Chromodynamics (QCD), the gauge field theory of quarks and gluons. These are the relevant degrees of freedom at high energies and short-distance scales, $r < 0.1\,\mathrm{fm}$, where the renormalized gauge coupling becomes weak (asymptotic freedom [1]). On the other hand, as we move towards low energy-momentum scales, the perturbative expansion breaks down, and the physical picture associated with Feynman diagrams derived from the QCD Lagrangian, expanding in powers of the gauge coupling, becomes invalid.

Dealing with the nucleon is a genuine non-perturbative problem. Lattice field theory provides a mathematically well-defined framework for a formulation of non-perturbative QCD [2]. The idea is to replace the four-dimensional Minkowski space-time continuum with a discrete lattice in a four-dimensional Euclidean space. In quantum field theory, information is obtained from correlation functions, which have a functional integral representation. Lattice field theory introduces an ultraviolet cutoff at the outset and gives a non-perturbative *definition* of the functional integral. For any lattice spacing a, the maximum momentum which can arise on the lattice is $p_{\max} \sim \pi/a$, which goes to infinity as $a \to 0$. The fermion fields $\psi(x)$ and $\bar{\psi}(x)$ live on lattice sites x. Gauge fields live on links through the variables

$$U_\mu(x) = \mathcal{P} \exp \int_0^a ds\, A_\mu(x + s\, e_\mu) \tag{1.1}$$

where $\mathcal{P}$ denotes the path ordering, $A_\mu = A_a^\mu\, \lambda^a/2$ (with A_a^μ the gluon fields and $\lambda^a/2$ the generators of the $SU(3)$ color gauge group), and e_μ is the unit vector in the μ direction. In lattice QCD the correlation function are expressed as [3]

$$\langle O_1 \dots O_n \rangle = \frac{1}{Z} \int \prod_{x,\mu} dU_\mu(x) \prod_x d\psi(x) d\bar{\psi}(x)\, O_1 \dots O_n\, e^{-S_{\mathrm{QCD}}} \tag{1.2}$$

where

$$Z = \int \prod_{x,\mu} dU_\mu(x) \prod_x d\psi(x) d\bar{\psi}(x)\, e^{-S_{\mathrm{QCD}}} \tag{1.3}$$

and S_{QCD} is the lattice QCD action. With quarks on sites and gluons on links, it is possible to devise lattice actions that respect gauge symmetry.

When a is taken to zero we must also specify how the lattice (bare) couplings behave. The proper continuum limit is taken with $a \to 0$ holding the physical quantities (*e.g.* hadron masses) fixed. Ultimately one must ensure that the dependence of any observable on the lattice spacing satisfies the appropriate renormalization group equation: the calculated values should scale correctly with a, as $a \to 0$.

In view of practical results, the breakthrough of the lattice formulation is that Eq.(1.2) turns quantum field theory into a mathematically well-defined problem in statistical mechanics. Numerical lattice QCD is concerned with numerical integration of the functional integral by Monte Carlo methods. On a computer with finite memory, one must introduce a finite space-time volume – providing an infrared cutoff – in order to keep under control the number of integration variables. Even with a finite lattice, this number is large. For N_S sites in each spatial direction and a temporal extent $L_4 = N_4\, a$, there are $(4 \times 8) N_S^3 N_4$ variables for gluons and $(4 \times 3) N_S^3 N_4$ for each flavor of quarks. If one only demands a volume a few times the size of the nucleon and also several grid points within nucleon's diameter, one already requires, say, 10 points along each direction. In four-dimensional space-time this leads to $\sim 32 \times 10^4$ gluonic variables. Therefore, the only feasible methods are based on Monte Carlo integration: an ensemble of random variables is generated according to Boltzmann weighting and the integrals involved in Eq.(1.2) are approximated by averages on the simulated ensemble. One first selects a desired level of precision, and then using appropriate theorems, determines an algorithm and a number of independent samples that yield such a precision. Apart from systematic effects due to non-zero lattice spacing and finite volume, lattice QCD "simulations" produce results that are exact on the given lattice, up to statistical errors.

Quarks pose problems. The functional integral formalism must be prepared to accommodate anticommuting fields. This is solved by describing the fermion fields using Grassmann variables. In all cases of interest, the quark lattice action can be written as [3]

$$S_q = \sum_{\alpha\beta} \bar{\psi}_\alpha \, M_{\alpha\beta} \, \psi_\beta \ , \tag{1.4}$$

where α and β collectively label discrete space-time, spin and internal quantum numbers. The matrix $M_{\alpha\beta}$ is a discretized version of the Dirac operator $\not{D} + m$, where m is the quark mass matrix. $M_{\alpha\beta}$ depends on the gauge field $U(x)$. Since the quark action is a quadratic form, the integral can be carried out exactly:

$$\int \prod_{\alpha\beta} d\bar{\psi}_\alpha \, d\psi_\beta \, e^{-\bar{\psi} M \psi} = \det M \ . \tag{1.5}$$

With the quarks integrated analytically, it is the gluons that are subject to the Monte Carlo method. The weighting factor in the path integrals in Euclidean space-time is now $e^{-S_g(U)} \det M$, where S_g is the lattice pure gauge action. Assuming that $\det M$ is positive, one can devise a Monte Carlo with "importance sampling". This is crucial to make lattice QCD numerically tractable. The random number generator creates gauge fields weighted according to $e^{-S_g(U)} \det M$. The appearance of the minus sign in front of $S_g(U)$ instead

of i is due to the use of imaginary time. Working in Euclidean space-time has also the important practical advantage that to isolate lowest-lying state and compute hadronic matrix elements can be done by looking at the asymptotic behavior of Euclidean-time correlation functions.

Generating statistically independent configurations of the U's involves computing how the effective action $S_g(U) - \ln \det M$ changes when the set of U's are varied. The presence of the fermion determinant makes this problem very difficult. The sampling involves the inversion of the fermion matrix $M(U)$ [1]. Moreover, the products of $\psi_\alpha \bar{\psi}_\beta$ in the integrand $O_1 \ldots O_n$ are replaced by quark propagators $[M^{-1}]_{\alpha\beta}$ by Wick contraction. The eigenvalues of M span a very large range, from 2π down to $m_q a$, where m_q is the quark mass. The ratio of the largest $\lambda_{\max}$ to the smallest $\lambda_{\min}$ of such eigenvalues determine the convergence rate of iterative methods to invert M. The CPU time needed for such calculations, even with the best algorithms, is proportional to

$$(\lambda_{\max}/\lambda_{\min})^p \sim \min\{1/(m_q a)^p, (L/a)^p\} \ . \tag{1.6}$$

The exponent p depends on the algorithm and is typically between 1 and 3 [5]. At fixed a, it is therefore costly to reduce m_q. The dependence of the ratio (1.6) on the lattice size L can be explained as follows. For a pure gauge theory, changing a variable at one location only affects the action at sites "near" the variable, so the attempt to update one link variable on the lattice involves a computational effort independent of the lattice volume. However, the fermion determinant is non-local and so, updating one gauge variable involves an amount of work proportional to the lattice volume. In addition to difficulties embodied in Eq.(1.6), statistical uncertainties increase as the quark mass decreases. With present techniques it is not yet possible to run lattice simulations at masses as small as those of the up and down quarks in nature.

The determinant of M generates sea quarks inside a hadron. An enormous numerical simplification occurs if one makes the so-called quenched approximation, replacing $\det M$ by 1 (no closed fermion loops) and compensating the corresponding omission of vacuum polarization effects with shifts in the bare couplings: valence quarks and gluons in hadrons are treated fully, while sea quarks are merely modeled or ignored altogether. The quenched approximation becomes exact in the limit of infinitely massive quarks. Only a full-QCD calculation can provide us with an answer to the question about the accuracy of such approximation. It is also very well established that as $m_q \to 0$, quenched QCD and full QCD, with non-zero flavor numbers, differ strongly [2].

The quenched approximation is now out-of-date. At present the challenge in lattice QCD is to devise efficient simulation methods for the full theory (including quark polarization effects) that will work well on large lattices and with small quark masses. The number of arithmetic operations that are required to generate the subsequent statistically

[1] For a comprehensive review of the algorithms used for present simulations with dynamical fermions see [4] and references therein.

[2] Cf. for example [5] and references therein.

independent field configurations can be estimated by the empirical formula [6][3]

$$\frac{\#\text{ operations}}{\text{field configurations}} \simeq 3.3 \left[\frac{140\,\text{MeV}}{m_\pi}\right]^6 \left[\frac{L}{3\,\text{fm}}\right]^5 \left[\frac{0.1\,\text{fm}}{a}\right]^7 \text{ Tflops years} \tag{1.7}$$

which shows the dependence on the lattice spacing a, lattice spatial size L and on the calculated value of m_π of the pion mass, which is related to the specified values of the quark masses. The result is given in Tflops years, the number of operations that a computer with a sustained speed of 1 Tflop (10^{12} floating-point operations per second) performs in 1 year of running time. While such machines are becoming available to the lattice community, the poor scaling behavior of the algorithms tells us that it will not be possible to vary the lattice parameters over a wide range. This unfavorable situation calls for new algorithmic ideas and theoretical guidance to realize the relevant extrapolations, in lattice spacing, lattice size and quark masses.

QCD is a multiscale problem: there is not only the energy scale Λ characteristic of non-perturbative gluonic effects but also a wide range of quark masses. Furthermore, two more scales are introduced in order to put QCD on a lattice. Firstly, for "light" quarks the lattice size must be such that $L \gg m_q^{-1}$, light quarks must "fit" into the lattice. Secondly, for "heavy" quarks the lattice spacing a must be smaller than the Compton wavelength of such quarks, $a \ll m_Q^{-1}$. The idealized hierarchy

$$L^{-1} \ll m_q \ll \Lambda \ll m_Q \ll a^{-1} \tag{1.8}$$

is forced by limited computing resources to be

$$L^{-1} < m_q < \Lambda < m_Q \sim a^{-1} \ . \tag{1.9}$$

Nevertheless, all the parameters a, L and m_q can be varied over certain ranges, providing numerical lattice QCD with one of its most important strength.

Effective field theories can provide sound theoretical guides to connect present lattice results with phenomenology [5]. Heavy quark effective theory and non-relativistic QCD are used in controlling and quantifying systematic uncertainties of lattice calculations for heavy quark systems. Lattice spacing effects can be described by an effective field theory due to Symanzik [7], while Lüscher developed a theoretical framework to study finite-volume effects [8] in terms of the asymptotically observed hadrons.

In our work we focus on the (light) quark mass dependence of nucleon observables and the so-called chiral extrapolation problem. In the limit of vanishing quark masses, QCD becomes a "theoretical paradise", being characterized by chiral symmetry. The spontaneous breakdown of this symmetry implies the absence of a mass gap in the spectrum of the asymptotically observed particles. Equipping up and down quarks with a small mass, the deviation from the chiral limit can be explored in a perturbative fashion. The pions are characterized by masses much smaller than those of all other hadrons, as they

[3] We use standard units $\hbar c = 1$ throughout this work.

are the Goldstone bosons associated with spontaneous chiral symmetry breaking in the two-flavor case. In Chiral Perturbation Theory [9–11], the effective low-energy theory of QCD, the relevant degrees of freedom are the hadrons observed in the low-mass meson and baryon spectrum. In the present context these are pions coupled to "heavy" nucleons and $\Delta\,(1232)$ states. Chiral symmetry imposes strong constraints on the form of the interactions among them. In particular, it enables a perturbative expansion of the QCD Green functions in terms of small external momenta and quark masses.

It is natural to combine both Chiral Perturbation Theory and lattice QCD to benefit from their respective advantages. For small enough quark masses, Goldstone bosons are expected to dominate the long-range behavior of correlation functions. On one side Chiral Perturbation Theory provides the dependence of low-energy observables on quark masses and external momenta. On the other side, the quark masses can be varied continuously in a lattice computation. In order to directly compare these two approaches, quarks have to be taken sufficiently light. The aim of our work is to investigate whether this is already achieved in present state-of-the-art simulations for the nucleon mass M_N and the axial vector coupling g_A, two quantities which have been extensively studied on the lattice in the very last years.

Chapter 2

Theoretical framework

Quarks and gluons are the fields that experience the strong interactions described by QCD [12]. The statement that QCD is a gauge theory based on the $SU(3)$ group with a "color" triplet of quark fields, fixes the QCD Lagrangian density to be

$$\mathcal{L} = -\frac{1}{4}\sum_{a=1}^{8} G^a_{\mu\nu} G^{\mu\nu}_a + \sum_{j=1}^{N_f} \bar{q}_j (i\gamma_\mu \mathcal{D}^\mu - m_j) q_j \ . \tag{2.1}$$

A summation over repeated Lorentz indices is implied. Here q_j are the quark fields of N_f flavors with mass m_j and $\mathcal{D}^\mu$ is the covariant derivative defined as

$$\mathcal{D}_\mu = \partial_\mu - ig \sum_{a=1}^{8} \frac{\lambda_a}{2} A^a_\mu \ , \tag{2.2}$$

where g is the gauge coupling, A^a_μ are the gluon fields and the $\lambda_a/2$ are the $SU(3)$ group generators in the triplet representation of the quarks. The gluon field strength tensor is given by

$$G^a_{\mu\nu} = \partial_\mu A^a_\nu - \partial_\nu A^a_\mu + g f_{ijk} A^j_\mu A^k_\nu \tag{2.3}$$

with f_{ijk} the totally antisymmetric structure constants of $SU(3)$. As far as gauge invariance is concerned, the QCD Lagrangian density could also include a term

$$\mathcal{L}_\theta = -\frac{\theta}{64\pi^2} \epsilon^{\mu\nu\rho\sigma} \sum_{a=1}^{8} G^a_{\mu\nu} G^a_{\rho\sigma} \ , \tag{2.4}$$

where $\epsilon_{\mu\nu\rho\sigma}$ is the totally antisymmetric Levi-Civita tensor, $\epsilon_{0123} = 1$. The inclusion of the term (2.4) would violate P and CP conservation. For example, a non-zero vacuum angle θ would generate a neutron electric dipole moment proportional to $|\theta|$. Present empirical information [13] gives the upper bound $|\theta| < 10^{-9}$ following [14] and even less according to Refs. [15]. In our work we do not consider P or CP violating effects. We will set $\theta = 0$ in the following.

The basic input of QCD is the dimensionless bare coupling g. The parameters are the bare quark masses m_j. In dimensional regularization [16] and using the modified minimal subtraction $\overline{\text{MS}}$ renormalization scheme [17], the β-function determining how

the *renormalized* coupling $g_{\rm ren}$ changes with the running scale μ, is independent of the quark masses:

$$\mu \frac{dg_{\rm ren}}{d\mu} = \beta(g_{\rm ren}) \ . \tag{2.5}$$

If $g_{\rm ren}(\mu)$ is small, we can compute $\beta(g_{\rm ren})$ in perturbation theory. The leading term in the perturbative expansion is of order g^3,

$$\beta(g) = -\beta_0 \frac{g^3}{(4\pi)^2} + \mathcal{O}(g^5) \ , \quad \beta_0 = \frac{1}{3}(11N_c - 2N_f) \ . \tag{2.6}$$

Here N_c is the number of colors. The last equation shows that, for small positive coupling g, β is negative, provided $11/2\, N_c$ exceeds the number of quark flavors with masses below the energy scale under consideration. For the case of physical interest, this condition is met, such that the theory is (ultraviolet) asymptotically free. Using Eq.(2.6) in Eq.(2.5) and integrating, one obtains

$$\alpha_s(\mu) \equiv \frac{g^2_{\rm ren}}{4\pi} = \frac{4\pi}{\beta_0 \ln(\mu^2/\Lambda^2_{\rm QCD})} \tag{2.7}$$

where $\Lambda_{\rm QCD}$ is an integration constant. The calculation at three-loop order together with the Particle Data Group average for α_S at the mass of the Z resonance, gives $\Lambda_{\rm QCD} = 217^{+25}_{-23}\,$MeV for 5 active quark flavors, in the $\overline{\rm MS}$ scheme of dimensional regularization [13]. The procedure of quantization, regularization and renormalization introduces the scale $\Lambda_{\rm QCD}$: the dimensionless coupling g in the Lagrangian is exchanged for a free dimensionful parameter.

In Eq.(2.6) it is justified to neglect higher-order contributions to the $\beta-$function only if the running coupling is small; accordingly, the above representation of the scale dependence of the coupling constant only holds for $\mu \gg \Lambda_{\rm QCD}$. Moreover, for small values of the running scale, the perturbative approach is no longer justified.

Analogously, the tuning of the quark masses is determined by the function γ_m, see for example Ref. [18],

$$\mu \frac{dm_{\rm ren}}{d\mu} = \gamma_m(g_{\rm ren})\, m_{\rm ren} \tag{2.8}$$

$$\gamma_m(g_{\rm ren}) = -\gamma_0 \frac{g^2_{\rm ren}}{(4\pi)^2} + \mathcal{O}(g^4_{\rm ren}) \,, \quad \gamma_0 = \frac{3(N_c^2-1)}{N_c} \ . \tag{2.9}$$

For large values of μ, the solution is of the form

$$m_{\rm ren} = \bar{m} \left(\ln \frac{\mu}{\Lambda_{\rm QCD}} \right)^{-\gamma_0/(2\beta_0)} \ . \tag{2.10}$$

The integration constant $\bar{m}$ is the renormalization group invariant quark mass. In the following we will work with running quark masses, even if we do not explicitly indicate that these quantities depend on μ.

As far as strong interactions are concerned, the different quark flavors u, d, ... have identical properties, except for their mass. The quark masses represent free parameters of the QCD Lagrangian — the theory makes sense for any value of m_u, m_d, ...

2.1 Chiral symmetry

If N_f quarks are massless, the Lagrangian does not contain any terms that connect the right- and left-handed components of the quark fields

$$q_{R,j} = \frac{1}{2}(1+\gamma_5)q_j\,, \quad q_{L,j} = \frac{1}{2}(1-\gamma_5)q_j\,, \tag{2.11}$$

for each flavor j. The Lagrangian of massless QCD therefore remains invariant under "chiral" rotations, *i.e.* independent global transformations of the right- and left-handed quark fields,

$$q_R \to V_R q_R \quad q_L \to V_L q_L \qquad V_R, V_L \in U(N_f)\,. \tag{2.12}$$

where $q_R = (q_{R,1} \dots q_{R,N_f})^T$ and the same for the left-handed quarks. The Noether currents associated with this symmetry are given by

$$V_a^\mu = \bar{q}\gamma^\mu \frac{\bar{\lambda}_a}{2} q\,, \quad A_a^\mu = \bar{q}\gamma^\mu\gamma_5 \frac{\bar{\lambda}_a}{2} q\,, \quad a = 1, \dots, N_f^2 - 1 \tag{2.13}$$

$$V_0^\mu = \bar{q}\gamma^\mu q\,, \qquad A_0^\mu = \bar{q}\gamma^\mu\gamma_5 q\,, \tag{2.14}$$

where the matrices $\bar{\lambda}_a$ form a complete set of traceless, Hermitian $N_f \times N_f$ matrices and $q = (q_1 \dots q_{N_f})^T$. The singlet axial current A_0^μ fails to be conserved at the quantum level (axial $U(1)$ anomaly [19]). Hence the actual symmetry group G of massless QCD, generated by the charges of the conserved currents, consists of those pairs of elements $V_R, V_L \in U(N_f)$ that obey the constraint $\det(V_R V_L^{-1}) = 1$, *i.e.*

$$G = SU(N_f) \times SU(N_f) \times U(1)_V\,. \tag{2.15}$$

The factor $U(1)_V$ is generated by the charge associated to the singlet vector current V_0^μ, referring to baryon number.

The next sections are devoted to the presentation of Chiral Perturbation Theory (ChPT), the effective low-energy theory of QCD which exploits the symmetry properties which we have described so far. We review the basic concepts underlying the construction and use of such a theory, emphasizing the aspects relevant for our analysis of the quark mass dependence of baryon properties. For clarity we will first focus on the mesonic sector of ChPT, where the Goldstone bosons associated with spontaneous chiral symmetry breaking are the only effective degrees of freedom. Particular attention will be paid to the explicit chiral symmetry breaking through non-vanishing quark masses and to the systematic, model-independent character of this theoretical approach. We will come to the meson-baryon system in Sec.2.8.

2.2 Spontaneous chiral symmetry breaking in QCD

In our work we concentrate on the $N_f = 2$ sector of the quarks u and d. There is strong evidence from hadron spectroscopy that the chiral $SU(2)_L \times SU(2)_R$ symmetry of the QCD Lagrangian is *spontaneously* broken, the ground state (vacuum) being invariant

only under the isospin subgroup generated by the charges of the vector currents V_a^μ. Indeed, if chiral symmetry were exact and unbroken, then the ground state would be invariant under chiral rotations, $G = SU(2)_L \times SU(2)_R \times U(1)_V$ being realized as a Wigner-Weyl symmetry. The hadron spectrum would consist of degenerate multiplets that transform irreducibly under G and thus contain degenerate states of opposite parity and equal spin, baryon number and strangeness. This is most strikingly *not* the case for the light pseudoscalar mesons which have masses much lower than the lightest scalar mesons. Moreover, if the axial charges would annihilate the vacuum, then the correlation functions of vector and axial currents $\langle 0|T\{V_a^\mu(x)V_b^\nu(0)\}|0\rangle$, $\langle 0|T\{A_a^\mu(x)A_b^\nu(0)\}|0\rangle$ should coincide. Consequently, the spectral distributions of vector and axial-vector mesonic excitations of the vacuum should also be identical, which they are not: the ρ mass is far smaller than the mass of the axial a_1 meson, $m_\rho \approx 0.77\,\mathrm{GeV} \ll m_{a_1} \approx 1.23\,\mathrm{GeV}$. Hence we are forced to conclude that if the massless limit with its chiral $SU(2) \times SU(2)$ symmetry is a good approximation at all, then it must be spontaneously broken to its isospin subgroup $SU(2)$, since the hadron spectrum can be organized in (nearly) degenerate isospin multiplets.

In the massless theory, a sufficient (but not a necessary) condition for spontaneous chiral symmetry breaking is a non-vanishing scalar quark condensate

$$\langle 0|\bar{u}u|0\rangle + \langle 0|\bar{d}d|0\rangle \equiv -\mathrm{Tr} \lim_{y\to x^+} \langle 0|\, T\{q(x)\bar{q}(y)\}|0\rangle \tag{2.16}$$

where the trace is taken over flavor indices. The available lattice results support the hypothesis of the formation of a non-vanishing scalar quark condensate [20], which is invariant under the subgroup generated by the vector charges, but correlates the right- and left-handed fields and thus is not chiral invariant.

Assuming that the spontaneous chiral symmetry breakdown gives rise to non-vanishing order parameters — vacuum expectation values of local operators which do not commute with all the charges of $SU(2)_L \times SU(2)_R$ —, Goldstone's theorem [21] asserts that the spectrum of the theory contains three *massless* particles (Goldstone bosons) with the same quantum numbers as the broken symmetry generators: spin zero, negative parity, unit isospin, zero baryon number and strangeness — the same quantum numbers of π^+, π^0, π^-. Let us denote as $|\pi_a(p)\rangle$ the one-particle state vectors of the Goldstone bosons, with four-momentum p^μ. Goldstone's theorem implies non-vanishing transition matrix elements of the axial current operators between the vacuum and $|\pi_a(p)\rangle$. Lorentz invariance and a suitable choice of phase for the states $|\pi_a(p)\rangle$ imply

$$\langle 0|A_a^\mu(x)|\pi_b(p)\rangle = ip^\mu \delta_{ab} f_\pi^0 e^{-ip\cdot x}\ , \tag{2.17}$$

with f_π^0 real and positive: this denotes the pion decay constant in the $SU(2)$ chiral limit, *i.e.* for vanishing u- and d-quark masses. Its magnitude cannot be determined by means of symmetry considerations alone but it is a dynamical issue.

Following Gasser and Leutwyler [10, 11], we introduce in the QCD Lagrangian with $\theta = 0$ the couplings of the conserved vector and axial currents as well as scalar and

pseudoscalar quark densities to the external c-number fields $v^\mu(x)$, $a^\mu(x)$, $s(x)$ and $p(x)$:

$$\mathcal{L} = \mathcal{L}^0_{\rm QCD} + \mathcal{L}_{\rm ext} = -\frac{1}{4} G^a_{\mu\nu} G^{\mu\nu}_a + \bar{q}\, i\gamma_\mu \mathcal{D}^\mu\, q + \bar{q}\, \gamma^\mu (v_\mu + \gamma_5 a_\mu)\, q - \bar{q}\, (s - i\gamma_5 p)\, q\ . \quad (2.18)$$

$\mathcal{L}^0_{\rm QCD}$ denotes the QCD Lagrangian for vanishing quark masses. The external fields are color-neutral, Hermitian 2×2 matrices in flavor space and commute with the Dirac matrices. Since we are not concerned with effects of the axial $U(1)$ anomaly, we omit the coupling to the singlet axial current and set $\mathrm{Tr}\, a_\mu = 0$. The ordinary two-flavor QCD Lagrangian is recovered by setting $v_\mu = a_\mu = p = 0$ and $s = \mathrm{diag}(m_u, m_d)$.

Let us define the generating functional $Z[v, a, s, p]$ by

$$\exp(iZ[v,a,s,p]) = \langle 0\,\mathrm{out}|0\,\mathrm{in}\rangle_{v,a,s,p} = \langle 0|\, T \exp\left[i \int d^4x\, \mathcal{L}_{\rm ext}(x) \right] |0\rangle\ , \quad (2.19)$$

where the external fields play the role of classical auxiliary variables. The expansion of the generating functional in powers of the external fields determines the Green functions of the theory. The quantity $\exp(iZ[v, a, s, p])$ is the vacuum-to-vacuum transition amplitude in the presence of external fields and describes the response of the system to the perturbations generated by them. The external field method has an important advantage: in the absence of anomalies, the Ward identities obeyed by the Green functions of the currents (the so-called chiral Ward identities) are equivalent to the statement that the generating functional is invariant under a *local* transformation of the external fields [22].

2.3 Low-energy expansion and effective Lagrangian

We are interested in determining the low-energy structure of the QCD Green functions, from Eq.(2.19). Let us first consider massless QCD. We will treat the case of non-vanishing quark masses in Sec.2.4. The Fourier transforms of the Green functions are dominated by the singularities generated by Goldstone bosons [22]. For example, the two-point function of the conserved axial current $A^a_\mu(x)$ exhibits a pole at $p^2 = 0$ corresponding to the propagation of a massless Goldstone boson,

$$\int d^4x\, e^{ip\cdot x} \langle 0|T\{A^\mu_a(x) A^\nu_b(0)\}|0\rangle = i f_\pi^{0\,2}\, \delta_{ab}\, \frac{p^\mu p^\nu}{p^2 + i\epsilon} + \ldots \quad (2.20)$$

The residue is proportional to $f_\pi^{0\,2}$ according to Eq.(2.17). The dots in Eq.(2.20) refer to cuts for multipion exchange as well as singularities associated with the exchange of massive particles.

Let us now suppose that at sufficiently small momenta, the Green functions are dominated by the one-particle-reducible contributions, namely the poles due to the exchange of Goldstone bosons. The corresponding residues are polynomial in the momenta. This assumption is called *pion pole dominance hypothesis* [22] and represents also the theoretical foundation of the venerable PCAC approach [23]. The singularities associated with multipion exchange occur only at subleading order in the low-energy expansion: the dots

in Eq.(2.20) refer to contributions beyond the leading order in the low-energy expansion. The vertices involving any number of pions, can be written as a Taylor series in the momenta. The S-matrix elements admit a low-energy expansion, which does not represent a Taylor series like for theories with mass gap [24], but involves singular functions of the momenta.

The hidden symmetry, which gives birth to the Goldstone bosons, at the same time also determines their low-energy properties. Indeed, starting from current conservation which requires

$$p_\mu \, \langle \pi^{a_1}(p_1)\pi^{a_2}(p_2)\ldots \text{out}|A^\mu(0)|0\rangle = 0 \ , \tag{2.21}$$

with $p^\mu = p_1^\mu + p_2^\mu + \ldots$ the four-momentum of the final state, and applying pion pole dominance, one can show that vertices involving any number of pions disappear if the pion momenta tend to zero, see for example Ref. [22]. At low-energies, the interaction among the Goldstone bosons is weak and pions of zero four-momentum do not interact at all. This crucial feature is the starting point of Chiral Perturbation Theory which treats the interaction among Goldstone bosons as a perturbation and the momenta as expansion parameters. The opposite behavior in the underlying quark-gluon theory prevents a perturbative low-energy analysis of the interaction in terms of the "fundamental" QCD degrees of freedom.

The one-particle-reducible contributions, which describe the pole terms occurring in the various Green functions, may be viewed as tree graphs of a local field theory, with *pion fields as dynamical variables*. Since the Goldstone bosons do not carry spin, they are described by scalar fields which we denote as $\pi^a(x)$, $a = 1, 2, 3$: they are in one-to-one correspondence with the massless one-particle states $|\pi^a(p)\rangle$ occurring in the spectrum of asymptotic states. The effective field theory is described by a local Lagrangian and the long-range correlations arise from the propagation of the local effective field $\pi^a(x)$. In this language, pole terms generated by pion exchange arise from propagation of the pion field and the vertices represent interactions among these fields. The Lagrangian of this effective pion field theory is called chiral effective Lagrangian.

The expansion of the vertices as a Taylor series in the momenta corresponds to a derivative expansion of the interaction Lagrangian. The various terms occurring in the Taylor series represent local interaction terms, containing the pion fields and their derivatives. Including the standard kinetic term, the effective Lagrangian with at most two derivatives can be cast into the form

$$\mathcal{L}^{\text{eff}} = \frac{1}{2}\,\partial_\mu\pi^a\partial^\mu\pi^a + v^1_{ab}(\pi)\,\partial_\mu\pi^a\partial^\mu\pi^b \ , \tag{2.22}$$

since Goldstone's theorem implies that terms without derivatives are absent. The function $v^1_{ab}(\pi)$ starts with a term quadratic in π and accounts for the leading term in the low-energy expansion of the four-pion vertex.

The coupling of the pion to the conserved currents may also be accounted for in the effective Lagrangian. Let us collectively denote the relevant external fields as $f^i_\mu(x) =$

$\{v_\mu^i(x), a_\mu^i(x)\}$. The full effective Lagrangian, which includes the purely pionic vertices as well as those involving external fields is of the form

$$\mathcal{L}_\pi^{\text{eff}} = \mathcal{L}_\pi^{\text{eff}}\,(\pi, \partial\pi, \partial^2\pi, \ldots;\; f, \partial f, \ldots)\;. \tag{2.23}$$

Using a symbolic notation, the general vertex occurring in this Lagrangian is of the type $\partial^{D_v} f^{F_v} \pi^{P_v}$, where D_v is the total number of derivatives, F_v specifies the number of external fields and P_v counts the pion fields entering the interaction term in question. It is convenient to define the order of the vertex as $O_v = D_v + F_v$, *i.e.* to treat the external fields as small quantities of the same order as the momentum. Note that in this ordering of the vertices, the number P_v of pion fields is left open. The sum of all vertices,

$$\mathcal{L}_\pi^{\text{eff}} = \frac{1}{2}\,\partial_\mu\pi^a\partial^\mu\pi^a + \sum_v g_v\,\partial^{D_v} f^{F_v}\pi^{P_v}\;, \tag{2.24}$$

amounts to an expansion of the function (2.23) in powers of the fields and their derivatives. Lorentz invariance implies that the effective Lagrangian only contains vertices of order $O_v = 2, 4, 6\ldots$ Counting powers of momentum associated with tree graphs, it turns out that the *leading* term in the low-energy expansion of the Green functions exclusively receives contributions from vertices with $O_v = 2$.

The virtue of the representation in terms of effective fields is that the Feynman graphs of a local field theory automatically obey the cluster decomposition property: whenever a given number number of pions and currents meet, the same vertex occurs, irrespective of the remainder of the graph. The sum of all contributions, involving the exchange of an arbitrary number of pions between the various vertices is given by the sum over all Feynman diagrams of the effective theory. While the tree graphs represent the classical limit, loops describe the quantum fluctuations. Accordingly, the representation of the generating functional $Z[f]$ in terms of effective fields takes the standard form of a Feynman path integral

$$\exp(iZ[f]) = \mathcal{Z}^{-1}\int[d\pi]\exp\left(i\int d^4x\,\mathcal{L}_\pi^{\text{eff}}(\pi, \partial\pi, \ldots;\; f, \partial f, \ldots)\right)\;, \tag{2.25}$$

where $\mathcal{Z}$ stands for the integral on the right-hand side evaluated at $f = 0$. The last equation represents the link between the underlying and the effective theories: the quantity $Z[f]$ one the left-hand side is the generating functional of the Green functions formed with the current operators *of the underlying theory*, while the right-hand side exclusively involves the effective field theory. Pion pole dominance hypothesis implies that the two sides coincide, order by order in the low-energy expansion.

The most remarkable property of the method is that it does not mutilate the theory under investigation: the effective field theory is no more than an efficient machinery to work out the low-energy expansion, within its radius of convergence, at any desired order. If the effective Lagrangian includes all the terms permitted by the symmetry of the underlying theory, ChPT is mathematically equivalent to QCD [9, 22]. The former

theory exclusively exploits the symmetry properties of the latter and involves an infinite number of effective coupling constants, which represent the Taylor coefficients of the modified expansion.

Although the symmetry of the underlying theory is spontaneously broken, it constrains the form of the effective Lagrangian [22,24]. The pion field variables can be viewed as the coordinates of a Riemannian manifold, the quotient space G/H, where G is the symmetry group of the QCD Hamiltonian, while H is the subgroup under which the ground state is invariant. In our case $G = SU(2) \times SU(2)$ and $H = SU(2)$. Since G/H is isomorphic to $SU(2)$ – a manifold with the topology of the three-dimensional sphere –, the pion field may be represented as a matrix field $U(x) \in SU(2)$. We can decompose the element $g = \{V_R, V_L\}$ of G into a product of the form nh, where n belongs to the quotient space and is a representative element in the equivalence class of g, while h is an element of the unbroken subgroup $SU(2)$. Under the action of the group G, the element $n = \{U, 1\}$ is taken into

$$gn = \{V_R U, V_L\} = \{V_R U V_L^\dagger, 1\}\{V_L, V_L\} \ , \tag{2.26}$$

so that gn and $n' = \{V_R U V_L^\dagger, 1\}$ belong to the same equivalence class. This shows that the field U transforms according to

$$U' = V_R U V_L^\dagger \ . \tag{2.27}$$

The choice of representatives in the equivalence class is not unique. One may also pick elements of the form $n = \{1, U\}$, which transform according to $U' = V_L U V_R^\dagger$. This amounts to replacing the pion field U by $U^\dagger$.

Since three coordinates are needed to parameterize the elements of $SU(2)$, the matrix field U is equivalent to a set of three scalar fields. We can, for example, express U as an exponential of the corresponding representation of the Lie algebra. In terms of the Pauli matrices τ_a, the generators of the Lie algebra are given by $\tau_a/2$. Accordingly, the canonical coordinates π^a of $U \in SU(2)$ are defined by

$$U = \exp\left(i \frac{\vec{\tau} \cdot \vec{\pi}}{2}\right) \ . \tag{2.28}$$

According to Eq.(2.27) the pion field π carries a nonlinear representation of the symmetry group.

If anomalies do not occur, Green functions of the currents obey Ward identities if and only if the generating functional $Z[f]$ is invariant under a gauge transformation of the external fields. Let us define

$$f_\mu^R = v_\mu + a_\mu \ , \quad f_\mu^L = v_\mu - a_\mu \tag{2.29}$$

which corresponds to the right- and left-handed currents, respectively. The right-handed fields transform like a gauge field of the first factor of G,

$$f_\mu^R(x)' = V_R(x) f_\mu^R(x) V_R(x)^\dagger - i \partial V_R(x) V_R(x)^\dagger \ , \tag{2.30}$$

and f_μ^L transforms in the same manner with $V_L(x)$. In the construction of the leading term in the derivative expansion of the effective Lagrangian with two traceless external vector fields, it is convenient to introduce a covariant derivative for the pion field,

$$D_\mu U(x) \equiv \partial_\mu U(x) - i f_\mu^R(x) U(x) + i U(x) f_\mu^L(x) \ . \tag{2.31}$$

One can show that the symmetries of the underlying theory fix the leading effective Lagrangian, except for an overall constant. There is only one gauge invariant expression of order p^2. The quantity $\mathrm{Tr}(D_\mu U\, D^\mu U^\dagger)$ is gauge invariant and the kinetic term assumes the standard form $1/2\,\partial_\mu\pi^a\partial^\mu\pi^a$ if in Eq.(2.28) π^a is replaced by $2\pi^a/f_\pi^0$. Therefore the leading term in the derivative expansion of the effective Lagrangian reads [10]

$$\mathcal{L}_\pi^{(2)} = \frac{1}{4} f_\pi^{0\,2}\,\mathrm{Tr}(D_\mu U\, D^\mu U^\dagger) \ , \tag{2.32}$$

with, for example,

$$U(x) = \exp\left(i\,\frac{\vec{\tau}\cdot\vec{\pi}}{f_\pi^0}\right) . \tag{2.33}$$

The generating functional is invariant under coordinate transformations. As already mentioned, in the low-energy expansion of the Green function formed with n currents, the vertices which are relevant at leading order are those described by $\mathcal{L}_\pi^{(2)}$: the remainder of the effective Lagrangian only matters if the low energy expansion of the n-point function is carried beyond leading order.

2.4 Explicit chiral symmetry breaking

Chiral symmetry is explicitly broken by non-vanishing quark masses. The relevant piece in the QCD Hamiltonian is

$$H_{\chi sb} = \int d^3x (m_u \bar{u}u + m_d \bar{d}d) \ . \tag{2.34}$$

Both lattice and continuum determinations of the quark masses show $m_{u,d}^{\overline{\mathrm{MS}}}\,(\mu = 2\,\mathrm{GeV}) < 10\,\mathrm{MeV}$ [13]. For "small" symmetry breaking parameters $m_{u,d}$, the energy eigenvalues are close to those of the symmetric theory. In particular, the spectrum must contain a set of one-particle states, whose masses tend to zero if the quark masses are turned off. As we are going to show, explicit chiral symmetry breaking does not remove the Goldstone bosons, but equips them with a mass. The approximate global $SU(2)_L \times SU(2)_R$ symmetry of QCD easily explains a crucial property of the observed hadronic mass pattern: the pion mass is remarkably small compared to the masses of all other hadrons.

Explicit symmetry breaking may be accounted for in the effective field theory, provided it is sufficiently weak [22]. If the masses of the Goldstone bosons are small, the poles which they generate still dominate the low-energy structure of the theory. Clearly, the excitation energy of all other levels must be large compared to the excitation energy of

the Goldstone bosons: if this condition is not met, the latter loose their distinguished role in the low-energy analysis. In the following we will assume that the explicit symmetry breaking part is weak and treat it as a perturbation. At low energies, we expect strong interaction physics to be governed by the softest excitations of the QCD ground state, the "light" degrees of freedom. Here "light" is meant compared to $M_{\rm nucleon}$ or $M_{\rho-{\rm meson}}$, the lightest masses of non-Goldstone states. Kaons and the η-meson indeed can be regarded as Goldstone bosons associated with spontaneous chiral symmetry breaking $SU(3)_L \times SU(3)_R \to SU(3)_V$. In our work we consider the expansion in powers of m_u and m_d, keeping the remaning quark masses fixed at their physical values. The pions are the only Goldstone bosons.

The symmetry breaking part of the QCD Lagrangian is of the form

$$\mathcal{L}_{\rm sb} = -\bar{q}_R\, m\, q_L - \bar{q}_L\, m^\dagger q_R \ , \tag{2.35}$$

where m is the quark mass matrix. Let us rewrite for convenience

$$\mathcal{L}_{\rm sb} = m^\alpha O_\alpha \tag{2.36}$$

where the operators $O^\alpha = (\bar{q}_R^i q_L^j, \bar{q}_L^i q_R^j)$ are bilinear in the quark fields. The elements of the quark mass matrix play the role of the symmetry breaking parameters m_α.

Compared to the case of vanishing quark masses, the Ward identities involve Green functions which do not only contain the currents but also the operators O^α. It is therefore convenient to extend the generating functional, treating also the symmetry breaking parameters formally as external fields $m^\alpha = m^\alpha(x)$, on the same footing as the $f_\mu^i(x)$ associated with the currents. As before, the effective action is defined by the vacuum-to-vacuum transition amplitude

$$\exp(iZ[f,m]) = \langle 0\,{\rm out}|0\,{\rm in}\rangle_{f,m} \ . \tag{2.37}$$

To obtain Green functions in the presence of explicit symmetry breaking, it is sufficient to set $m^\alpha(x) = m_0^\alpha + \tilde{m}^\alpha(x)$ and expand the functional $Z[f,m]$ in powers of $f_\mu^i(x)$ and $\tilde{m}^\alpha(x)$. We expand around the non-zero, constant value of the light quark masses m^α which occurs in $\mathcal{L}_{\rm QCD}$. In the following we will be concerned with the two-flavor case.

The symmetry breaking also manifests itself in the effective theory. Including explicit chiral symmetry breaking, the low-energy analysis then involves a combined expansion, which treats both the momenta and the quark masses as small parameters. The effective Lagrangian now contains an external scalar field $m^\alpha(x)$,

$$\mathcal{L}_\pi^{\rm eff} = \mathcal{L}_\pi^{\rm eff}\,(\pi, \partial\pi, \ldots; f, \partial f, \ldots; m, \partial m, \ldots) = \mathcal{L}_{\rm eff}^0 + \mathcal{L}_{\rm eff}^{\rm sb} \ . \tag{2.38}$$

The effective Lagrangian considered in Sec.2.3 is what remains if the symmetry breaking field $m^\alpha(x)$ is turned off, *i.e.* $\mathcal{L}_{\rm eff}^0$. The extra term is the effective field theory analogue of the symmetry breaking piece which occurs in the original QCD Lagrangian.

Since we assume that the symmetry breaking is small, $\mathcal{L}_{\rm sb}$ may be treated as a perturbation. The corresponding perturbation series is ordered according to the powers of

the external field $m^\alpha(x)$. The effective Lagrangian can be expanded accordingly. The leading term in $\mathcal{L}_{\text{eff}}^{\text{sb}}$ is of first order in $m^\alpha(x)$. Since derivatives can be removed by partial integration, we can, without loss of generality, write the leading term in the form

$$\mathcal{L}_{\text{eff}}^{\text{sb}} = m^\alpha l_\alpha\,(\pi, \partial\pi, \dots; f, \partial f, \dots) + \mathcal{O}(m^2)\ . \tag{2.39}$$

At low energies, $l_\alpha(\pi, \dots)$ is dominated by the leading term in the derivative expansion. Both the derivative and the field $f_\mu^i(x)$ count as quantities of order p, the pion external momenta. Lorentz invariance only permits even powers of p. It is convenient to simplify the bookkeeping by counting the external field $m^\alpha(x)$ as a quantity of order p^2, such that both the symmetric and the symmetry breaking part of the Lagrangian consist of a series of terms of even order in p, starting at $\mathcal{O}(p^2)$. At leading order, the symmetry breaking term does not contain derivatives of the pion field and is independent of $f_\mu^i(x)$,

$$\mathcal{L}_{\text{eff}}^{\text{sb}} = m^\alpha l_\alpha(\pi) + \mathcal{O}(p^4)\ . \tag{2.40}$$

The explicit form of the function $l_\alpha(\pi)$ can be worked out using the constraint imposed by the symmetry [22, 24]. Using matrix notation,

$$\mathcal{L}_{\text{eff}}^{\text{sb}} = \text{Tr}\{m\, l(\pi) + m^\dagger\, l^\dagger(\pi)\} + \mathcal{O}(p^4)\ , \tag{2.41}$$

where $l(\pi)$ is a 2×2 matrix. Gauge invariance requires this matrix to transform in the same manner as the operator $q_L \times \bar{q}_R$ [24],

$$l(\pi) \to V_L l(\pi) V_R^\dagger\ , \tag{2.42}$$

which apart from an interchange of V_L and V_R, coincides with the transformation of the covariant pion field $U(\pi)$. Since the transformation law fixes the matrix up to a multiplicative constant, this implies $l(\pi) = \lambda U(\pi)^\dagger$. We write the effective coupling constant λ in the form $1/2\, f_\pi^0 B$. Parity conservation implies that B is real. At leading order in the low-energy expansion, the effective Lagrangian thus contains two real coupling constants,

$$\mathcal{L}_\pi^{(2)} = \frac{1}{4} f_\pi^{0\,2}\, \text{Tr}\{D_\mu U D^\mu U^\dagger\} + \frac{1}{2} f_\pi^{0\,2} B\, \text{Tr}\{m\, U^\dagger + m^\dagger\, U\}\ . \tag{2.43}$$

In order to interpret the new parameter B, let us consider the energy density of the ground state ($U = 1$),

$$\langle 0|\mathcal{H}_{\text{eff}}|0\rangle = -f_\pi^{0\,2} B(m_u + m_d) \tag{2.44}$$

and compare its derivative with respect to any of the light quark masses with the corresponding quantity in QCD, using the fact that the vacuum is invariant under $SU(2)_V$,

$$\left.\frac{\partial\langle 0|\mathcal{H}_{\text{QCD}}|0\rangle}{\partial m_q}\right|_{m_u = m_d = 0} = \langle 0|\bar{u}u|0\rangle_0 = \langle 0|\bar{d}d|0\rangle_0 \equiv \langle 0|\bar{q}q|0\rangle_0\ , \tag{2.45}$$

where $\langle 0|\bar{q}q|0\rangle_0$ denotes the scalar quark condensate in the $SU(2)$ chiral limit. Therefore, at first order in m, we obtain

$$\langle 0|\bar{q}q|0\rangle_0 = -f_\pi^{0\,2} B \ . \tag{2.46}$$

As we are taking the quark masses m_u, m_d to be real and positive, the configuration $\pi^a = 0$ represents a minimum of the potential arising from explicit symmetry breaking

$$V_{\rm eff}(\pi) = -\frac{1}{2} f_\pi^{0\,2} B \,{\rm Tr}\{m(U(\pi) + U(\pi)^\dagger)\} \tag{2.47}$$

provided B is positive. For the ground state of the effective theory to be stable against decay into multipion configurations, B must therefore be positive.

Let us consider the leading effective Lagrangian in Eq.(2.43). We switch off the external vector field and take a constant diagonal quark mass matrix $m = {\rm diag}(m_u, m_d)$ with $m_{u,d} \geq 0$. Since for unitary, unimodular 2×2 matrices U, the quantity $U + U^\dagger$ is a multiple of the unit matrix, the leading term of the effective Lagrangian only involves ${\rm Tr}\, m = m_u + m_d$. Using the parameterization in Eq.(2.33) and expanding in powers of the pion field, we get

$$\mathcal{L}_\pi^{(2)} = f_\pi^{0\,2} B(m_u + m_d) + \frac{1}{2}\left[\, \vec{\tau}\cdot\partial_\mu\vec{\pi}\,\vec{\tau}\cdot\partial^\mu\vec{\pi} - B(m_u + m_d)(\vec{\tau}\cdot\vec{\pi})^2 \right] \ . \tag{2.48}$$

Up to a sign, the first term represents the vacuum energy generated by the quark masses. The contribution of order π^2 describes a free pion of mass

$$M_{\pi^+}^2 = M_{\pi^0}^2 = M_{\pi^-}^2 = B(m_u + m_d) \ . \tag{2.49}$$

Expressing the low-energy constant B in terms of the order parameter $\langle 0|\bar{q}q|0\rangle_0$, the last equation leads to the Gell-Mann – Oakes – Renner relation [25]:

$$m_\pi^2 f_\pi^{0\,2} = -(m_u + m_d)\,\langle 0|\bar{q}q|0\rangle_0 + \mathcal{O}(m_{u,d}^2) \ . \tag{2.50}$$

As required by the Goldstone theorem, the pion mass disappears when the quark masses are turned off — the approximate chiral symmetry becomes an exact one. As long as the symmetry breaking is small, the pions only pick up a small mass proportional to the square root of the symmetry breaking parameter $m_u + m_d$. As the symmetry breaking term grows, higher powers of m_u and m_d are expected to become increasingly important. Since the effective Lagrangian used here neglects these terms, the above result for m_π^2 only holds up to corrections of $\mathcal{O}(m^2)$.

The explicit symmetry breaking shifts the poles generated by one-pion exchange. Accordingly, the Feynman propagator of the effective field is modified, $1/(p^2 + i\epsilon) \to 1/(p^2 - m_\pi^2 + i\epsilon)$. In the counting of powers which treats the quark masses as quantities of order p^2, the two terms occurring in the denominator are of the same order of magnitude, according to Eq.(2.50). We can also evaluate on-shell matrix elements without running into conflict with the power counting: the mass shell $p^2 = m_\pi^2$ links two quantities of the same algebraic order.

We notice that while the quark masses and the condensate depend on renormalization scheme and scale used in QCD, the product $B(m_u + m_d)$ does not. According to the expression of $m_\pi(m_{u,d})$ in ChPT, one can always translate the quark mass dependence of physical observables into a pion-mass dependence, avoiding complications with renormalization-group non-invariant quantities.

The leading effective Lagrangian is characterized by two scales, namely f_π^0 and B. Such parameters not fixed by the symmetry are called low-energy constants (LECs). They have to be determined by fits to experimental data or according to some model. The LECs encode information on underlying short-distance effects. All the low-energy constants are in principle calculable from QCD. They do not depend on the light quark masses, but are determined by the scale $\Lambda_{\rm QCD}$ and the masses of the heavy quarks. In practice, however, such calculations are not feasible yet. In Sec.2.9 we will discuss in detail present knowledge of the low-energy constants relevant for our work.

2.5 Loops and power counting in the mesonic sector

The perturbative expansion of a local field theory generates a unitary scattering matrix, provided all graphs are taken into account, including those containing loops. The corresponding path integral representation of the effective action is given by Eq.(2.25). The tree graphs represent the classical limit of this path integral. The quantum fluctuations described by the graphs containing loops contribute at non-leading order. At this point the effective Lagrangian method shows its full strength: the path integral not only yields all the pole terms, but automatically also accounts for all singularities due to multipion exchange contributions. Moreover, this approach *systematically* accounts for all singularities relevant at a given order in the low-energy expansion.

Dimensional regularization for ultraviolet divergences in loop integrals maintains the Ward identities in the context of Chiral Perturbation Theory. It avoids power-law divergences and momentum independent contributions generated by a cutoff regularization. Of course, there is no physics in the regularization and it is perfectly legitimate to use cutoff procedures, see for example [26, 27]. Since the effective Lagrangian contains all possible vertices, involving any number of derivatives, the divergences may be absorbed in a renormalization of the bare couplings, quite irrespective of the regularization used. The Ward identities may then be imposed order by order in the loop expansion. The net result for the low-energy representation of the Green function does not depend on the method used. The contributions from individual graphs, however, do depend on the regularization. Moreover, as we are going to show, using dimensional regularization, the renormalization of the coupling constants of a given order in $\mathcal{L}_\pi^{\rm eff}$ can be worked out, *once for all*, by analyzing the low-energy expansion to that order. If the expansion is carried further, the renormalized coupling constants do not change. In particular, the bare couplings f_π^0 and B, which enter the leading term of the effective Lagrangian, represent quantities of physical interest. Employing dimensional regularization, the leading order relations which connect these quantities with the pion decay constant and the quark condensate of massless QCD are not modified by higher-order contributions.

Weinberg [9] pointed out that at any given order in momenta or quark masses, only graphs with a *limited* number of loops contribute and the derivative expansion of the effective Lagrangian is needed only to that corresponding order. This is crucial to turn the effective Lagrangian with its infinite number of terms into a practical tool. The effective field theory does not get out of control when extended beyond leading order. Using dimensional regularization, indeed, the path integral over the effective field can be evaluated in a controlled manner, order by order in the low-energy expansion. The effective Lagrangian

$$\mathcal{L}_\pi^{\text{eff}} = \mathcal{L}_\pi^{\text{eff}}(\pi, \partial\pi, \dots; f, \partial f, \dots; m, \partial m, \dots) \ . \tag{2.51}$$

is represented as an infinite series of the type

$$\mathcal{L}_\pi^{\text{eff}} = \frac{1}{2}\,\partial\pi\partial\pi + \sum_v g_v\, \partial^{D_v} f^{F_v} m^{M_v} \pi^{P_v} \ , \tag{2.52}$$

where the integers D_v, F_v, M_v and P_v count the overall number of derivatives and fields entering the vertex v. Counting the external fields $f_\mu^i(x)$ and $m^\alpha(x)$ as quantities of $\mathcal{O}(p)$ and $\mathcal{O}(p^2)$, respectively, the order of a vertex is given by

$$O_v = D_v + F_v + 2M_v \ . \tag{2.53}$$

It is convenient to decompose the Lagrangian accordingly, collecting all of the vertices of a given order into a corresponding contribution to the effective Lagrangian

$$\mathcal{L}_\pi^{\text{eff}} = \mathcal{L}_\pi^{(2)} + \mathcal{L}_\pi^{(4)} + \mathcal{L}_\pi^{(6)} + \dots \tag{2.54}$$

Consider now a Green function formed with n_1 currents and n_2 scalar operators. The perturbative evaluation of the path integral leads to a representation for this quantity in the form of a sum of contributions arising from an infinite set of Feynman diagrams. The tree graphs are given by a product of vertices and propagators. The expressions for the loop diagrams involve similar products, integrated over the loop momenta. In dimensional regularization, the loop integrals extend over a d-dimensional momentum space, each loop contributing with a volume element of the form d^dq. The integrand is a homogeneous function of the external and internal momenta: scaling all external momenta by the same factor t and the light quark masses by t^2, the integrand remains the same, except for an overall power of t [1]. For the graph γ to contribute, we must have

$$\sum_{v\in\gamma} F_v = n_1 \ , \quad \sum_{v\in\gamma} M_v = n_2 \ . \tag{2.55}$$

Looking at the topology of loop graphs, one can show that a graph γ with L_γ independent loops [2] gives a contribution to the generating functional of order p^{O_γ} with

$$O_\gamma = \sum_{v\in\gamma}(O_v - 2) + (d-2)L - n_1 - 2n_2 + 2 \tag{2.56}$$

[1] The issue of convergence has to be addressed in order for the procedure of rescaling to be well-defined.
[2] L_γ is the maximum number of internal lines that can be cut without disconnecting the diagram.

where the sum extends over all vertices of the graph [24]. Clearly, for sufficiently small momenta and quark masses, the diagrams with small O_γ should dominate. According to Eq.(2.56), if the space-time dimension is larger that two, the occurrence of loops suppresses the magnitude of the graph at low-energies: in four dimensions, graphs containing one loop are suppressed by two powers of momentum compared to tree graphs, those with two loops by four powers and so on. This property is crucial for Chiral Perturbation Theory to be a coherent framework [9]. It implies that the standard perturbation series, organized accordingly to the number of loops, goes along perfectly well with the low-energy expansion. In the mesonic sector there is a one-to-one correspondence between chiral and loop expansion.

Chiral effective field theory leads to a double expansion in "small" momenta and quark masses. The effective couplings have the dimensionality of negative powers of mass and the theory is expected to loose its predictive power at energies of the order of the common mass scale that characterizes the various couplings.

The question of how large the radius of convergence of the low-energy expansion is, has been explored by Georgi and Manohar [28]. They argue that since higher-order terms are required as counterterms for loops involving lower-order interactions, it is inconsistent to assume that the size of these terms is smaller than the typical loop corrections. Any running coupling $L(\mu)$ in a counterterm should be at least as big as its anomalous dimension $\mu\, dL(\mu)/d\mu$ [29]. Since higher-order terms in the effective Lagrangian are identified by more powers of ∂ and m, dimensional analysis suggests that these terms should be associated with inverse powers of a dimensional parameter Λ_χ that controls the convergence of the expansion. Therefore, in general, a term in $\mathcal{L}_\pi^{\rm eff}$ with $2i$ derivatives and j powers of m is expected to have coupling constants of the form $c/\Lambda_\chi^{2(i+j)}$, with c of order one. Then the momentum and quark mass expansion converges for $p/\Lambda_\chi \ll 1$ and $m_\pi/\Lambda_\chi \ll 1$. The calculation of the $\pi\pi$ scattering amplitude, for example, can be carried to arbitrary order in Q (the typical pion energy), always with the net result that at each order we encounter a finite number of new couplings whose renormalization serves to eliminate the scale dependence of physical amplitudes. The ratio of the $\mathcal{O}(p^2)$, to the $\mathcal{O}(p^4)$ corrections is of order $Q^2/(16\pi^2 f_\pi^{0\,2})$. The factor $16\pi^2$ is generic for one-loop integrals in $3+1$ dimensions. This leads to the "naive" dimensional estimate $\Lambda_\chi \lesssim 4\pi f_\pi^0$. A more refined analysis investigated how the bound on Λ_χ varies with the number of flavors N_f [30, 31]. The loop expansion is found to be yield $\Lambda_\chi \lesssim 4\pi f_\pi^0/\sqrt{N_f}$. This pattern persists to all orders in the loop expansion.

A more quantitative picture can be achieved, for example, by saturating suitable dispersion relations with contributions from resonances. The low-energy structure is dominated by the poles and cuts generated by the lightest particles. The effective theory is constructed using the asymptotic (color singlet hadron) states of QCD. In the sector with zero baryon number and light quarks only, the Goldstone bosons form a complete set of such states, all other mesons being unstable against decay into these. The Goldstone degrees of freedom are explicitly accounted for in the effective theory — they represent the dynamical variables. All other levels manifest themselves only indirectly through the

values of the effective coupling constants. In some channels, like the $I = J = 1$ channel, the scale of the chiral expansion is set by the mass of the ρ meson, in others by the masses of the scalar or pseudoscalar states occurring around 1 GeV. The cuts generated by the Goldstone pairs are significant in some cases and are negligible in others, depending on the numerical value of the relevant Clebsch-Gordan coefficient. A case-by-case analysis is mandatory to formulate quantitative statements about convergence of the chiral expansion.

Let us now examine the runnings of m_π and f_π with the light quark masses, which are of particular relevance for our study. In the following we will not take into account isospin-breaking effects and work with degenerate light u- and d- quark masses, $m_u = m_d = m_q$.

2.6 Pion mass versus quark mass

In our study we translate the functional dependence of physical observables on the (light) quark mass m_q into a pion-mass dependence according to the Gell-Mann – Oakes – Renner relation, Eq.(2.50), which represents the leading term in the quark-mass expansion of m_π in the so-called "standard symmetry breaking scenario". As pointed out in Ref. [32], if the term proportional to m_q^2 in Eq.(2.50) were comparable or even larger than the linear one, a different bookkeeping for the chiral perturbation series would be required. The leading correction to the Gell-Mann–Oakes–Renner relation is given by

$$m_\pi^2 = 2Bm_q - \frac{\bar{l}_3}{32\pi f_\pi^{0\,2}} (2Bm_q)^2 + \mathcal{O}(m_q^3) \ , \tag{2.57}$$

where $\bar{l}_3$ is a m_q-dependent coefficient related to the low-energy constant l_3 in $\mathcal{L}_\pi^{(4)}$ [10]. The standard chiral power counting is adequate only if $\bar{l}_3$ is not too large.

In the low-energy regime the phases of the form factors relevant for the decay $K^+ \to \pi^+\pi^- e^+\nu_e$ are related to the corresponding phases of $I = 0$ S-wave and $I = 1$ P-wave elastic $\pi\pi$ scattering. Using a dispersion theoretical approach in terms of Roy equations, Colangelo, Gasser and Leutwyler obtained a value for the scattering length a_0^0 which gives the upper limit $|\bar{l}_3| \leqslant 16$ [33]. Even with this coarse estimate, the Gell-Mann-Oakes-Renner relation turns out to be a decent starting point: more than 94% of the physical pion mass stems from the first term in Eq.(2.57). This supports the conjecture that the quark condensate is the leading order parameter of the spontaneously broken chiral symmetry and there is no need for a reordering of the ChPT series in the two-flavor case.

Of course, higher-order terms in the quark-mass expansion of m_π are expected to become more important with increasing m_q. For reasons not yet understood, fully dynamical lattice QCD simulations show a linear relationship between m_π^2 and the explicit chiral symmetry breaking parameter m_q even for pion masses ranging from beyond the physical kaon mass up to 1 GeV. A recent systematic analysis [34] of full $N_f = 2$ lattice QCD simulations by the CP-PACS and UKQCD collaborations shows that the leading-order result, Eq.(2.50), agrees with the data up to 1 GeV in m_π, at least. However, this

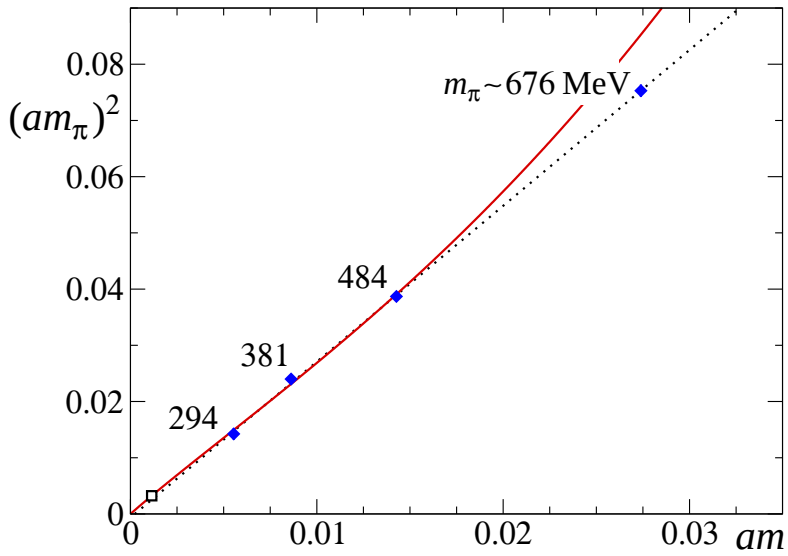

Figure 2.1: The square of the pion mass versus the current quark mass, in lattice units. Recent data for $N_f = 2$ are compared with leading- (dotted) and next-to-leading-order formulae (full curve) in Chiral Perturbation Theory [35]. The lattice spacing is determined, at the specified values of the gauge coupling, by setting the Sommer scale [36] $r_0 = 0.5\,\mathrm{fm}$ at the quark mass where $r_0 m_\pi = 1.26$. The point represented by an open square is obtained by extrapolation to the physical pion mass.

amazing feature is not shared by higher-order ChPT expressions for $m_\pi(m_q)$ for such an extended range in quark mass. In order to assess the convergence behavior of m_π^2 versus m_q, in Ref. [34] leading and next-to-leading-order predictions for a given quark mass have been compared. It turns out that the chiral expansion is sufficiently well behaved up to pion masses of about 600 MeV. In this analysis the low-energy constants have been fixed consistently with empirical information and the estimate $\bar{l}_3(m_q^{\mathrm{phys}}) = 2.9 \pm 2.4$ [10] has been used.

Fig.2.1 from Ref. [35] shows very recent results with dynamical standard Wilson fermions, on a 32×24^3 lattice, with spacing of about 0.08 fm and spatial size close to 2 fm. Pion and current quark masses are extracted from the correlation functions of the isovector axial current and density. The dotted line, which is a linear fit of all four lattice data points, passes through the origin within errors. If we omit the point at the largest mass and fit to the three remaining lattice data with Eq.(2.57), we obtain the solid curve in Fig.2.1, and the values of the fit parameters B and $\bar{l}_3$ come out close to the phenomenologically expected ones, see Ref. [35]. One-loop chiral perturbation theory with phenomenologically acceptable values of the coupling constants is able to make contact with the quark-mass range that can be reached in present simulations with dynamical quarks.

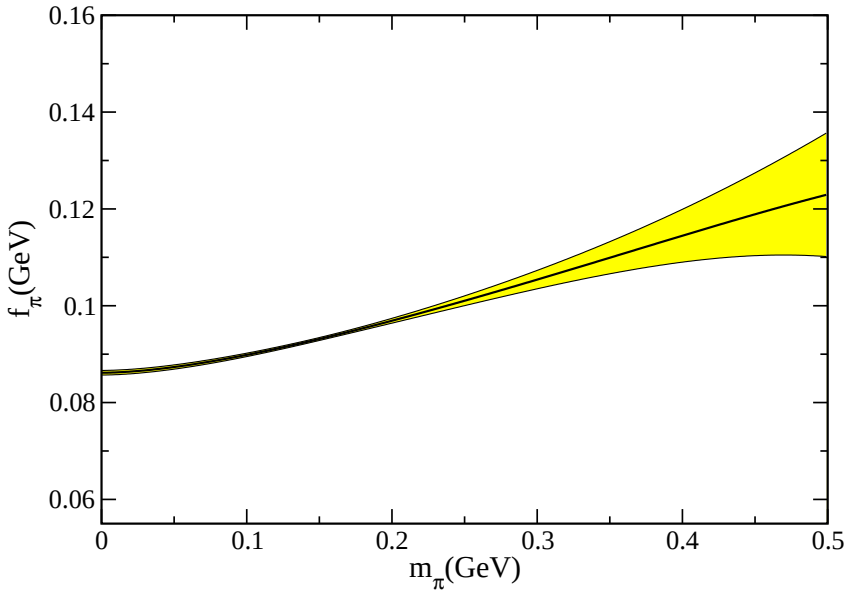

Figure 2.2: The 1-σ band of the pion mass dependence of f_π at NNLO, as determined in Ref. [37].

2.7 Pion mass dependence of f_π

At next-to-leading order, the quark mass expansion for f_π reads [10]

$$f_\pi = f_\pi^0 \left[1 + \frac{(2B\, m_q)^2\, \bar{l}_4}{16\pi^2 f_\pi^{0\,2}} + \mathcal{O}(m_q^4) \right] \ . \tag{2.58}$$

In this case the relevant effective coupling is known rather well: chiral symmetry implies that it also determines the slope of the scalar form factor of the pion. Let us define

$$\bar{l}_4 \equiv \ln \frac{\Lambda_4^2}{(2B\, m_q)^2} \ . \tag{2.59}$$

Analyticity relates the pion scalar form factor to the $I = 0$ S-wave phase shift of $\pi\pi$ scattering. Evaluating the relevant dispersion relation with the remarkably accurate information about this phase shift that follows from the Roy equations, Colangelo, Gasser and Leutwyler found [33]

$$\Lambda_4 = 1.26 \pm 0.14\,\mathrm{GeV} \ . \tag{2.60}$$

This information determines the quark mass dependence of the pion decay constant to within rather narrow limits, see Fig.2.2 from Ref. [37], where the plot refers to the next-to-next-to-leading order formula. Here the impact of the relevant combination of $\mathcal{O}(p^6)$ couplings has been neglected since this contribution is small. The analysis of Ref. [37] gives the estimate $f_\pi^0 \approx 86.2\,\mathrm{MeV}$.

Fig.2.3 from Ref. [35] shows recent results with standard Wilson fermions on a 32×24^3 lattice, with spacing of about 0.08 fm and spatial size close to 2 fm. Tadpole improved

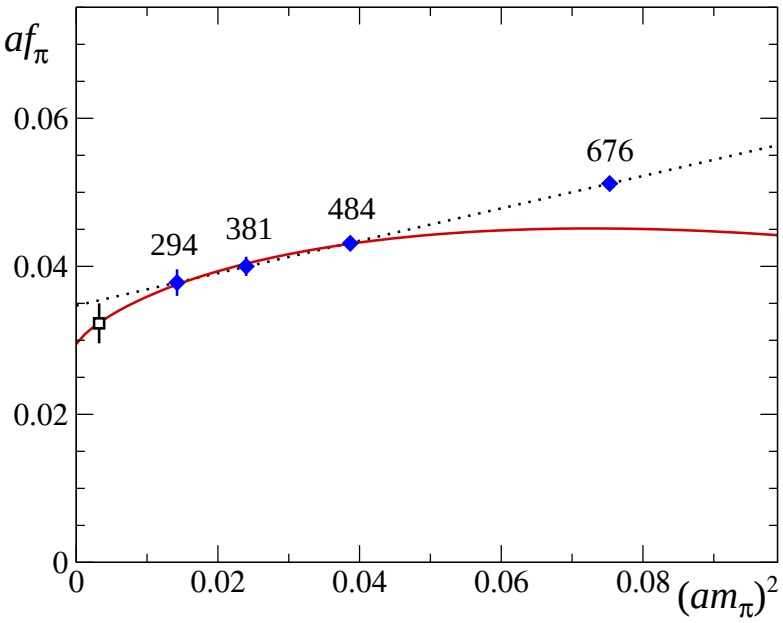

Figure 2.3: Simulation results for the pion decay constant, plotted versus the pion mass squared, in lattice units [35]. The lattice spacing is determined by setting the Sommer scale [36] $r_0 = 0.5\,\mathrm{fm}$ at the quark mass where $r_0 m_\pi = 1.26$. The curves are linear and leading-one-loop chiral fits. The point represented by an open square is obtained by extapolation to the physical pion mass.

perturbation theory has been used to estimate the renormalization factor relevant for the pion decay constant and a small finite-volume correction, computed according to one-loop ChPT, has been applied to data. The three smallest pion mass points are fitted using Eq.(2.58), treating f_π^0 and Λ_4 as free parameters. The fit result for the latter comes out to be in agreement with the range (2.60), while the value for f_π at the physical pion mass, $f_\pi = 80(7)\,\mathrm{MeV}$, is slightly lower than the empirical one. However, uncontrolled systematic errors affect this preliminary set of data points. The results need to be confirmed at several lattice spacings, due to the absence of $\mathcal{O}(a)$-improvement terms in the Wilson action presently employed [35].

2.8 The pion-nucleon system

In this section we discuss the inclusion of baryons in Chiral Perturbation Theory. We will make use of the resulting effective field theory to systematically investigate the impact of spontaneous and explicit chiral symmetry breaking on the long-distance structure of the nucleon. After an introduction to the formalism, both in the manifestly covariant formulation and in the non-relativistic limit, we will focus on the infrared regularization method, the framework we use for our analysis of the quark mass dependence of nucleon observables.

The relativistic formalism for the low-energy πN effective field theory dates back to Weinberg [39], Coleman *et al.* [40], Langacker and Pagels [41] and others, see Ref. [42]. The connection to QCD Green functions was performed in a systematic fashion by Gasser, Sainio and Švarc [43] and Krause [44]. Here we specialize to the case of two flavors, with pions and nucleons as the asymptotically observed fields — the explicit degrees of freedom of the effective field theory.

The time-ordered nucleon matrix elements of the quark currents are generated by the nucleon-to-nucleon transition amplitude

$$\mathcal{F}(\vec{p}\,',\vec{p};v;a;s;p) = \langle \vec{p}\,' \,\mathrm{out}|\vec{p}\,\,\mathrm{in}\rangle^{\mathrm{connected}}_{v,a,s,p}, \quad \vec{p}\,' \neq \vec{p} \tag{2.61}$$

determined by the Lagrangian (2.18). Here $|\vec{p}\,\mathrm{in}\rangle$ denotes an incoming one-nucleon state of momentum $\vec{p}$. The idea is to construct, in analogy with Eq.(2.25), a pion-nucleon field theory which allows to evaluate the functional $\mathcal{F}$ to any order in the low-energy expansion [43].

First we consider the general structure of the effective πN Lagrangian, $\mathcal{L}^{\mathrm{eff}}_{\pi N}$. The pions are collected in the $SU(2)$ matrix-valued field $U(x)$ while proton and neutron are combined in the isospinor $\Psi = (p,n)^T$. To construct a theory incorporating nucleons, we must first decide how the nucleon field transform under $SU(2)_L \times SU(2)_R$. There is a variety of ways to describe these transformation properties. All of them lead to the same physics: different representations in a theory containing Goldstone bosons are connected via field redefinitions [45]. We can therefore choose a maximally convenient description, where both $\pi\pi$ and πN interactions are of derivative nature: these interactions are easy to classify according to their contribution to the low-energy expansion. This calls for a non-linear realization of chiral symmetry. Following Refs. [39, 40], we introduce a matrix-valued function K, defined as

$$V_R u = u' K \tag{2.62}$$

with $u^2(x) = U(x)$ and $U'(x) = V_R U(x) V_L^\dagger = u'^2(x)$ and $V_R, V_L \in SU(2)$. The baryon field transforms as

$$\Psi \to K(V_L, V_R, U)\ . \tag{2.63}$$

The most general effective πN Lagrangian for processes with one incoming and one outgoing nucleon and no nucleon loops which

- has a *local* $SU(2)_L \times SU(2)_R \times U(1)_V$ symmetry in order that single-nucleon Green functions satisfy chiral Ward identities,
- is a Hermitian Lorentz scalar,
- is even under the discrete symmetries C, P and T,
- has the smallest number of derivatives

is given by [43]

$$\mathcal{L}_{\pi N}^{(1)} = \bar{\Psi}\left(i\not{D} - M_0 + \frac{g_A^0}{2}\gamma^\mu\gamma_5 u_\mu\right)\Psi \ . \tag{2.64}$$

where

$$\begin{aligned} D_\mu &= \partial_\mu + \Gamma_\mu \\ \Gamma_\mu &= \frac{1}{2}[u^\dagger, \partial_\mu u] - \frac{i}{2}u^\dagger r_\mu\, u - \frac{i}{2}u\, l_\mu u^\dagger \\ u_\mu &= i\{u^\dagger, \partial_\mu u\} + u^\dagger r_\mu\, u - u\, l_\mu u^\dagger \\ r_\mu &= v_\mu + a_\mu, \quad l_\mu = v_\mu - a_\mu \\ \chi_\pm &= u^\dagger\chi u^\dagger \pm u\chi^\dagger u, \quad \chi = 2B(s+ip) \ . \end{aligned} \tag{2.65}$$

$\mathcal{L}_{\pi N}^{(1)}$ contains two parameters not determined by chiral symmetry, which must be pinned down by a fit to data: the nucleon mass M_0 and the axial-vector coupling constant of the nucleon g_A^0, both taken in the chiral limit, *i.e.*

$$M_N = M_0\,[1 + \mathcal{O}(m_q)] \qquad g_A = g_A^0\,[1 + \mathcal{O}(m_q)] \ . \tag{2.66}$$

The overall normalization in Eq.(2.64) is chosen in such a way that in the case of no external fields and no pion fields, $\mathcal{L}_{\pi N}^{(1)}$ reduces to the Lagrangian of a free nucleon.

The nucleon mass does not vanish in the chiral limit and represents an additional, "large" scale comparable to Λ_χ [3]. This means that the zeroth component of the partial derivative acting on a nucleon field does not produce a "small" quantity: $D_\mu\Psi = \mathcal{O}(p^0)$ whereas $(i\not{D} - M_0)\Psi = \mathcal{O}(p)$ where p denotes a generic (external) nucleon *three*-momentum. As pointed out by Gasser, Sainio and Švarc, in dimensional regularization and $\overline{\rm MS}$ scheme [43], the fact that the nucleon mass does not vanish in the chiral limit spoils the exact one-to-one correspondence between loop and small momentum expansions characterizing ChPT in the mesonic sector. An amplitude of a specific chiral order may receive contributions from diagrams with an arbitrary number of loops. More precisely, in the manifestly Lorentz invariant framework with dimensional regularization and $\overline{\rm MS}$ scheme, the chiral expansion of loop graphs involving nucleon propagators in general starts at the same chiral order as the corresponding tree graphs, so that the renormalization of divergences requires also the tuning of effective couplings appearing at *lower* order [4]. Furthermore, the lowest order coefficients M_0 and g_A^0 get renormalized at every order of the series. In this framework it is complicated to establish a systematic method of assessing the relative importance of diagrams generated by $\mathcal{L}_{\pi N}^{\rm eff}$.

2.8.1 The non-relativistic limit

To overcome such a mismatch between chiral and loop expansion in the baryonic sector, the so-called Heavy-Baryon projection has been proposed [47–49]. It is modeled after

[3] Cf. the analysis of the quark mass dependence of the nucleon mass in Chapter 3.

[4] This also happens when employing a mass-dependent regularization scheme, like a momentum cutoff, see for example Refs. [29, 46].

heavy-quark effective field theory methods and historically it is the first scheme including baryons with a power counting analogous to the mesonic sector. If one considers the baryons as very heavy, with masses large compared to the typical external momenta transferred by pions or any external source, only baryon momenta relative to the rest mass will count and these can be small. The emerging picture is that of an almost static source surrounded by a cloud of light pions.

Jenkins and Manohar [47, 48] formulated Heavy-Baryon Chiral Perturbation Theory (HBChPT) taking the extreme non-relativistic limit of the manifestly covariant theory and performing a systematic expansion in powers of the nucleon mass. The approach is analogous to the Foldy-Wouthuysen non-relativistic reduction [50] which provides a systematic procedure to block-diagonalize a relativistic Dirac Hamiltonian in powers of the inverse of the mass M of the Dirac field and produce a decoupling of the large and small components of this field to any desired order in $1/M$, see for example Ref. [51] [5].

For a general four-vector v^μ with the properties $v^2 = 1$ and $v^0 \geq 1$, one defines the projection operators

$$P_v^\pm = \frac{1}{2}(1 \pm \not{v}), \quad P_v^+ + P_v^- = 1, \quad P_v^{\pm 2} = P_v^\pm, \quad P_v^\pm P_v^\mp = 0 \ . \tag{2.67}$$

For a nucleon of four-momentum p^μ and mass M_N, the particular choice $v^\mu = p^\mu/M_N$ correspond to its world velocity. Let us decompose the nucleon field Ψ into the so-called velocity-dependent fields H_v and h_v defined as

$$H_v \equiv \exp[iM_0\, v\cdot x]\, P_v^+\Psi, \qquad h_v \equiv \exp[iM_0\, v\cdot x]\, P_v^-\Psi \ . \tag{2.68}$$

In the nucleon rest-frame $v^\mu = (1,0,0,0)$ this decomposition leads to the standard non-relativistic reduction of a Dirac spinor into upper (large) and lower (small) components. Using Eq.(2.68) in the equation of motion for Ψ from the relativistic πN effective Lagrangian in Eq.(2.64), one finds that the component h_v is suppressed by powers of $1/M_0$ compared to H_v. The nucleon mass disappears from the leading-order πN Lagrangian, it only shows up in an infinite string of higher-order vertices suppressed by powers of $1/M_0$. These terms together with new chiral structures from the most general chiral πN effective Lagrangian at higher orders allow to systematically go beyond the extreme non-relativistic (static) limit.

An ordinary partial derivative acting on a Heavy-Baryon field H_v produces a small "residual" four-momentum k^μ appearing in the separation $p_\mu = M_0\, v_\mu + k_\mu$. In the Heavy-Baryon approach, four-momenta are considered small if their components are much less than the nucleon mass or $4\pi f_\pi^0$, which are indeed comparable in size. This leads to a low-energy expansion in terms of $p/(4\pi f_\pi^0)$ and p/M_0, where p collectively denotes external pion momenta, four-momenta transferred by external sources, residual nucleon momenta and Goldstone boson masses.

The power counting scheme in HBChPT can be formulated in close analogy to the mesonic sector, cf. Sec.2.5. The chiral order O_γ of a given diagram with exactly one

[5] A criterion for the Foldy-Wouthuysen method to work is that the potential in the Hamiltonian are small in comparison with the mass of the Dirac field. This can be regarded as the analogue of treating external fields as small quantities, of order p or p^2 in ChPT.

baryon in the initial and one baryon in the final state, in four space-time dimensions, reads [53, 54]

$$O_\gamma = 2N_L + 1 + \sum_{n=1}^{\infty} 2(n-1)N_{2n}^{\pi} + \sum_{n=1}^{\infty}(n-1)N_n^{\pi N} \geq 2N_L + 1 \ . \tag{2.69}$$

Here N_L is the number of independent loop momenta, N_{2n}^{π} the number of vertices originating from the purely mesonic Lagrangian $\mathcal{L}_\pi^{(2n)}$ and $N_n^{\pi N}$ the number of vertices from the pion-nucleon Lagrangian of order n, $\mathcal{L}_{\pi N}^{(n)}$. In the baryonic sector the chiral order of the effective Lagrangian increases in units of one, because of the possibility of forming Lorentz invariants by contracting derivatives with Dirac matrices.

According to Eq.(2.69), loops start contributing at $O_\gamma = 3$, which means that the low-energy constants in the second order πN effective Lagrangian are not needed to absorb infinities from one-loop calculations. Moreover, the parameters of the lowest-order Lagrangian do not get modified due to higher order corrections in the chiral limit, like in the mesonic sector.

2.8.2 Infrared regularization

A vast majority of applications of ChPT in the one-nucleon sector were performed in the Heavy-Baryon framework [47, 49, 52]. However, such an approach may generate Green functions which do not satisfy the analytic properties resulting from a fully relativistic theory. This is crucial for connections with dispersion relations. An instructive example is the triangle-graph, Fig.2.4. One needs to consider the properties of the integral

$$\gamma(t) \equiv i \int \frac{d^4k}{(2\pi)^4} \frac{1}{k^2 - m_\pi^2 + i\epsilon} \frac{1}{(k-q)^2 - m_\pi^2 + i\epsilon} \frac{1}{(p-k)^2 - M_0^2 + i\epsilon} \ , \tag{2.70}$$

where q is the four-momentum transferred to the virtual pion (for example by an external source) and $t \equiv q^2$. A diagram of this type appears in many calculations such as the scalar or electromagnetic form factors of the nucleon, πN or Compton scattering. The analytic properties of such a graph as a function of t are determined by the pole structure of the propagators.

Counting powers one can see that the integral (2.70) converges. The function $\gamma(t)$ is analytic in t except for a cut along the positive real axis starting at $t = 4\,m_\pi^2$ corresponding to the fact that two on-shell pions can be produced for $t \geq 4\,m_\pi^2$. This diagram has also a singularity in the second Riemann sheet, at $t_c = 4m_\pi^2 - m_\pi^4/M_N^2 = 3.98\,m_\pi^2$, *i.e.* very close to physical threshold. To leading order in the Heavy Baryon approach, this singularity coalesces with the threshold [55]. Near $t = 4\,m_\pi^2$, $\gamma(t)$ does not admit an expansion in powers of meson momenta and quark masses. The Heavy-Baryon representation does not make sense there and, within such approach, an infinite series of internal line insertions must be summed up to properly describe the behavior near two-pion threshold. In a fully relativistic treatment, such constraints from analyticity are automatically fulfilled, since the *full* function $\gamma(t)$ is involved and not the first terms in its chiral expansion.

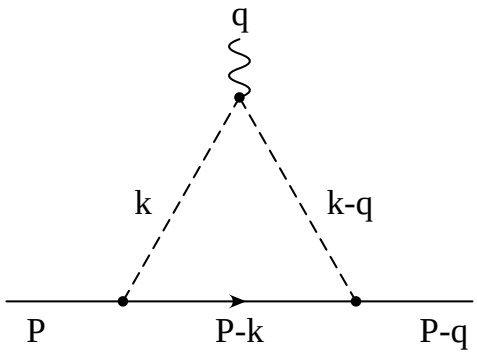

Figure 2.4: Triangle graph. The solid, dashed and wiggly lines represent nucleons, pions and an external scalar source, respectively.

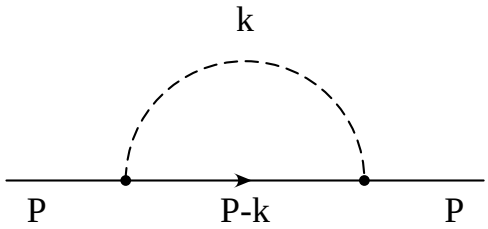

Figure 2.5: Self-energy graph analyzed in the text.

Methods which produce both the correct analytic structure and a consistent power counting have been developed. Ellis and Tang [56] argued that relativistic one-loop integrals can be separated into "soft" and "hard" parts, according to the portion of internal loop momenta involved: while for the former the HBChPT power counting applies, the contributions from the latter can be absorbed in some LECs. A more formal implementation of such a program, called infrared regularization [57], is due to Becher and Leutwyler [6]. Let us illustrate this method by means of the *dimensionally regularized* scalar one-loop integral, Fig.2.5,

$$H(p^2,d) = \frac{1}{i}\int \frac{d^dk}{(2\pi)^d}\frac{1}{k^2-m_\pi^2+i\epsilon}\frac{1}{k^2-2p\cdot k+(p^2-M_N^2)+i\epsilon}\ . \tag{2.71}$$

Here d is an arbitrary space-time dimension and the right-hand side is thought to be analytically continued as a function of d. Infrared regularization relies on dimensional regularization, it is a variant thereof which preserves low-energy power counting rules underlying HBChPT. The integral (2.71) converges for $d<4$. In the limit $m_\pi \to 0$, this integral develops an infrared singularity, generated by small values of $k=\mathcal{O}(p)$. In that region the first factor in the integrand counts as $\mathcal{O}(p^{-2})$ while the second is of order p^{-1}.

[6] For a procedure, alternative to infrared regularization, to overcome the problems of covariant Baryon ChPT with dimensional regularization and $\overline{\rm MS}$, we refer to [58].

We therefore naively expect the part originating the infrared singularity to be of order $\mathcal{O}(p^{d-3})$. On the other hand, for "large" loop momenta (of the order of the nucleon mass) we expect power counting to fail.

Let us introduce the dimensionless variables

$$\alpha = \frac{m_\pi}{M_N} , \qquad \Omega = \frac{p^2 - M_N^2 - m_\pi^2}{2M_N m_\pi} , \tag{2.72}$$

which count as $\mathcal{O}(p)$ and $\mathcal{O}(p^0)$ respectively, since we analyze nucleon momenta close to the mass shell. Using the standard Schwinger-Feynman parameterization

$$\frac{1}{AB} = \int_0^1 \frac{dz}{[(1-z)A + zB]^2} , \tag{2.73}$$

we perform the shift $k \to k + pz$ in the integration variable and obtain

$$H = \frac{1}{i} \int_0^1 dz \int \frac{d^d k}{(2\pi)^d} \frac{1}{[k^2 - A(z) + i\epsilon]^2} \tag{2.74}$$

where

$$A(z) = z^2 p^2 - z(p^2 - M_N^2 + m_\pi^2) + m_\pi^2 = M_N^2 [z^2 - 2\alpha\Omega z(1-z) + \alpha^2 (1-z)^2] . \tag{2.75}$$

The last equivalence has been written in order to facilitate the comparison with the result in Ref. [57]. Performing the integration over k we get

$$H = f(d) \int_0^1 dz \, [A(z) - i\epsilon]^{d/2-2} \tag{2.76}$$

with

$$f(d) = \frac{\Gamma(2 - d/2)}{(4\pi)^{d/2}} . \tag{2.77}$$

In this representation, the infrared singularity arises from small values of z: $A(z)$ becomes correspondingly small if m_π tends to zero. We can isolate this divergent part by scaling the variable of integration, $z = \alpha x$. The upper limit then becomes large: $x = 1/\alpha \to \infty$ as $m_\pi \to 0$. An integral I having *the same infrared singularity* as the integral H is then defined as

$$I \equiv f(d) \int_0^\infty dz \, [A(z) - i\epsilon]^{d/2-2} . \tag{2.78}$$

Accordingly, the infrared regular part of H is defined as

$$R \equiv -f(d) \int_1^\infty dz \, [A(z) - i\epsilon]^{d/2-2} \tag{2.79}$$

so that $H = I + R$. In the terminology of Ellis and Tang [56], I represents the "soft" component of the amplitude, while R is the "hard" component. For arbitrary values of

d, the explicit expressions for H, I and R involve hypergeometric functions. The chiral expansion of I has the form

$$I = \mathcal{O}(p^{d-3}) + \mathcal{O}(p^{d-2}) + \mathcal{O}(p^{d-1}) + \dots \tag{2.80}$$

while for any value of d the corresponding expansion of R is

$$R = \mathcal{O}(p^0) + \mathcal{O}(p^1) + \mathcal{O}(p^2) + \dots \tag{2.81}$$

The integral (2.78) converges for $d < 3$. The analytical continuation to $d = 4$ is performed via partial integration. We notice that the factor $f(d)$ in Eq.(2.77) contains a pole there. Throughout this work the subtraction of the $1/(d-4)$ poles is done via the definition of

$$L(\lambda) = \frac{\lambda^{d-4}}{16\pi^2}\left\{\frac{1}{d-4} - \frac{1}{2}\left[\ln(4\pi) + \Gamma'(1) + 1\right]\right\} , \tag{2.82}$$

where λ is a (mass) regularization scale which makes the logarithms appearing in the expansion of I to have dimensionless arguments. According to the last equation,

$$I = -2L(\lambda)\,\frac{\alpha(\Omega+\alpha)}{1+2\alpha\Omega+\alpha^2} + \bar{I} \tag{2.83}$$

where $\bar{I}$ denotes the renormalized amplitude after removing the pole as $d \to 4$:

$$\begin{aligned}\bar{I} = &-\frac{1}{8\pi^2}\frac{\alpha\sqrt{1-\Omega^2}}{1+2\alpha\Omega+\alpha^2}\,\arccos\left(-\frac{\Omega+\alpha}{\sqrt{1+2\alpha\Omega+\alpha^2}}\right)\\ &-\frac{1}{16\pi^2}\frac{\alpha(\Omega+\alpha)}{1+2\alpha\Omega+\alpha^2}\left(2\ln\frac{m_\pi}{\lambda} - 1\right) ,\end{aligned} \tag{2.84}$$

for $-1 < \Omega < 1$. The chiral expansion of $\bar{I}$ *starts* at order p, in agreement with power counting. Furthermore, the series giving the chiral expansion of I converges if Ω is in the disk [57]

$$|\alpha| < |\Omega \pm \sqrt{\Omega^2 - 1}| , \tag{2.85}$$

a range which covers the entire low-energy region.

At threshold, $p^2 = (M_N + m_\pi)^2$, we get

$$H_{\rm thr} = \frac{\Gamma(2-d/2)}{(4\pi)^{d/2}(d-3)}\left(\frac{m_\pi^{d-3}}{M_N+m_\pi} + \frac{M_N^{d-3}}{M_N+m_\pi}\right) , \tag{2.86}$$

where the first term is the infrared singular part $I_{\rm thr}$ and the second represents $R_{\rm thr}$. From the previous expressions of the chiral expansions of I and R, Eqs.(2.80) and (2.81), it is clear that the distinguishing feature between I and R is the following: for non-integer values of the space-time dimension d, I gives rise to non-integer powers of p, whereas the regular part may be expanded in an ordinary Taylor series in momenta and quark masses. For the integrals at threshold this can be nicely seen by expanding in powers of m_π counting as $\mathcal{O}(p)$. For the "soft" contribution the power counting is respected. On the other hand, it is the regular part which does not satisfy counting rules and contains the

problematic polynomial terms in M_0. However, at any order, R can be absorbed in the LECs of the effective Lagrangian. In the standard renormalization procedure, *ultraviolet infinite* contributions from loop integrals are absorbed in the coupling constants; in the infrared regularization, not only the infinite parts are moved to the couplings, but also *finite parts* originating from the propagation of very massive states. The latter mess up the power counting in dimensional regularization and $\overline{\rm MS}$ scheme, giving rise to terms of the type $(M_0/\Lambda_\chi)^n$ which obscure the convergence of the chiral expansion — possibly saved by unnaturally large counterterms.

On the other hand, the infrared singular part I has the same analytical properties as the full integral H in the low-energy region. Its chiral expansion leads to the non-trivial momentum and quark mass dependence (unambiguously predicted) in ChPT, leading to chiral logarithms or fractional powers of the quark masses.

Becher and Leutwyler also showed that their procedure to separate infrared and regular parts through a suitable Feynman parametrization leads to a unique result, in agreement with the chiral Ward identities of QCD. The proof is essentially based on the fact that terms with fractional versus integer powers in the pion mass must be separately chirally symmetric. Consequently, the infrared regularization prescription, which replaces any dimensionally regularized one-loop integral H with its infrared singular part I, defines a symmetry preserving regularization scheme.

As discussed in detail in Ref. [57], the infrared regularization method can be easily generalized to any one-loop integral in Baryon Chiral Perturbation Theory. All of these integrals can be reduced to the form

$$H^{\mu_1\cdots\mu_r}_{mn} = \frac{1}{i}\int \frac{d^dk}{(2\pi)^d}\frac{k^{\mu_1}\ldots k^{\mu_r}}{a_1\ldots a_m\, b_1\ldots b_m}\ , \tag{2.87}$$

where the denominator involves meson and nucleon propagators

$$\begin{aligned} a_i &= (k+q_i)^2 - m_\pi^2 + i\epsilon \\ b_j &= (p_j-k)^2 - M_N^2 + i\epsilon\ . \end{aligned} \tag{2.88}$$

The numerator arises from both the derivative couplings characteristic of ChPT and the term $\not{k}$ that occurs in the numerator of the nucleon propagator.

In view of Lorentz invariance, the integral (2.87) can be decomposed in a basis formed with tensor polynomials of the external momenta p_j^μ and q_k^μ. The other Lorentz covariant object involved is the metric tensor $g_{\mu\nu}$. Contracting with k^ρ and $g^{\rho\sigma}$, the coefficients of the decomposition can be expressed in terms of scalar integrals of the form

$$H_{mn} = \frac{1}{i}\int \frac{d^dk}{(2\pi)^d}\frac{1}{a_1\ldots a_m\, b_1\ldots b_m}\ , \tag{2.89}$$

which can easily be related to the "master" scalar integral H in Eq.(2.71) through partial derivatives with respect to m_π^2 and M_N^2. In Appendix C we explicitly show the tensor reduction for all integrals relevant for our analysis.

Baryon Chiral Perturbation Theory with infrared regularization is fully systematic and model-independent. It is able to account for all contributions arising to a given order in the low-energy expansion of the various observables. The price to pay is that the loop integrals cannot be interpreted directly in physical terms. The machinery does incorporate the finite extension of the nucleon, but only indirectly, through pion loops and effective coupling constants, which parameterize short-distance physics contributing to the internal structure of the nucleon. The replacement of pointlike vertices by form factors [46, 59], resulting in an effective cutoff of the virtual meson momenta, gives a more intuitive physical picture but in general ruins the Ward identities of chiral symmetry and messes up the systematic power counting. On the other hand, when loop diagrams are calculated, the reliable part of the result comes only from the low-energy portion of the loop, for which ChPT is appropriate. In a cutoff approach one can check whether a loop integral is saturated by low-momentum modes. Using dimensional regularization or variants thereof, in addition to the correct long-distance behavior, there is a residual dependence on the short-distance portion of the loop integral, whose "weight" is not under direct control: indeed any of such high-energy contributions can be accounted for by a shift in the coefficients of the effective Lagrangian. After renormalization, an incorrect short-distance effect can still be removed by adjusting parameters. However, those parameters can consequently turn out to be unnaturally large, obscuring the convergence pattern at finite order in the low-energy expansion. Finally, we notice that by construction infrared regularization does enhance the contribution from small internal loop momenta, if m_π is sufficiently small.

2.8.3 Comparison between infrared regularization and the Heavy-Baryon approach

Let us now establish the connection between the infrared singular part I of the integral H and the corresponding result in HBChPT. In the Heavy-Baryon framework, the scalar self-energy diagram of Fig.2.5 is replaced by an infinite string of one-loop graphs, involving an arbitrary number of internal line insertions. This can be understood looking at the relativistic nucleon propagator and expressing the four-momentum as $p^\mu = M_0 v^\mu + r^\mu$,

$$\begin{aligned} &\frac{i}{\not p - M_0 + i\epsilon} = i\,\frac{\not p + M_0}{2M_0\, v\cdot r + r^2 + i\epsilon} \\ &\longrightarrow\ \frac{\not p + M_0}{2M_0}\frac{i}{v\cdot r + i\epsilon}\left[1 + \frac{ir^2}{2M_0}\frac{i}{v\cdot r + i\epsilon} + \left(\frac{ir^2}{2M_0}\frac{i}{v\cdot r + i\epsilon}\right)^2 + \ldots\right] \end{aligned} \tag{2.90}$$

where we assumed r^μ small enough to allow for an expansion in terms of a geometric series. The result is shown in Fig.2.6 and can be interpreted as an infinite series in terms of the Heavy-Baryon propagator and self-energy insertions which have the form of a non-relativistic kinetic energy.

Let us apply the expression (2.90) to the loop integral H in Eq.(2.71) by *first* expanding and *then* performing the summation: the integral over the first term in (2.90) converges

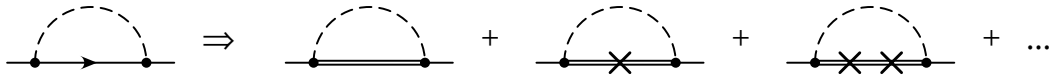

Figure 2.6: Internal line insertions. The double line denotes the Heavy-Baryon propagator $[v \cdot (k-r) + i\epsilon]^{-1}$ and the cross an insertion of $(k-r)^2/(2M_0)$, where k is the pion loop momentum.

for $d < 3$ and gives a contribution of order p^{d-3}, the integral over the second term converges for $d < 2$ and yields a term of order p^{d-2} and so on. For $d < 3 - n$, the region $k = \mathcal{O}(p)$ yields all the terms in the chiral expansion of H, up to and including p^{d-3+n}. In that region of integration it is legitimate to interchange the integration with the expansion. Hence, the infrared singular part of the relativistic one-loop integral represents the (infinite) sum of the corresponding integrals occurring in the Heavy-Baryon series. The difference between the two formulations of Baryon ChPT is in the regular part: in the Heavy-Baryon approach it is zero, order by order.

The advantage of the relativistic scheme is clear: for a general one-loop amplitude it may be very difficult, if not impossible, to obtain a closed expression for the sum of all insertions. Infrared regularization produces a reordering of the Heavy-Baryon series, which can lead to an improvement of the convergence properties [57]. The chiral expansion of an infrared regularized graph of a certain order defined in Eq.(2.69), *starts* with the corresponding contribution at that order in dimensionally regularized HBChPT and includes a whole series of terms suppressed in HBChPT by higher powers of $1/M_0$. This full tower of recoil correction can be recovered in the non-relativistic framework only going to higher orders in the calculation. Moreover, as mentioned before for the triangle-graph, the chiral expansion in HBChPT is known to break down in certain regions of phase space and a coherent Heavy-Baryon representation only results if the insertions required by relativistic kinematics are summed up to all orders. This problem arises from the interchange of the loop integration with the non-relativistic expansion, which is not always legitimate. The infrared regularization method avoids these difficulties *ab initio*, because it does not rely on a non-relativistic expansion of the loop integrals. This fact has a consequence on renormalization within the relativistic approach. In general, infrared singular parts of loop integrals contain ultraviolet divergent pieces that can be absorbed only by higher-order counterterms. This means that in order to get a regularization scale independent result while keeping the full tower of recoil corrections, in general it is not sufficient to tune the coupling constants of those terms in the effective Lagrangian that enter at the order at which one works. This is in marked contrast both with the mesonic sector and the Heavy-Baryon framework. In order to avoid the unphysical scale dependence, Becher and Leutwyler suggest to set the regularization scale $\lambda = M_0$ since the nucleon mass represents a "natural" scale in this context. In our work we do *not* set $\lambda = M_0$, but either introduce higher-order counterterms or numerically study the effects of the residual scale dependence.

2.9 Effective Lagrangian and low-energy constants

In our analysis of the quark mass dependence of the nucleon mass M_N and nucleon axial coupling g_A up to chiral order p^4, the relevant effective Lagrangian has the following form:

$$\mathcal{L}^{\rm eff} = \mathcal{L}^{(1)}_{\pi N} + \mathcal{L}^{(2)}_{\pi N} + \mathcal{L}^{(3)}_{\pi N} + \mathcal{L}^{(4)}_{\pi N} + \mathcal{L}^{(2)}_{\pi} \ . \tag{2.91}$$

Eq.(2.43) gives the expression of the leading pion effective Lagrangian. We use

$$\begin{aligned}
\mathcal{L}^{(1)}_{\pi N} &= \bar\Psi \left(i\gamma_\mu D^\mu - M_0\right)\Psi + \frac{1}{2}\, g_A^0\, \bar\Psi\, \gamma_\mu\gamma_5 u^\mu\, \Psi \\
\mathcal{L}^{(2)}_{\pi N} &= c_1\, {\rm Tr}(\chi_+)\bar\Psi\Psi - \frac{c_2}{4M_0^2}\, {\rm Tr}(u_\mu u_\nu)\, (\bar\Psi D^\mu D^\nu \Psi + {\rm h.c.}) \\
&\quad + \frac{c_3}{2}\, {\rm Tr}(u_\mu u^\mu)\, \bar\Psi\Psi - \frac{c_4}{4}\, \bar\Psi\, \gamma^\mu\gamma^\nu [u_\mu, u_\nu]\, \Psi + ... \\
\mathcal{L}^{(3)}_{\pi N} &= \frac{1}{2} B_9\, \bar\Psi\gamma^\mu\gamma_5\, u_\mu \Psi\, {\rm Tr}(\chi_+) + B_{20}\, \bar\Psi(i\gamma_\mu D^\mu - M_0)\Psi\, {\rm Tr}(\chi_+) \ + \ldots \\
\mathcal{L}^{(4)}_{\pi N} &= e_{38}\, [{\rm Tr}(\chi_+)]^2 \bar\Psi\Psi + \frac{e_{115}}{4}\, {\rm Tr}(\chi_+^2 - \chi_-^2)\bar\Psi\Psi \\
&\quad - \frac{e_{116}}{4}\, \left[{\rm Tr}(\chi_-^2) - ({\rm Tr}(\chi_-))^2 + {\rm Tr}(\chi_+^2) - ({\rm Tr}(\chi_+))^2\right] \bar\Psi\Psi + \ldots \ ,
\end{aligned} \tag{2.92}$$

cf. Eq.(2.65). $\mathcal{L}^{(3)}_{\pi N}$ is written according to Ref. [60]. For $\mathcal{L}^{(4)}_{\pi N}$ we follow Ref. [61]. The B_9-term is needed for renormalization of g_A to leading one-loop level. The counterterm proportional to B_{20} is related to nucleon wave-function renormalization. Such a term can be transformed away through a nucleon field redefinition [62], using the nucleon equation of motion from the lowest order πN Lagrangian [7].

In our study we ignore the effects of isospin breaking and work with degenerate masses for the up and down quarks.

One of our aims is to check whether present lattice calculations are consistent with the quark mass dependence of nucleon observables in ChPT. Crucial in this respect is a precise knowledge of the low-energy constants. In this section we will be concerned with empirical determinations of dimension-two, -three and -four LECs of relevance for our analysis.

Second-order low-energy constants

The constants c_i carry the dimension of an inverse mass and according to "naive" dimensional arguments should be of order $1/\Lambda_\chi$. These low-energy constants have been determined (to some accuracy) from low-energy hadron phenomenology. Consider first c_1. It is related to the so-called pion-nucleon sigma term, defined as the limit for vanishing momentum transfer $t = (p' - p)^2$ of the nucleon scalar form factor

$$\sigma_N(t) = \langle N(p')|m_u\bar u u + m_d \bar d d|N(p)\rangle \ . \tag{2.93}$$

[7] This convention has been adopted in Ref. [61], where, moreover, the coupling corresponding to B_9 is called d_{16}.

We will show in Sec.3.5 that c_1 drives the quark-mass expansion of the pion-nucleon sigma term [43]:

$$\sigma_N \equiv \sigma_N(0) = -4\, c_1 m_\pi^2 - \frac{9 {g_A^0}^2 m_\pi^3}{64\pi {f_\pi^0}^2} + \mathcal{O}(m_\pi^4)\ . \tag{2.94}$$

Neglecting higher-order terms and using as input the empirical values $f_\pi^0 \equiv f_\pi = 92.4\,\mathrm{MeV}$, $m_\pi = 138\,\mathrm{MeV}$ and $g_A^0 \equiv g_A = 1.267$, together with the outcome of the analysis by Gasser, Leutwyler and Sainio in the early 1990's, $\sigma_N(0) = 45 \pm 8\,\mathrm{MeV}$ [63], Eq.(2.94) gives

$$c_1 = -0.88 \pm 0.11\,\mathrm{GeV}^{-1}\ . \tag{2.95}$$

However, the value of the pion-nucleon sigma term is still an open issue. For a detailed discussion we refer the reader to Sec.3.5. Recent studies of πN scattering data suggest larger values for $\sigma_N(0)$ [64], outside one-standard deviation from the central value in Ref. [63]. Just to fix ideas, $\sigma_N(0) = 60\,\mathrm{MeV}$ corresponds to $c_1 = -1.08\,\mathrm{GeV}^{-1}$, according to Eq.(2.94).

The constants c_2, c_3 and c_4, contributing to the $\pi N \to \pi N$ process, have been determined from πN phase-shifts using the expressions for the relevant scattering amplitudes in HBChPT, both at the leading [65] and next-to-leading [66] one-loop level. In these studies three different partial-wave analyses [67–69] have been used as input to pin down LECs by fitting to S- and P-wave phase-shifts in the range of pion momenta in the nucleon rest frame between 40 [66] - 50 [65] and 100 MeV. At leading-one-loop order, $\mathcal{O}(p^3)$, the following intervals for the central values in units of GeV^{-1} have been obtained [65]:

$$\begin{aligned} c_1 &= (-1.53 \cdots - 1.23) \qquad c_2 = (3.13 \ldots 3.28) \\ c_3 &= (-6.20 \cdots - 5.85) \qquad c_4 = (3.47 \ldots 3.51)\ . \end{aligned} \tag{2.96}$$

The spread of values corresponds to the different data sets used as input for the fits. The values of c_1 found in this analysis are sizeably bigger in magnitude than the estimate (2.95) and lead to a very large pion-nucleon σ-term, between 73 and 96.4 MeV, which is difficult to reconcile with phenomenology. However, fixing c_1 corresponding to a σ-term of 47.6 MeV the authors report only somewhat worse χ^2 per degree of freedom for the fits based on the input data in Refs. [67,69]. Furthermore, c_1, c_2, c_3 and c_4 receive significant contributions in going from the tree to the one-loop level. The $\mathcal{O}(p^2)$ best fits based again on [67–69] leads indeed to

$$\begin{aligned} c_1 &= (-1.06 \cdots - 0.77) \qquad c_2 = (2.36 \ldots 2.69) \\ c_3 &= (-4.04 \cdots - 3.78) \qquad c_4 = (2.35 \ldots 2.64) \end{aligned} \tag{2.97}$$

in units of GeV^{-1}. These values are in good agreement with the tree level analysis of elastic πN scattering performed in Ref. [70]. Indeed, taking as input Koch's values for the *threshold* parameters [67], Becher and Leutwyler obtain [70]

$$\begin{aligned} c_1 &= -0.9\, M_N^{-1} \qquad c_2 = 2.5\, M_N^{-1} \\ c_3 &= -4.2\, M_N^{-1} \qquad c_4 = 2.3\, M_N^{-1}\ , \end{aligned} \tag{2.98}$$

while using as input *subthreshold* coefficients in Ref. [71], the same authors get [57]

$$\begin{aligned} c_1 &= -0.6\, M_N^{-1} \qquad & c_2 &= 1.6\, M_N^{-1} \\ c_3 &= -3.4\, M_N^{-1} \qquad & c_4 &= 2.0\, M_N^{-1}\ . \end{aligned} \tag{2.99}$$

The bulk of the discrepancy between the results (2.98) and (2.99) for $c_{2,3,4}$ is argued to be due to the $\Delta\,(1232)$ [70].

An analysis to order p^4 seems to be mandatory in this context. The fits in Ref. [66] at next-to-leading one-loop level, $\mathcal{O}(p^4)$, in HBChPT do not, however, provide further constraints on these LECs. At this order indeed it is impossible to disentangle the effects of the c_i from the contributions of higher-order couplings, without information on the latter from other processes.

In the scattering process $\pi(q) + N(p) \to \pi(q') + N(p')$, the Mandelstam variables are defined as follows:

$$\begin{aligned} s &= (p+q)^2 \ = (p'+q')^2 \\ t &= (q'-q)^2 = (p'-p)^2 \\ u &= (p-q')^2 = (p'-q)^2\ . \end{aligned} \tag{2.100}$$

These kinematic variables are subject to the constraint $s + t + u = 2M_N^2 + 2m_\pi^2$. The chiral expansion is expected to converge best inside the so-called Mandelstam triangle, the region of the Mandelstam plane bounded by the three lines $s = (M_N + m_\pi)^2$, $u = (M_N + m_\pi)^2$ and $t = 4\,m_\pi^2$. In Ref. [72] Büttiker and Meißner reconstruct the πN amplitude inside this unphysical region by means of dispersion relations, taking as input the Karlsruhe partial-wave analysis [67]. The determination of the c_i has then been performed by fitting the $\mathcal{O}(p^3)$ HBChPT result to the extrapolated amplitude. The LEC c_2 is basically an undetermined quantity since its contribution carries a kinematical prefactor which turns out to be very small around the center of the Mandelstam triangle. Büttiker and Meißner perform two fits, around $\nu = t = 0$ (Fit 1) and around $\nu = 0$, $t = 2m_\pi^2/3$ (Fit 2), which represent the "ideal points" in the chiral limit and for *physical* nucleons and pions, respectively. They obtain

$$\begin{aligned} &c_1 = -0.81 \pm 0.15 \quad c_3 = -4.69 \pm 1.34 \quad c_4 = 3.40 \pm 0.04 \quad \text{(Fit1)} \\ &c_1 = -0.80 \pm 0.07 \quad c_3 = -4.70 \pm 0.95 \quad c_4 = 3.40 \pm 0.04 \quad \text{(Fit2)} \end{aligned} \tag{2.101}$$

in units of GeV^{-1}. These results are consistent *within the large error bars* with previous studies at leading one-loop in HBChPT, see Refs. [73, 74]. However, the uncertainties quoted in Ref. [72] must be taken with care, since no error analysis is available for KA84 phase-shifts and elasticities [67]. It is therefore impossible to reliably quantify theoretical errors for the dispersive amplitudes inside the Mandelstam triangle. The authors of Ref. [72] simply assume an error of 10% for the amplitudes of interest.

In Chapter 3 we will show that the precise value of the low-energy coupling c_3 is crucial in the discussion of the quark mass dependence of the nucleon mass, at least for the large

quark masses accessible to present lattice calculations. A relatively large magnitude for c_3 is in agreement with constraints imposed by the isospin-even pion-nucleon scattering amplitude *at threshold*. Consider the on-shell πN forward scattering amplitude for a nucleon at rest. Denoting by b and a the isospin of the outgoing and incoming pion, respectively, the scattering amplitude takes the form

$$T^{ba} = T^+(\omega)\,\delta^{ba} + T^-(\omega)\,i\epsilon^{bac}\tau^c \ . \tag{2.102}$$

Defining q^μ as the pion four-momentum, $\omega = q^0$. At threshold, $\vec{q} = 0$, and the pertinent scattering lengths are defined by

$$a^\pm = \frac{1}{4\pi}\left(1 + \frac{m_\pi}{M_N}\right)^{-1} T^\pm(m_\pi) \ . \tag{2.103}$$

Crossing symmetry implies that $\mathcal{L}^{(2)}_{\pi N}$ contributes to $T^+(\omega)$ only via the terms proportional to $c_{1,\,2,\,3}$. For the isospin-even threshold amplitude the following chiral expansion holds at the leading-one-loop level in HBChPT [52]:

$$T^+(m_\pi) = \frac{2m_\pi^2}{f_\pi^{0\,2}}\left(c_2 + c_3 - 2c_1 - \frac{g_A^{0\,2}}{8M_0}\right) + \frac{3g_A^{0\,2}m_\pi^3}{64\pi f_\pi^{0\,4}} + \mathcal{O}(m_\pi^4) \ . \tag{2.104}$$

The expression for the pion-mass dependence of a^+ at next-to-leading one-loop level, $\mathcal{O}(p^4)$, has been worked out in Ref. [66]. Here the authors checked that keeping the dimension-two LECs fixed to the central values (2.96), the fourth-order contributions to a^+ are small. This is not surprising since with $c_{1,2,3}$ in Eq.(2.96), the right-hand side of Eq.(2.104) is already compatible with the empirical T^+ at threshold. Without further input on the relevant fourth-order couplings, no firmer statement can be made about higher-order corrections in Eq.(2.104).

Measurements of the hadronic energy shift and width of the $1s$ level in the pionic hydrogen and deuterium atoms performed by the PSI group [75] give

$$a^+ = (-0.22 \pm 0.43)\cdot 10^{-2}\, m_\pi^{-1} \ , \tag{2.105}$$

and therefore

$$T^+_{\rm thr} = (-0.045 \pm 0.088)\,{\rm fm} \ . \tag{2.106}$$

For a thorough investigation of pion-deuteron scattering at threshold in the framework of low-energy effective field theories we refer to [76], where the authors establish limits of accuracy for extracting πN scattering lengths from the measured πd scattering lengths. A comparison with existing approaches is also included in Ref. [76]. An updated analysis by the PSI group [77] which gives

$$a^+ = -0.0001^{+0.0009}_{-0.0021}\, m_\pi^{-1} \tag{2.107}$$

and consequently $T^+_{\rm thr} = -0.045 \ldots 0.016\,{\rm fm}$, has been examined in Ref. [78]: here an improved description of the deuteron effects gives, in the isospin limit,

$$a^+ = (-12 \pm 2({\rm statistical}) \pm 8({\rm systematic}))\cdot 10^{-4}\, m_\pi^{-1} \ . \tag{2.108}$$

which corresponds to $T^+_{\rm thr} = -0.041 \cdots - 0.004\,{\rm fm}$.

Assuming that higher-order effects in Eq.(2.104) are negligible, one can regard that relation as a constraint on the combination $c_2+c_3-2c_1$ of dimension-two LECs. However, one should keep in mind that the next-to-leading order term $3g_A^2 m_\pi^3/(64\pi f_\pi^4) = 0.174\,{\rm fm}$ is much larger than the typical accuracy of the most recent estimates of T^+ at threshold. According to the empirical values of $T^+(m_\pi)$, c_1 and c_2 in literature, Eq.(2.104) implies $c_3 \approx -5\,{\rm GeV}^{-1}$.

Such a large value in magnitude for c_3 is not compatible with the analysis of nucleon-nucleon phase-shifts in Ref. [79]. Here Entem and Machleidt evaluate the impact of the complete set of two-pion exhange contributions at two-loop, fourth chiral order, on peripheral partial waves of NN scattering [79]. Their results are not affected by the variations of c_1 and c_2 within the ranges

$$c_1 = -0.81 \pm 0.15\,{\rm GeV}^{-1} \quad c_2 = 3.28 \pm 0.23\,{\rm GeV}^{-1}\ , \tag{2.109}$$

while c_3 is crucial. The input $c_3 = -3.4\,{\rm GeV}^{-1}$ is found to be consistent with empirical peripheral NN phase-shifts, whereas values which substantially differ from that, turn out to be unacceptable in this analysis [79]. The same input value is also successfully used in the study of nucleon-nucleon scattering at next-to-next-to-next-leading order by Epelbaum *et al.* in Ref. [80]. For a comprehensive and updated discussion on c_3 in the context of NN phase shift analyses, we refer to [81].

We will show in Sec.3.3.2 that the discrepancy with the previous estimate $c_3 \approx -5\,{\rm GeV}^{-1}$ can be understood in terms of resonance exchange and $\Delta\,(1232)$ dominance, taking into account the different kinematical regions effectively probed by πN and NN scattering. The latter kind of process provides the better (more indirect though) estimate of c_3 in the chiral, static limit.

Third- and fourth-order couplings

Dimension-three and -four LECs absorb infinities from ultraviolet divergent loop integrals. Each of those couplings decompose as

$$b_i \equiv b_i^r(\lambda) + \frac{\beta_i}{f_\pi^{0\,2}}\,L(\lambda)\ , \tag{2.110}$$

where any infinity in the limit $d \to 4$ is subsumed in

$$L(\lambda) = \frac{\lambda^{d-4}}{16\pi^2}\left\{\frac{1}{d-4} - \frac{1}{2}\left[\ln(4\pi) + \Gamma'(1) + 1\right]\right\}\ . \tag{2.111}$$

Here λ is the regularization scale and $b_i^r(\lambda)$ is the remaining finite piece that has to be fixed from phenomenology.

In the infinite part, β_i denotes the β-function associated with the corresponding counterterm. The renormalized LECs $b_i^r(\lambda)$ are measurable quantities satisfying the renormalization group equations

$$\lambda\,\frac{d}{d\lambda} b_i^r(\lambda) = -\frac{\beta_i}{16\pi^2 f_\pi^{0\,2}}\ . \tag{2.112}$$

In HBChPT for the couplings B_9 and B_{20} in Eq.(2.92), we have [60]

$$\beta_9 = \frac{1}{8} g_A^0 (4 - {g_A^0}^2) \qquad \beta_{20} = -\frac{9 {g_A^0}^2}{16} \; . \tag{2.113}$$

When analyzing the chiral tensors in Eq.(2.92), one notices that B_9 also contributes in inelastic pion-nucleon scattering processes like $\pi N \to \pi\pi N$ [82]. In Ref. [83] this process was analyzed to $\mathcal{O}(p^3)$ in HBChPT. Values for the couplings of interest were obtained by fitting to differential and total cross-sections and setting all the relevant dimension-two and -three LECs already determined in Ref. [65] equal to their central values. A second analysis of $\pi N \to \pi\pi N$ scattering [84] unfortunately does not specify the value for the analogue of the coupling B_9 they used. We quote here the results of the revised study in Ref. [85]. Translating these findings into our conventions we obtain

$$B_9^r(\lambda = m_\pi^{\rm phys}) = (-1.4 \pm 1.2)\,{\rm GeV}^{-2} \; , \quad B_{20}^r(\lambda = m_\pi^{\rm phys}) \equiv 0 \; . \tag{2.114}$$

The central value of B_9 is the average of the central values for the three fits described in Ref. [85]. The error bar is the superposition of the corresponding uncertainties. We note that Refs. [83, 85] follow the convention of Ref. [62] to apply a nucleon field transformation to eliminate all equation-of-motion-dependent terms from the effective Lagrangian: according to Eq.(2.92), $B_{20}^r(\lambda)$ is therefore equal to zero *at the scale of their analysis*, which corresponds to $\lambda = 139.57\,{\rm MeV}$.

Concerning the fourth-order couplings e_{38}, e_{115}, e_{116} in Eq.(2.92), dimensional analysis suggest that they should be of order $1/\Lambda_\chi^3$. No estimate of the numerical value of the couplings $e_{115,\,116}$ is available. The term involving e_{38} gives rise to a quark mass renormalization of c_1; e_{38} enters in a linear combination of LECs whose value cannot be pinned down accurately from fits to phase-shifts, even if input values from $\mathcal{O}(p^3)$ fits are used [66]. Therefore we will treat e_{38}, e_{115}, e_{116} as free parameters in our numerical analysis.

2.10 Including the $\Delta\,(1232)$ as an explicit degree of freedom

In Baryon Chiral Perturbation Theory, pions and nucleons are the dynamical degrees of freedom, *i.e.* the fields appearing in the chiral effective Lagrangian. Resonances are also included implicitly, in the form of local counterterms. However, the $\Delta\,(1232)$ resonance has a special status in two respects. First its mass lies only about 300 MeV above the nucleon mass. Treating it as a heavy state compared to the nucleon is of questionable validity from the phenomenological point of view. It also couples very strongly to the πN system, and contributes substantially through resonance exchange graphs in those channels where such effects are possible [8]. The experimental $\pi^+ p$ and $\pi^- p$ total cross-sections show the dominant role of the $\Delta\,(1232)$ resonance in the P-wave spin-3/2 isospin-3/2

[8] The same holds true for the full decuplet in relation to the baryon octet [48].

channel. Moreover, for $N_c \to \infty$ the nucleon and the delta resonance become degenerate in mass. The special role played by the $\Delta(1232)$ in low-energy nuclear and particle physics can be understood in terms of the quark model: the octet and decuplet baryons have wave-functions differing only in the arrangement of their quark spins. The higher resonances, on the other hand, differ in their orbital wave-functions. A spin-flip does not cost much energy, because the hyperfine spin-spin interaction is rather weak. Thus it is relatively easy for an octet baryon to be converted into a decuplet baryon, whereas it is more difficult to convert it into other excited states.

We have computed the quark mass dependence of M_N and g_A using a chiral effective Lagrangian of pions, nucleons and deltas coupled to external sources. In the two-flavor chiral effective field theory which we describe in this section, the $\Delta(1232)$ occur as a dynamical variable, as an independent baryonic species. Quantum fluctuations also generate graphs that contain delta propagators instead of nucleon propagators. The scheme we adopt allows to *systematically* account for all contributions arising to a given order in the chiral expansion of the various observables. It also enables us to go beyond the extreme non-relativistic limit, described by the Δ-isobar model in the 1970's [86]. The power counting scheme we follow is the so-called Small Scale Expansion (SSE) [87]: the delta-nucleon mass splitting in the chiral limit, $\Delta = M_\Delta^0 - M_0$, is treated as a "small" parameter together with external momenta and pion masses. In the literature the usual collective label for the small scale is ϵ. Δ is a dimensionful parameter of the theory which stays *finite* in the chiral limit. The choice to treat it as a "small" parameter corresponds to the fact that the nucleon spin-isospin polarizability is large and it is therefore easy to excite the nucleon and get the $\Delta(1232)$. For alternative approaches to the inclusion of spin-3/2 particles in chiral effective field theories we refer to [88, 89]. Other counting schemes rely, for example, on the $SU(6)$ limit where the nucleon and delta states are degenerate to leading order or the "heavy resonance" limit, where Δ counts as a parameter of order p^0.

The effective Lagrangian relevant for our study up to leading-one-loop order, can be organized as follows:

$$\mathcal{L}^{\rm eff} = \mathcal{L}_{\pi N}^{(1)} + \mathcal{L}_{\pi N}^{(2)} + \mathcal{L}_{\pi N}^{(3)} + \mathcal{L}_{\pi N\Delta}^{(1)} + \mathcal{L}_{\pi\Delta}^{(1)} + \mathcal{L}_{\pi}^{(2)} + \mathcal{L}_{\Delta} \ . \tag{2.115}$$

Here $\mathcal{L}_\Delta$ denotes the Lagrangian of the free $\Delta(1232)$ field.

The standard form of the relativistic Lagrangian for a free spin-3/2 field $\psi(x)$ is

$$\mathcal{L}_{3/2} = \bar{\psi}^\alpha \, \Lambda_{\alpha\beta}(A) \psi^\beta \tag{2.116}$$

where α, β are Lorentz indices and the matrix Λ depends on a free, unphysical parameter A, with $A \neq -1/2$ [90], see Ref. [87] for notation. This Lagrangian is invariant under the so-called point transformation [91],

$$\begin{aligned} \psi_\alpha(x) &\to \psi_\alpha(x) + a\gamma_\alpha\gamma_\beta\psi^\beta(x) \\ A &\to \frac{A-2a}{1+4a} \ , \end{aligned} \tag{2.117}$$

where a is an arbitrary parameter, except that $a \neq -1/4$. Point-invariance means that an admixture a of "spurious" spin-1/2 components (which are always present in the relativistic spin-3/2 field ψ) can be compensated by a corresponding change in A. Physical quantities are guaranteed to be independent of the choice of the parameter A by the "KOS-theorem" [92].

The matrix $\Lambda_{\alpha\beta}(A)$ can be decomposed as

$$\Lambda_{\alpha\beta}(A) = O^A_{\alpha\mu}\,\bar{\Lambda}^{\mu\nu}\,O^A_{\nu\beta} \tag{2.118}$$

where the tensor

$$O^A_{\alpha\beta} = g_{\alpha\beta} + \frac{2A}{d}\gamma_\alpha\gamma_\beta \tag{2.119}$$

takes care of the point-invariance [87] and d is the number of space-time dimensions.

The first-order $\pi N\Delta$ Lagrangian has the form [87]

$$\mathcal{L}^{(1)}_{\pi N\Delta} = c_A\,\bar{\psi}^i_\alpha O^{\alpha\beta}_A\,\Theta^\gamma_\beta(Z)\,w^i_\gamma\Psi_N + \text{h.c.}\,, \tag{2.120}$$

with

$$\begin{aligned} w^i_\mu &= \mathrm{Tr}(\tau^i u_\mu)/2 \\ \Theta^{\mu\nu} &= g^{\mu\nu} - (Z+1/2)\gamma^\mu\gamma^\nu\,, \end{aligned} \tag{2.121}$$

where τ^i, $i = 1, 2, 3$, denote the Pauli matrices in isospin space and Z is a so-called off-shell parameter, involved in the coupling with the spin-1/2 components. In Eq.(2.120), ψ^α_i denotes the spin-3/2 isospin-3/2 delta field in Rarita-Schwinger notation, see Appendix A for details. The chiral tensors u_β, w^i_β encode couplings to pions and external sources. The low-energy constant c_A represents the leading axial-N-Δ coupling, frequently called $g_{\pi N\Delta}$ in the literature. In Ref. [87] all (non-relativistic) Lagrangians are written in terms of the transformed fields

$$\Psi_\mu(x) = O^A_{\mu\nu}\,\psi(x) \tag{2.122}$$

and are therefore A-independent.

Tang and Ellis showed that in the framework of effective field theories, the off-shell parameters in $\mathcal{L}_{\pi N\Delta}$ and $\mathcal{L}_{\pi\Delta}$ can be absorbed in the infinite number of parameters in the effective Lagrangian [94]. Neglecting them, the term in Eq.(2.115) describing the delta propagation and its coupling to pions and external sources, reads [87]

$$\mathcal{L}^{(1)}_{\pi\Delta} = -\bar{\psi}^i_\alpha O^{\alpha\mu}_A\left\{\left[i\not{D}^{ij} - M^0_\Delta\delta^{ij} + \frac{g_1}{2}\not{u}^{ij}\gamma_5\right]g_{\mu\nu} - \frac{\gamma_\mu\gamma_\lambda}{4}\left(i\not{D}^{ij} - M^0_\Delta\delta^{ij}\right)\gamma^\lambda\gamma_\nu\right\}O^{\nu\beta}_A\psi^j_\beta\,,$$

where

$$\begin{aligned} D^{ij}_\mu &= D_\mu\delta^{ij} - i\epsilon^{ijk}\,\mathrm{Tr}(\tau^k D_\mu) \\ u^{ij}_\mu &= \xi^{ik}_{3/2}\,u_\mu\,\xi^{kj}_{3/2} \end{aligned} \tag{2.123}$$

and $\xi^{ij}_{3/2}$ denotes the isospin-3/2 projector, $\xi^{ij}_{3/2} = \delta^{ij} - \tau^i\tau^j/3$, see Appendix A. Furthermore, g_1 denotes the axial-Δ-Δ coupling in the $SU(2)$ chiral limit, whereas M^0_Δ is the delta mass in the chiral limit.

Including explicit $\Delta\,(1232)$ degrees of freedom, in the Small Scale Expansion counting scheme, the $\mathcal{O}(\epsilon^3)$ πN Lagrangian contain these additional terms allowed by symmetry:

$$\mathcal{L}^{(3)}_{\pi N} = \bar{\Psi}\left[B_{23}\,\Delta\mathrm{Tr}(\chi_+) + \Delta^2\,B_{30}\,(i\gamma_\mu D^\mu - M_0) + \Delta^2\,B_{31}\,\frac{1}{2}\gamma_\mu\gamma_5 u^\mu + B_{32}\,\Delta^3\right]\Psi + \ldots \tag{2.124}$$

Here we follow the nomenclature of Ref. [95] where a complete set of counterterms is listed, appropriate for renormalization of both leading-one-loop HBChPT and non-relativistic SSE calculations. The generalization to the relativistic framework is straightforward. We notice that $B_{23,30,31,32}$ are identically zero in absence of explicit $\Delta\,(1232)$ degrees of freedom, but are required for a leading-one-loop calculation in the Small Scale Expansion. All the B_i have a finite, regularization scale λ dependent part $B^r_i(\lambda)$ as well as an infinite part as $d \to 4$, cf. Eq.(2.110).

The terms in Eq.(2.124) make sure that the chiral limit values for M_N and g_A are the same in HBChPT and SSE. They guarantee the decoupling of the delta. If the $\Delta\,(1232)$ is regarded to be too heavy to propagate, its effects are encoded into couplings between the light fields, pion and nucleons. The decoupling theorem [96, 97] describes how the heavy particles must enter into the low-energy theory. According to that theorem, $\Delta\,(1232)$ effects are characterized by inverse powers of the delta mass and renormalize coupling constants. Inverse powers of heavy-particle mass arise from propagators involving virtual exchange of this particle. This result is in accord with physical intuition. If the heavy-particle mass becomes infinite, one would expect that the direct influence of the particle disappears. Any shift in the couplings is not directly observable since they have to be determined from experiment.

The decoupling of the delta represents an important constraint and a consistency check of the theory: in the limit of an infinitely heavy delta, the SSE result should reproduce that in the scheme with πN degrees of freedom, at any given chiral order.

2.10.1 The $\Delta\,(1232)$ propagator

Choosing $A = -1$, the propagator for a spin-3/2 isospin-3/2 particle in the Rarita-Schwinger formalism has the general form:

$$S^\Delta_{\mu\nu}(p) = S^{ij}_{\mu\nu}(p)\,\xi^{ij}_{3/2} \tag{2.125}$$

where

$$S^{ij}_{\mu\nu}(p) = -i\,\frac{\not{p} + M^0_\Delta}{p^2 - (M^0_\Delta)^2 + i\epsilon}\left[g_{\mu\nu} - \frac{1}{d-1}\,\gamma_\mu\gamma_\nu - \frac{(d-2)\,p_\mu p_\nu}{(d-1)\,(M^0_\Delta)^2} + \frac{p_\mu\gamma_\nu - p_\nu\gamma_\mu}{(d-1)\,M^0_\Delta}\right]. \tag{2.126}$$

The Dirac tensor $S_{\mu\nu}$ can be written as a linear combination of spin-3/2 and spin-1/2 projection operators $P^{3/2}_{\mu\nu}$, $P^{1/2}_{\mu\nu}$, see Appendix A:

$$-i\,S^{\Delta}_{\mu\nu}(p) = -\frac{\not{p}+m^0_\Delta}{p^2-(M^0_\Delta)^2+i\epsilon}\,P^{3/2}_{\mu\nu} - \frac{1}{\sqrt{d-1}\,M^0_\Delta}\left(\left(P^{1/2}_{12}\right)_{\mu\nu}+\left(P^{1/2}_{21}\right)_{\mu\nu}\right) + \frac{d-2}{(d-1)\,(M^0_\Delta)^2}\,(\not{p}+M^0_\Delta)\left(P^{1/2}_{22}\right)_{\mu\nu}\,. \tag{2.127}$$

Only the spin-3/2 components are associated with a propagation, whereas the (spurious) spin-1/2 components correspond to local contact operators [93, 98]. Since the chiral effective field theory for a coupled pion-nucleon-delta system contains the most general set of local contact operators allowed by chiral symmetry, we can just take into account the propagation of the spin-3/2 degrees of freedom since the effects of the spurious off-shell spin-1/2 components are completely absorbed by the counterterms of the theory. In the low-energy theory also the field theoretical deficiencies of the Rarita-Schwinger approach discussed in Ref. [99], can be accounted for via counterterms. Bernard, Hemmert and Meißner have proposed the decomposition [93]

$$S^{\Delta}_{\mu\nu} = -i\,\frac{\not{p}+M^0_\Delta}{p^2-(M^0_\Delta)^2+i\epsilon}\,\frac{p^2}{(M^0_\Delta)^2}\,P^{3/2}_{\mu\nu} + i\,R_{\mu\nu}\,, \tag{2.128}$$

where

$$R_{\mu\nu} = \frac{\not{p}+M^0_\Delta}{(M^0_\Delta)^2}\left[g_{\mu\nu}-\frac{1}{d-1}\,\gamma_\mu\gamma_\nu\right] + \frac{1}{(d-1)\,(M^0_\Delta)^2}\,(p_\mu\gamma_\nu-\gamma_\mu p_\nu) \tag{2.129}$$

is not connected with the spin-3/2 propagation, is local and only generates contributions which can be subsumed in counterterms. The propagator [93]

$$G^{ij}_{\mu\nu}(p) = -i\,\frac{\not{p}+M^0_\Delta}{p^2-(M^0_\Delta)^2+i\epsilon}\,\frac{p^2}{(M^0_\Delta)^2}\,P^{3/2}_{\mu\nu}\,\xi^{ij}_{3/2}\,. \tag{2.130}$$

is therefore sufficient to incorporate the physics of the delta in the low-energy theory. In our analysis, we work with the propagator in Eq.(2.130). This form facilitates the comparison with the non-relativistic formulation of SSE where only the spin-3/2 components propagate [87, 100].

2.10.2 Low-energy parameters in the framework with explicit $\Delta\,(1232)$

In view of investigating the quark mass dependence of M_N and g_A in SSE to one-loop order, we summarize what is known about the low-energy parameters of interest in the effective Lagrangian with explicit $\Delta\,(1232)$ degrees of freedom.

The delta-nucleon mass difference

Lattice data show an almost parallel running of M_N and M_Δ with m_π [101]. Although present simulations are performed with relatively large quark masses, it is reasonable to assume that the delta-nucleon mass splitting at the *physical* pion mass is a good approximation of the low-energy parameter Δ.

The position of the $\Delta(1232)$ resonance pole in the (complex) total center-of-mass energy plane has been determined from the magnetic dipole $M_{1+}^{(3/2)}$ and electric quadrupole $E_{1+}^{(3/2)}$ amplitudes of pion photoproduction: $M_\Delta - i\Gamma_\Delta/2 = (1211 - i\,50)\,\mathrm{MeV}$, according to Ref. [102]. According to the Particle Data Group average [13], the $\Delta(1232)$ pole position in the complex energy plane leads to $M_\Delta = 1210\,\mathrm{MeV}$ and $\Gamma_\Delta = 100\,\mathrm{MeV}$. According to that, $M_\Delta - M_N = 271.1\,\mathrm{MeV}$.

If we look at the 90^0 πN phase-shift in the spin-3/2 isospin-3/2 channel, the Particle Data Group average gives $M_\Delta = 1232\,\mathrm{MeV}$ [13]. In this case, $M_\Delta - M_N = 293\,\mathrm{MeV}$.

A recent study indicates that the delta-nucleon mass splitting becomes slightly larger in the chiral limit: in Ref. [93] the quark mass dependences of the nucleon and the delta mass are analyzed in the framework of manifestly covariant SSE at next-to-leading one-loop accuracy, $\mathcal{O}(\epsilon^4)$. The comparison of the relevant formulae with lattice data from Ref. [101] suggests $\Delta \approx 330\,\mathrm{MeV}$.

The couplings c_A and g_1

In our numerical analysis we used for c_A estimates at the physical value of m_π since nothing is known about the quark mass dependence of this coupling. The expression for the strong $\Delta \to N\,\pi$ decay width Γ in the relativistic framework can be deduced from the tree graphs of $\mathcal{L}^{(1)}_{\pi N\Delta}$. In the rest frame of the decaying delta it reads

$$\Gamma_{\Delta\to N\pi} = \frac{c_A^2\, q_\Delta^3}{24\pi f_\pi^{0\,2} M_\Delta^{0\,2}} \left[(M_\Delta^0 + M_0)^2 - m_\pi^2\right] = \frac{c_A^2}{6\pi f_\pi^2}(E_\pi^2 - m_\pi^2)^{3/2}\, \frac{M_\Delta^0 + M_0 - E_\pi}{2\,M_\Delta^0}\ , \tag{2.131}$$

where q_Δ is the momentum of the decay products for the decay at rest and

$$E_\pi = \frac{M_\Delta^{0\,2} - M_0^2 + m_\pi^2}{2\,M_\Delta^0}\ . \tag{2.132}$$

Using in Eq.(2.131) the empirical Breit-Wigner width of the $\Delta(1232)$, $\Gamma_{\Delta\to N\pi} = 120 \pm 5\,\mathrm{MeV}$ [13], together with $M_\Delta = 1232\,\mathrm{MeV}$ and physical values of f_π, m_π and M_N, we get c_A between 1.4 and 1.5. If we look at the position of the delta pole in the complex W-plane we have $\Gamma_{\Delta\to N\pi} \approx 100\,\mathrm{MeV}$, which corresponds to $c_A \approx 1.5$ for $M_\Delta = 1210\,\mathrm{MeV}$. In our numerical study we set the estimate corresponding to Eq.(2.131) as $c_A = 1.5$, a value somewhat larger than the spin-flavor $SU(4)$ relation

$$c_A = 3/(2\sqrt{2})\, g_A = 1.34\ . \tag{2.133}$$

The calculation in the non-relativistic framework, at leading order in HBChPT, gives [103]

$$\Gamma^{\rm HB}_{\Delta\to N\pi} = \frac{c_A^2}{6\pi f_\pi^2}(\Delta^2 - m_\pi^2)^{3/2}\ . \tag{2.134}$$

Here $\Gamma_{\Delta\to N\pi} = 120 \pm 5\,\text{MeV}$ gives $c_A \approx 1$, while for $\Gamma_{\Delta\to N\pi} = 100\,\text{MeV}$, $c_A = 1.125$.

Little is known about the value of the axial-Δ-Δ coupling g_1:

- using $SU(4)$ spin-flavor quark symmetry, one finds

$$g_1 = \frac{9}{5}\,g_A\ . \tag{2.135}$$

  The non-relativistic $SU(4)$ quark model (where no spin-dependent interaction between quarks is considered) predicts $g_A = 5/3$ and consequently $g_1 = 3$. According to Eq.(2.135), if $g_A = 1.267$ then $g_1 = 2.28$.

- A special quartet scheme of chiral symmetry realization for even- and odd-parity baryon resonances was proposed in Ref. [105]. According to such a scheme the authors found that the parity non-changing couplings such as $\pi\Delta_\pm\Delta_\pm$ are forbidden at leading order.

- Fettes and Meißner analyzed elastic πN scattering to $\mathcal{O}(\epsilon^3)$ in the framework of non-relativistic Small Scale Expansion [104]. By fitting to S- and P-wave amplitudes for different sets of available pion-nucleon phase-shifts in the physical region at low energies, the authors could not determine reliably g_1.

Chapter 3

Quark mass dependence of the nucleon mass

We have studied the nucleon mass M_N in the framework of the effective low-energy theory of QCD in the one-nucleon sector and for the two-flavor case. In particular, we have analyzed the functional dependence of this nucleon observable on the explicit chiral symmetry breaking parameter m_q, comparing two versions of $SU(2)$ Baryon Chiral Effective Field Theory (BChEFT): with and without *explicit* $\Delta\,(1232)$ degrees of freedom. The main features of the formalism have been described in Chapter 2. Here we present the relevant formulae both at leading- and next-to-leading one-loop level. We then discuss the outcome of a numerical analysis performed using as input a selected set of the most recent full-QCD lattice data. The basic results appear in two papers, Refs. [106] and [107].

3.1 The nucleon mass in QCD and in ChEFT

Consider the matrix element of the QCD energy-momentum tensor $\Theta^{\mu\nu}$ at zero momentum transfer between one-nucleon states $|N_s(\vec{p})\rangle$. Lorentz invariance requires

$$\langle N_s(\vec{p})\,|\Theta^{\mu\nu}|\,N_s(\vec{p})\rangle = a\,p^\mu p^\nu + b\,g^{\mu\nu} \tag{3.1}$$

where a and b are scalar constants. Using the normalization

$$\langle N_{s'}(\vec{p}\,')\,|\,N_s(\vec{p})\rangle = \frac{E_{\vec{p}}}{M_N}\,\delta_{s's}\,(2\pi)^3\,\delta^3(\vec{p}\,'-\vec{p})\ ,$$

where $E_{\vec{p}} = \sqrt{\vec{p}^{\,2}+M_N^2}$ and $s, s' = \pm 1/2$ are the spin projections, the Hamiltonian

$$H = \int d^3\vec{x}\,\Theta^{00}(0,\vec{x}\,) \tag{3.2}$$

has the following matrix element in the one-nucleon state:

$$\langle N_s(\vec{p})\,|H|\,N_s(\vec{p})\rangle = \frac{E_{\vec{p}}^{\,2}}{M_N}(2\pi)^3\,\delta^3(\vec{0})\ . \tag{3.3}$$

Comparing Eq.(3.3) with Eq.(3.1), we get

$$\langle N_s(\vec{p})\,|\Theta^{\mu\nu}|\,N_s(\vec{p})\rangle = p^\mu p^\nu/M_N\ . \tag{3.4}$$

The nucleon mass is therefore given by the forward matrix element of the trace of the symmetric QCD energy-momentum tensor in the one-nucleon state:

$$M_N = \langle N_s(\vec{p}) \, | \Theta^\mu_\mu | \, N_s(\vec{p}) \rangle \ . \tag{3.5}$$

If the quark masses were set equal to zero, the Lagrangian of QCD would exhibit scale invariance *at the classical level*. This would lead to a traceless energy-momentum tensor and would imply zero nucleon mass. However, *at the quantum level* one gets

$$\Theta^\mu_\mu = \frac{\beta(g)}{2g} G^a_{\mu\nu} G^{\mu\nu}_a + (1+\gamma_m)\, \bar{q} m q \ , \tag{3.6}$$

as far as matrix elements between physical states are concerned [108]. Here g is the $SU(3)$ gauge coupling of QCD, $G^{\mu\nu}_a$ the gluon field strength tensor and $\beta(g)$ is the QCD β-function; m denotes the quark mass matrix in flavor space and γ_m is the anomalous dimension of the mass operator $\mathcal{O}_m = \bar{q} m q$, cf. Eq.(2.9) and Ref. [18],

$$\gamma_m = \mu \, \frac{d \ln Z_m}{d\mu} \tag{3.7}$$

where Z_m is the renormalization factor for the quark masses and μ is the renormalization scale. Renormalization introduces a scale parameter and the quantum corrections destroy scale invariance. The trace of the energy-momentum tensor, which is equal to the divergence of the scale current, shows an anomaly.

Neglecting consistently γ_m and higher order terms in $\beta(g)$ in Eq.(3.6), Eq.(3.1) implies

$$M_N = \langle N_s(\vec{p}) \, | \, \frac{\alpha_s}{8\pi} \left(\frac{2}{3} N_f - 11 \right) G^a_{\mu\nu} G^{\mu\nu}_a + m_u \, \bar{u}u + m_d \, \bar{d}d + m_s \, \bar{s}s + \ldots \, | \, N_s(\vec{p}) \rangle \tag{3.8}$$

where N_f is the number of quark flavors with masses much less than the typical energy under consideration. The dots indicate contributions from quarks heavier than the strange. This fundamental expression emphasizes the important role played by gluons in building up the nucleon mass. Note that $G^a_{\mu\nu} G^{\mu\nu}_a = \vec{B}^2 - \vec{E}^2$, in terms of the color magnetic and electric fields. As already mentioned, the matrix element

$$\langle N_s(\vec{p}) \, | m_u \bar{u}u + m_d \bar{d}d | \, N_s(\vec{p}) \rangle \tag{3.9}$$

is the so-called pion-nucleon sigma-term σ_N, the nucleon scalar form factor at zero momentum transfer. Although its precise empirical value is currently still under debate and an even larger uncertainty affects the strange-quark mass term (see Sec.3.5), the gluon trace is by far the dominant contribution on the right-hand side of Eq.(3.8).

According to Eq.(3.9), the physical nucleon mass has the following decomposition:

$$M_N = M_0 + \sigma_N$$

where M_0 is the nucleon mass in the $SU(2)$ chiral limit, *i.e.* for vanishing $u-$ and $d-$quark masses.

In a chiral effective field theory, formulated in terms of the asymptotically observed fields, the physical (renormalized) nucleon mass is defined by the position of the pole in the two-point function of the nucleon Dirac field $\Psi(x)$:

$$\int \mathrm{d}^4x\, e^{ip\cdot x}\langle 0|\, T\{\Psi(x)\bar{\Psi}(0)\}\,|0\rangle = \frac{i}{\not{p} - M_0 - \Sigma(\not{p})}\,, \tag{3.10}$$

where $\Sigma(\not{p})$, the nucleon self-energy, is the one-particle irreducible contribution to the full propagator $S_F(p)$. The position of the pole,

$$M_N = M_0 + \delta M\ , \tag{3.11}$$

where δM is the nucleon mass-shift, is given by the solution of the equation

$$[\not{p} - M_0 - \Sigma(\not{p})]|_{\not{p}=M_N} = 0\ . \tag{3.12}$$

Expanding the nucleon self-energy around M_N,

$$\Sigma(\not{p}) = \Sigma(\not{p})|_{\not{p}=M_N} + (\not{p} - M_N)\,\Sigma'(\not{p})|_{\not{p}=M_N} + \mathcal{O}(\not{p} - M_N)^2\ , \tag{3.13}$$

using Eq.(3.12) we have

$$\not{p} - M_0 - \Sigma(\not{p}) = (\not{p} - M_N)\left[1 - \Sigma'(\not{p})|_{\not{p}=M_N}\right] + \mathcal{O}(\not{p} - M_N)^2\ . \tag{3.14}$$

We can express the full nucleon propagator as

$$S_F(p) = \frac{i\,Z_N}{\not{p} - M_N - \Sigma_R(\not{p})} \tag{3.15}$$

where

$$\Sigma_R(\not{p})|_{\not{p}=M_N} = 0 \quad \text{and} \quad \frac{\partial}{\partial\,\not{p}}\,\Sigma_R(\not{p})|_{\not{p}=M_N} = 0\ . \tag{3.16}$$

The renormalization factor Z_N is evaluated as the residue of the full propagator $S_F(p)$ at the pole $\not{p} = M_N$:

$$Z_N^{-1} = 1 - \Sigma'(\not{p})|_{\not{p}=M_N}\ . \tag{3.17}$$

3.2 Analytic results

In our study we neglect isospin breaking effects and work with equal $u-$and $d-$ quark masses, $m_{u,d} = m_q$. Furthermore, we translate the functional dependence on the (light) m_q into a pion-mass dependence according to the Gell-Mann – Oakes – Renner relation, consistently with our power counting scheme (see Sec.2.6):

$$m_\pi^2 = 2Bm_q + \mathcal{O}(m_q^2, m_q^2\,\ln m_q/\lambda)\ . \tag{3.18}$$

Let us concentrate first on the ChEFT scheme with nucleons and pions as the only explicit degrees of freedom.

$$\mathcal{L} = \mathcal{L}_{\pi N}^{(1)} + \mathcal{L}_{\pi N}^{(2)} + \mathcal{L}_{\pi N}^{(4)} + \mathcal{L}_{\pi}^{(2)} \tag{3.19}$$

is the effective Lagrangian needed to work out the quark mass dependence of M_N up to and including chiral order p^4, see Sec.2.9. The vertices relevant for our calculations are collected in Appendix B.

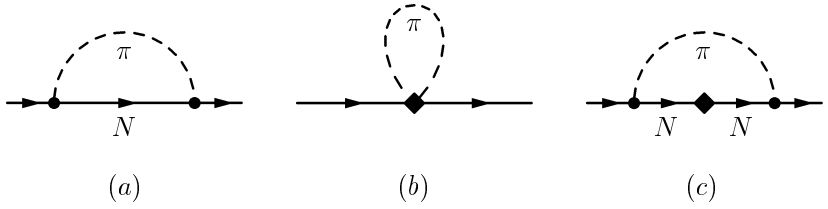

Figure 3.1: One-particle-irreducible one-loop graphs of NLO (a) and NNLO (b, c) contributing to the nucleon self-energy in Baryon ChPT (without explicit $\Delta(1232)$ degrees of freedom). The solid dot denotes a vertex from $\mathcal{L}^{(1)}_{\pi N}$, the diamond a vertex from $\mathcal{L}^{(2)}_{\pi N}$.

3.2.1 $\mathcal{O}(p^3)$ results

The leading-order (LO) term in the nucleon mass-shift comes from the explicit chiral symmetry breaking piece in $\mathcal{L}^{(2)}_{\pi N}$, involving c_1. The next-to-leading order (NLO) contribution is represented by the diagram (a) of Fig.3.1, with the πN vertex appearing in $\mathcal{L}^{(1)}_{\pi N}$.

We have evaluated all the relevant one-loop integrals using infrared regularization, in order to match chiral power counting and manifest Lorentz invariance. In our approach we keep the whole tower of recoil corrections attached to any infrared regularized one-loop diagram with baryon propagators. It has been shown that this can improve the convergence properties in the low-energy region [57]. Besides, it permits a more efficient numerical analysis of the m_π-dependence for the relatively large pion masses presently accessible to fully dynamical lattice QCD simulations.

In terms of the loop functions in Appendix C, graph (a) gives [57]

$$\Sigma_a(\not{p}) = \frac{3{g_A^0}^2}{4f_\pi^{0\,2}}\,(M_0+\not{p})\left[m_\pi^2\, I_N(p^2,m_\pi^2) + (M_0-\not{p})\not{p}\, I_N^{(1)}(p^2,m_\pi^2)\right]\ , \tag{3.20}$$

which develops an ultraviolet divergence proportional to m_π^4. In order to have a finite, regularization-scale-independent result, we include the contact term $-4\,e_1 m_\pi^4 \bar{\Psi}\Psi$ generated by $\mathcal{L}^{(4)}_{\pi N}$. In the notation of Eq.(2.92), *at fourth chiral order*, $e_1 = -(4e_{38} + e_{115}/2 + e_{116}/2)$.

The expression for the m_π-dependence of M_N at NLO reads:

$$\begin{aligned} M_N = M_0 - 4c_1 m_\pi^2 + \left[4\,e_1^r(\lambda) + \frac{3{g_A^0}^2}{64\pi^2 f_\pi^{0\,2} M_0}\left(1 - 2\ln\frac{m_\pi}{\lambda}\right)\right] m_\pi^4 \\ - \frac{3{g_A^0}^2}{16\pi^2 f_\pi^{0\,2}}\, m_\pi^3 \sqrt{1-\frac{m_\pi^2}{4M_0^2}}\,\arccos\left(-\frac{m_\pi}{2M_0}\right)\ , \end{aligned} \tag{3.21}$$

where $e_1^r(\lambda)$ is defined as the finite (regularization scale λ dependent) part of e_1,

$$e_1 = e_1^r(\lambda) + \frac{3\,{g_A^0}^2}{8 f_\pi^{0\,2}\, M_0}\, L(\lambda)\ . \tag{3.22}$$

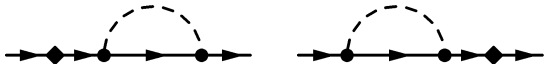

Figure 3.2: One-particle-reducible one-loop graphs contributing to $M_N(m_\pi)$ at chiral order p^4. The diamond denotes the quark-mass insertion involving the coupling c_1 in $\mathcal{L}^{(2)}_{\pi N}$.

Any ultraviolet divergences are subsumed in $L(\lambda)$, Eq.(C.2). According to Eq.(3.22), $e_1^r(\lambda)$ scales in such a way that the overall right-hand side of Eq.(3.21) is scale independent.

For further discussion we show the expansion of Eq.(3.21) in powers of the pion mass:

$$M_N = M_0 - 4c_1 m_\pi^2 - \frac{3{g_A^0}^2}{32\pi f_\pi^{0\,2}} m_\pi^3 + \left[4\, e_1^r(\lambda) - \frac{3{g_A^0}^2}{64\pi^2 f_\pi^{0\,2} M_0} (1 + 2\ln\frac{m_\pi}{\lambda}) \right] m_\pi^4 + \frac{3{g_A^0}^2}{256\pi f_\pi^{0\,2} M_0^2} m_\pi^5 + \mathcal{O}(m_\pi^6). \tag{3.23}$$

The sum of the first three terms coincides with the leading-one-loop expression for M_N in Heavy Baryon Chiral Perturbation Theory (HBChPT) [52]. The third piece is the leading non-analytic term in the quark-mass expansion of M_N. The counterterm that controls the contributions at m_π^4 encodes short-distance dynamics, including effects of the $\Delta\,(1232)$ and possibly other resonance excitations of the nucleon. We notice that the parameters c_1 and $e_1^r(\lambda)$ absorb the leading correction to the Gell-Mann – Oakes – Renner relation (2.50), corresponding to the choice of expressing the quark mass dependence of M_N in terms of $m_\pi(m_q)$ at next-to-leading order.

3.2.2 $\mathcal{O}(p^4)$ analysis

Both tree and one-loop diagrams contribute at next-to-next-to-leading order (NNLO). The latter are labelled by (b) and (c) in Fig.3.1 and include vertices generated by $\mathcal{L}^{(2)}_{\pi N}$. The $\mathcal{O}(p^4)$ one-particle reducible one-loop diagrams are drawn in Fig.3.2.

In d space-time dimensions, diagram (b) gives [57]

$$\Sigma_b = \frac{3m_\pi^2\,\Delta_\pi}{f_\pi^{0\,2}} \left(2c_1 - \frac{p^2}{M_0^2 d}\, c_2 - c_3 \right) , \tag{3.24}$$

where Δ_π is the tadpole integral in Appendix C. Graph (c), together with those in Fig.3.2, can be calculated from Eq.(3.20). Indeed, for small m_π,

$$\frac{i}{\not p - M_0 - 4\,c_1 m_\pi^2} = \frac{i}{\not p - M_0} + \frac{i}{\not p - M_0}\,(i\,4\,c_1 m_\pi^2)\,\frac{i}{\not p - M_0} + \dots \ . \tag{3.25}$$

We can therefore compute the c_1-insertions by a simple shift of the pole of the nucleon propagator, from the "bare" nucleon mass to its renormalized value at second chiral order

$$M_N \to M_0 - 4\,c_1 m_\pi^2 \ . \tag{3.26}$$

Afterwards, in order to avoid higher-order terms, we have to expand the result in powers of c_1 and retain the term linear in c_1.

Finally, at NNLO we have

$$\begin{aligned} M_N =& \frac{1}{128\,\pi^2\,f_\pi^{0\,2}\,M_0^3\,\sqrt{4-m_\pi^2/M_0^2}}\Bigg\{12\,\arccos\left(\frac{-m_\pi}{2\,M_0}\right)\,g_A^{0\,2}\,m_\pi^3\,(4\,c_1\,m_\pi^4+m_\pi^2\,M_0-4\,{M_0}^3) \\ &+M_0\,\sqrt{4-\frac{m_\pi^2}{{M_0}^2}}\,\Bigg[-24\,c_1\,g_A^2\,m_\pi^6+6\,g_A^2\,m_\pi^4\,M_0-512\,c_1\,\pi^2 f_\pi^{0\,2}\,M_0^2\,m_\pi^2 \\ &+3\,c_2\,m_\pi^4\,M_0^2+128\,\pi^2 f_\pi^{0\,2}\,M_0^3-12\,m_\pi^4\,\ln\frac{m_\pi}{\lambda}\,\Bigg(M_0^2(-8\,c_1+c_2+4\,c_3) \\ &+g_A^{0\,2}\,(4\,c_1\,m_\pi^2+M_0)\Bigg)\Bigg]\Bigg\}+4\,e_1^r(\lambda)\,m_\pi^4+64\,e_2^r(\lambda)\,m_\pi^6\,. \end{aligned} \tag{3.27}$$

Here $e_2^r(\lambda)$ is the finite part of the sixth-order coupling needed to compensate of the scale dependence at this level,

$$e_2 = e_2^r(\lambda)+\frac{6\,c_1 g_A^{0\,2}}{f_\pi^{0\,2}\,M_0^2}\,L(\lambda)\,.$$

The factor 64 in front of it reminds that e_2 is the coupling which should be of "natural size" according to "naive" dimensional arguments [28], see Sec.2.5. Indeed

$$\mathcal{L}_{\pi N}^{(6)} = \bar\Psi\,\epsilon_2\,[\mathrm{Tr}(\chi_+)]^3\Psi+\cdots = 64\,\epsilon_2\,m_\pi^6+\cdots \tag{3.28}$$

for which we expect that ϵ_2 is of order $1/\Lambda_\chi^5$.

In Eq.(3.27),

$$e_1 = e_1^r(\lambda)+\frac{3L(\lambda)}{8f_\pi^{0\,2}}\left(\frac{g_A^{0\,2}}{M_0}-8c_1+c_2+4c_3\right).$$

The β-function describing the λ-dependence of the renormalized effective coupling e_1^r has changed from $\mathcal{O}(p^3)$ to $\mathcal{O}(p^4)$. However, infrared regularization has the property that the fourth-order β-function in question will not be affected by higher orders.

Eq.(3.27) contains too many parameters to be useful for our numerical analysis, based on a low-statistics set of input lattice data. Hence we have expanded the expression (3.27) around $m_\pi = 0$ and truncated up to and including $\mathcal{O}(m_\pi^5)$:

$$\begin{aligned} M_N =& M_0-4c_1m_\pi^2-\frac{3g_A^{0\,2}}{32\pi f_\pi^{0\,2}}m_\pi^3 \\ &+\left[4\,e_1^r(\lambda)-\frac{3}{64\pi^2 f_\pi^{0\,2}}\left(\frac{g_A^{0\,2}}{M_0}-\frac{c_2}{2}\right)-\frac{3}{32\pi^2 f_\pi^{0\,2}}\left(\frac{g_A^{0\,2}}{M_0}-8c_1+c_2+4c_3\right)\ln\frac{m_\pi}{\lambda}\right]m_\pi^4 \\ &+\frac{3g_A^{0\,2}}{256\pi f_\pi^{0\,2}M_0^2}m_\pi^5+\mathcal{O}(m_\pi^6)\,. \end{aligned} \tag{3.29}$$

The terms up to m_π^4 have already been discussed in [43]: their sum represent the $\mathcal{O}(p^4)$ Heavy Baryon result. Up to m_π^5 no counterterm other than the combination denoted by

e_1 is required to achieve scale independence. We will argue numerically that the Eq.(3.29) does represent a good approximation of the full expression.

The relativistic result truncated at m_π^5, Eq.(3.29), has the same structure as the expansion of the nucleon mass in HBChPT to $\mathcal{O}(p^5)$, since there are no genuine two-loop graph contributions at this order in the chiral expansion [109]. More specifically, in the evaluation of the nucleon mass-shift in the Heavy-Baryon framework, the sum of the terms proportional to m_π^3 and m_π^5 gives [109]

$$\delta m^{(3)} + \delta m^{(5)} = -\frac{3 g_{\pi NN}^2}{32\pi M_N^2} m_\pi^3 \left(1 - \frac{m_\pi^2}{8 M_N^2}\right) \ , \tag{3.30}$$

where

$$\frac{g_{\pi NN}}{M_N} = \frac{g_A^0}{f_\pi^0}\left[1 - m^2\left(\frac{{g_A^0}^2}{16\,\pi^2 {f_\pi^0}^2} + \frac{\bar{l}_4}{{f_\pi^0}^2} - \frac{4\bar{d}_{16} - 2\bar{d}_{18}}{g_A^0}\right)\right] \tag{3.31}$$

and

$$m_\pi^2 = m^2\left(1 + \frac{2\,\bar{l}_3 m^2}{{f_\pi^0}^2}\right) \tag{3.32}$$

with $m^2 = 2Bm_q$; $\bar{d}_i$, $\bar{l}_i$ are suitable LECs, defined to absorb $\ln(m/\lambda)$-terms [65]. In Eq.(3.30) the fifth-order contribution to M_N in the non-relativistic framework is expressed through the quark mass dependence of quantities which enter at order m_π^3: the m_π^5 term represents just a $1/M_N^2$ recoil correction of the $\mathcal{O}(m_\pi^3)$ result. In the relativistic approach, the running of g_A and f_π gives rise to contributions starting at $\mathcal{O}(p^5)$ with the term proportional to m_π^5 in Eq.(3.30).

3.2.3 Inclusion of $\Delta\,(1232)$: $\mathcal{O}(\epsilon^3)$ results

An EFT with a Lagrangian involving only pions and nucleons still feels the effects of heavy fields - like the $\Delta\,(1232)$ - through virtual contributions encoded in various couplings between the light fields. When integrating out the heavy fields from the Lagrangian, effects of particles that "decouple" are characterized by inverse powers of their mass and contribute to coupling constant renormalization. Since we are working at limited perturbative order, "freezing" the $\Delta\,(1232)$ and relegating its effects to higher order terms could reduce the degree of accuracy of the approximation and the range of applicability of the formulae worked out in the standard BChPT approach. The inclusion of the $\Delta\,(1232)$ as an *explicit* degree of freedom can represent more effectively the physics responsible of the low-energy behaviour of the observable under study. Furthermore, such extension of standard BChPT represents a way to explore the influence of higher-order effects in the scheme restricted to πN degrees of freedom only.

We have described the manifestly Lorentz invariant formulation of the so-called Small Scale Expansion in Sec.2.10: the $\Delta\,(1232)$ contributions are treated in a systematic expansion in ϵ, which collectively denotes soft external momenta, pion mass and delta-nucleon mass difference in the $SU(2)$ chiral limit. We have worked out the expression

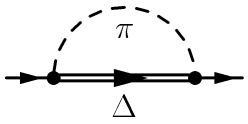

Figure 3.3: Leading-one-loop diagram contributing to the nucleon self-energy with an intermediate $\Delta\,(1232)$. The vertex comes from $\mathcal{L}^{(1)}_{\pi N\Delta}$.

for the pion mass dependence of M_N within the fully relativistic approach because it enables us to recover immediately the non-relativistic result and examine the importance of recoil effects.

The leading-one-loop contribution to the nucleon self-energy with an intermediate $\Delta\,(1232)$ is represented by the graph in Fig.3.3. The leading $\pi N\Delta$ interaction Lagrangian, Eq.(2.120), contains the relevant vertex. The dependence on the so-called off-shell parameter Z is spurious (see Sec.2.10) and its effects can be absorbed by a redefinition of the couplings. In terms of the basic integrals in Appendix C, the $\mathcal{O}(\epsilon^3)$ graph yields the following shift to the nucleon mass in d space-time dimensions [1]:

$$\begin{aligned}\delta M_N^{3/2} = &-\frac{c_A^2\,(d-2)}{4(d-1)f_\pi^{0\,2}M_0{M_\Delta^0}^2}\times\\ &\Big\{I_\Delta\,(M_0^2-2M_\Delta^0M_0+{M_\Delta^0}^2-m_\pi^2)(M_0^2+2M_\Delta^0M_0+{M_\Delta^0}^2-m_\pi^2)^2\\ &+\Delta_\pi\left[M_0^4+2M_\Delta^0M_0^3+4m_\pi^2M_0^2-2({M_\Delta^0}^3-M_\Delta^0m_\pi^2)M_0-({M_\Delta^0}^2-m_\pi^2)^2\right]\\ &-\frac{4}{d}\,\Delta_\pi M_0^2m_\pi^2\Big\}\ .\end{aligned}\tag{3.33}$$

At $\mathcal{O}(\epsilon^3)$ the full result is schematically given by

$$M_N = M_0 - 4\,c_1m_\pi^2 + \delta M_N^{\pi N} + \delta M_N^{3/2} + \text{ counterterms }\,,\tag{3.34}$$

where $\delta M_N^{\pi N}$ is the nucleon mass-shift at order p^3 in the scheme with πN degrees of freedom:

$$\delta M_N^{\pi N} = \Sigma_a(\not{p}=M_0)\ ,\tag{3.35}$$

according to Eq.(3.20).

The spin-1/2 components of the delta field give rise to purely polynomial terms in m_π starting to contribute at m_π^4. They can consequently be accounted for by a redefinition of higher-order couplings.

Let us have a closer look at the terms in Eq.(3.33) which diverge in the limit $d\to 4$.

[1] See Ref. [93] for the $\mathcal{O}(\epsilon^4)$ result.

Expanding in powers of m_π and Δ, we get

$$\begin{aligned}
\delta M_N^{3/2}\Big|_{\rm inf} = & \left(-\frac{16L\,c_A^2\Delta^3}{3f_\pi^{0\,2}} - \frac{8L\,c_A^2\Delta^4}{3f_\pi^{0\,2}M_0} + \mathcal{O}(\Delta^5)\right) \\
& + \left(\frac{8L\,c_A^2\Delta}{f_\pi^{0\,2}} + \frac{4L\,c_A^2\Delta^2}{f_\pi^{0\,2}M_0} + \frac{22L\,c_A^2\Delta^3}{3f_\pi^{0\,2}M_0^2} + \mathcal{O}(\Delta^4)\right) m_\pi^2 \\
& + \left(-\frac{5L\,c_A^2}{f_\pi^{0\,2}M_0} - \frac{5L\,c_A^2\Delta^2}{f_\pi^{0\,2}M_0^3} + \frac{5L\,c_A^2\Delta^3}{f_\pi^{0\,2}M_0^4} + \mathcal{O}(\Delta^4)\right) m_\pi^4 \\
& + \left(\frac{5L\,c_A^2}{3f_\pi^{0\,2}M_0^3} - \frac{5L\,c_A^2\Delta}{3f_\pi^{0\,2}M_0^4} + \frac{7L\,c_A^2\Delta^2}{3f_\pi^{0\,2}M_0^5} - \frac{3L\,c_A^2\Delta^3}{f_\pi^{0\,2}M_0^6} + \mathcal{O}(\Delta^4)\right) m_\pi^6 \\
& + \left(-\frac{L\,c_A^2}{6f_\pi^{0\,2}M_0^5} + \frac{L\,c_A^2\Delta}{3f_\pi^{0\,2}M_0^6} - \frac{L\,c_A^2\Delta^2}{2f_\pi^{0\,2}M_0^7} + \frac{2L\,c_A^2\Delta^3}{3f_\pi^{0\,2}M_0^8} + \mathcal{O}(\Delta^4)\right) m_\pi^8 \,. \qquad (3.36)
\end{aligned}$$

In order to obtain a renormalized expression for $M_N(m_\pi)$, an infinite number of counterterms would be required. In the following we discuss different approaches to give a meaning to Eq.(3.34).

First, we note that in the non-relativistic limit $M_0 \to \infty$, two counterterms would be sufficient:

$$\mathcal{L}_{\pi N}^{(3)} = \bar\Psi \left[B_{32}\,\Delta^3 + B_{23}\,\Delta\,{\rm Tr}(\chi_+)\right]\Psi + \dots \,, \qquad (3.37)$$

see Sec.2.10. These terms are, among the whole set needed for renormalization in Eq.(3.34), the only ones appearing in $\mathcal{L}_{\pi N}^{(3)}$, all the others being of higher order in the standard power counting. Keeping the leading term in the $1/M_0$ expansion in Eq.(3.33), one recovers the $\mathcal{O}(\epsilon^3)$ result in non-relativistic SSE:

$$\begin{aligned}
M_N(m_\pi) = & M_0 - B_{32}^r(\lambda)\Delta^3 - 4\,c_1 m_\pi^2 - 4B_{23}^r(\lambda)\,\Delta m_\pi^2 - \frac{3{g_A^0}^2 m_\pi^3}{32 f_\pi^{0\,2}\pi} \\
& - \frac{c_A^2\Delta^3}{3\pi^2 f_\pi^{0\,2}}\ln\frac{m_\pi}{\lambda} + \frac{c_A^2\Delta^3}{9\pi^2 f_\pi^{0\,2}} + \frac{c_A^2\Delta}{2\pi^2 f_\pi^{0\,2}}\,m_\pi^2\ln\frac{m_\pi}{\lambda} - \frac{c_A^2 m_\pi^2\Delta}{12\pi^2 f_\pi^{0\,2}} \\
& - \frac{c_A^2}{3\pi^2 f_\pi^{0\,2}}(\Delta^2 - m_\pi^2)^{3/2}\ln\left(\frac{\Delta}{m_\pi} + \sqrt{\frac{\Delta^2}{m_\pi^2} - 1}\right) + \mathcal{O}(\epsilon^4) \,. \qquad (3.38)
\end{aligned}$$

The expansion around the chiral limit,

$$\begin{aligned}
M_N^{\rm chir}(m_\pi) = & M_0 - \frac{\Delta^3}{(4\pi f_\pi^0)^2}\left(16\pi^2 f_\pi^{0\,2}\,B_{32}^r(\lambda) + \frac{16}{3}c_A^2\ln\frac{2\Delta}{\lambda} - \frac{16}{9}c_A^2\right) \\
& - 4c_1 m_\pi^2 - \frac{\Delta}{(4\pi f_\pi^0)^2}\left(64\pi^2 f_\pi^{0\,2}B_{23}^r(\lambda) - 8c_A^2\ln\frac{2\Delta_0}{\lambda}\right)m_\pi^2 \\
& - \frac{3{g_A^0}^2}{32\pi f_\pi^{0\,2}}m_\pi^3 - \frac{3c_A^2}{32\pi^2 f_\pi^{0\,2}\Delta}m_\pi^4 + \frac{c_A^2}{8\pi^2 f_\pi^{0\,2}\Delta}m_\pi^4\ln\frac{m_\pi}{2\Delta} + \mathcal{O}(m_\pi^6) \,,
\end{aligned}$$

makes clear how we can achieve scale-independent decoupling of the delta for $m_\pi/M_\Delta \to 0$. Setting indeed $B_{23}^r(\lambda)$ and $B_{32}^r(\lambda)$ such that the first two terms in the chiral expansion

of $M_N(m_\pi)$ coincide with those in the πN sector,

$$B^r_{23}(\lambda) = \frac{1}{(4\pi f_\pi^0)^2}\, 2c_A^2 \ln\frac{2\Delta}{\lambda}\ , \tag{3.39}$$

$$B^r_{32}(\lambda) = \frac{1}{(4\pi f_\pi^0)^2}\left(-\frac{16}{3}c_A^2 \ln\frac{2\Delta}{\lambda} + \frac{16}{9}c_A^2\right)\ , \tag{3.40}$$

we obtain the result [103, 110]

$$\begin{aligned} M_N^{\rm SSE} = M_0 - 4\,c_1 m_\pi^2 - \frac{3\,{g_A^0}^2 m_\pi^3}{32 f_\pi^{0\,2}\pi} - \frac{c_A^2\Delta m_\pi^2}{12 f_\pi^{0\,2}\pi^2} + \frac{c_A^2\Delta}{f_\pi^{0\,2}\pi^2}\left(\frac{m_\pi^2}{2} - \frac{\Delta^2}{3}\right)\ln\frac{m_\pi}{2\Delta} \\ - \frac{c_A^2(\Delta^2 - m_\pi^2)^{3/2}}{3 f_\pi^{0\,2}\pi^2}\ \ln\left[\sqrt{-1 + \frac{\Delta^2}{m_\pi^2}} + \frac{\Delta}{m_\pi}\right]\ . \end{aligned} \tag{3.41}$$

Coming back to the relativistic case, our "full formula" has been worked out as follows, cf. Ref. [93]. We take care of divergences at m_π^0 and m_π^2 in Eq.(3.36) via two terms, $-\dot{B}_{32}\Delta^3$ and $-4\dot{B}_{23}\Delta m_\pi^2$: each of them is thought to absorb an infinite string of divergences in powers of Δ. Scale dependence at order m_π^4 has been removed by introducing the counterterm $-4\dot{e}_1 m_\pi^4\bar{\Psi}\Psi$, as we did at order p^3 in the πN sector. Like in the non-relativistic calculation, we choose the finite parts $\dot{B}^r_{23,32}(\lambda)$ in such a way that the chiral expansion of $M_N(m_\pi)$ at order ϵ^3 starts as

$$M_N = M_0 - 4\,c_1 m_\pi^2 + \mathcal{O}(m_\pi^3)\ . \tag{3.42}$$

The decoupling of the $\Delta\,(1232)$ is now realized up to and including $\mathcal{O}(m_\pi^3)$. Since we are going to compare our expressions for $M_N(m_\pi)$ with a data sample of limited statistics, we do not introduce other free parameters and live with uncompensated scale dependence at m_π^6 and m_π^8. Both effects of partial implementation of the decoupling and residual scale dependence are of higher order in the chiral expansion and therefore are part of the "systematic uncertainty" attached to the covariant SSE calculation. We will show the numerical impact of these effects in Sec.3.3.4.

If we truncate the relativistic SSE expression up to and including the term proportional to $1/M_0$, the counterterms $\tilde{B}_{32}\Delta^3\bar{\Psi}\Psi$, $4\tilde{B}_{23}\Delta m_\pi^2\bar{\Psi}\Psi$ and $-4\tilde{e}_1 m_\pi^4\bar{\Psi}\Psi$ are sufficient to ensure both renormalization and exact decoupling, cf. Eq.(3.36). Setting

$$\begin{aligned} \tilde{B}^r_{23}(\lambda) &= \frac{1}{(4\pi f_\pi^0)^2}\left[2c_A^2\ln\frac{2\Delta}{\lambda} + \frac{\Delta}{M_0}c_A^2\left(1 + \ln\frac{2\Delta}{\lambda}\right)\right] \\ \tilde{B}^r_{32}(\lambda) &= \frac{1}{(4\pi f_\pi^0)^2}\left[-\frac{16}{3}c_A^2\ln\frac{2\Delta}{\lambda} + \frac{16}{9}c_A^2 - \frac{16\Delta c_A^2}{9M_0} - \frac{8\Delta c_A^2}{3M_0}\ln\frac{2\Delta}{\lambda}\right]\ , \end{aligned} \tag{3.43}$$

these two renormalized couplings do not appear in the final equation, which reads

$$
\begin{aligned}
M_N = M_0 &- 4\,c_1 m_\pi^2 - \frac{3{g_A^0}^2 m_\pi^3}{32 f_\pi^{0\,2}\pi} - \frac{3{g_A^0}^2 m_\pi^4}{64\, f_\pi^{0\,2} M_0 \pi^2} - \frac{9 c_A^2 m_\pi^4}{64 f_\pi^{0\,2} M_0 \pi^2} \\
&- \frac{c_A^2 \Delta^4}{6 f_\pi^{0\,2} M_0 \pi^2} \ln\frac{m_\pi}{2\Delta} - \frac{c_A^2 \Delta^3}{3 f_\pi^2 \pi^2} \ln\frac{m_\pi}{2\Delta} + \frac{c_A^2 m_\pi^2 \Delta^2}{4 f_\pi^{0\,2} M_0 \pi^2} \ln\frac{m_\pi}{2\Delta} - \frac{c_A^2 m_\pi^2 \Delta^2}{24 f_\pi^{0\,2} M_0 \pi^2} \\
&+ \frac{c_A^2 m_\pi^2 \Delta}{2 f_\pi^{0\,2} \pi^2} \ln\frac{m_\pi}{2\Delta} - \frac{c_A^2 m_\pi^2 \Delta}{12 f_\pi^{0\,2} \pi^2} - \frac{3{g_A^0}^2}{32 f_\pi^{0\,2} M_0 \pi^2}\, m_\pi^4 \ln\frac{m_\pi}{\lambda} - \frac{5 c_A^2}{16 f_\pi^{0\,2} M_0 \pi^2}\, m_\pi^4 \ln\frac{m_\pi}{\lambda} \\
&- \frac{c_A^2}{6 f_\pi^{0\,2} M_0 \pi^2}\, \Delta (\Delta^2 - m_\pi^2)^{3/2} \ln\left(\frac{\Delta}{m_\pi} + \sqrt{\frac{\Delta^2}{m_\pi^2} - 1}\right) \\
&- \frac{c_A^2}{3 f_\pi^{0\,2} \pi^2}\, (\Delta^2 - m_\pi^2)^{3/2} \ln\left(\frac{\Delta}{m_\pi} + \sqrt{\frac{\Delta^2}{m_\pi^2} - 1}\right) + 4\,\tilde{e}_1^r(\lambda) m_\pi^4 \ . \qquad (3.44)
\end{aligned}
$$

Eqs.(3.41) and (3.44) are valid only for $m_\pi \leq \Delta$ —as it is in Nature. Since in our numerical analysis we take input lattice data at pion masses larger than the physical one, we need the analytic continuation of the expressions above to $m_\pi \geq \Delta$. This is achieved via the replacement

$$
\sqrt{\Delta^2 - m_\pi^2}\, \ln\left[\sqrt{-1 + \frac{\Delta^2}{m_\pi^2}} + \frac{\Delta}{m_\pi}\right] \;\to\; -\sqrt{m_\pi^2 - \Delta^2}\, \arccos\frac{\Delta}{m_\pi} \ .
$$

In the same way we worked out the analytic continuation of the full relativistic formula.

3.3 Numerical analysis and contact with lattice QCD

Let us now assume that there is an overlap between the region of validity for the expressions in Sec.3.2 and the range of quark masses presently accessible to full-QCD lattice simulations. In this section we describe our numerical study of Eqs.(3.21), (3.27), (3.29), (3.34), (3.44) and (3.41), in the ChEFT schemes with and without explicit $\Delta\,(1232)$ degrees of freedom, in the continuum and infinite volume limit. Parameters not fixed by chiral symmetry have been determined by fitting to a combined set of fully dynamical two-flavor lattice QCD results by the CP-PACS [111], JLQCD [112] and QCDSF-UKQCD [113] collaborations. Let us first examine our data sample.

3.3.1 Brief survey of lattice QCD results

In lattice QCD calculations, hadron masses are extracted analyzing the large Euclidean time behavior of correlation functions for zero-momentum operators $O_H(\tau)$ carrying the appropriate quantum numbers to create the hadron of interest. In this way, nucleon and pion masses are deduced by studying the fall-off pattern for large values of τ of

correlation functions

$$\mathcal{C}(\tau) = \langle 0|\, O_H^\dagger(\tau)\, O_H(0)|0\rangle = \frac{\int \mathcal{D}U\mathcal{D}\bar{\psi}\mathcal{D}\psi\, e^{-S_{\rm QCD}}\, O_H^\dagger(\tau)\, O_H(0)}{\int \mathcal{D}U\mathcal{D}\bar{\psi}\mathcal{D}\psi\, e^{-S_{\rm QCD}}} \quad , \tag{3.45}$$

where $S_{\rm QCD}$ is the (Euclidean) lattice action of QCD, *i.e.* the sum of the gauge field action and the action of fermions (quarks) coupled to gauge fields. If $|\Omega\rangle$ is the state created from the vacuum by the operator $O_H(0)$ and E_n denotes the energy of the n-th eigenstate $|n\rangle$ of the Hamiltonian, we have

$$\mathcal{C}(\tau) = \sum_n |\langle n|\Omega\rangle|^2\, e^{-E_n\,\tau} \quad . \tag{3.46}$$

Hence, in the large τ limit, $\mathcal{C}(\tau)$ is dominated by the lowest energy state carrying the quantum numbers of O_H.

The actual quantity computed on the lattice is the hadron mass in units of the inverse of the lattice spacing a. In order to convert this dimensionless quantity into physical units, one has to determine a by comparison with phenomenology. The presence of systematic errors due to large quark masses, lattice spacing and finite-volume effects, makes it non-trivial to set the scale for the simulation results. A popular method is to use the force parameter r_0 [36], calculated assuming that the QCD static $q\bar{q}$ potential coincides with the phenomenological effective potential which describes the energy levels of heavy quarkonia. The scale r_0 is implicitly defined through

$$r^2\, \frac{d\,V(r)}{dr}\bigg|_{r=r_0} = 1.65 \tag{3.47}$$

where $V(r)$ denotes the static quark-antiquark potential. The numerical value on the right-hand side is adjusted such that fitting to the bottomonium spectrum with phenomenological or lattice potentials yields $r_0 \approx 0.5\,\text{fm}$. In the following we shall adopt this procedure to set the scale and use $r_0 = 0.5\,\text{fm}$ [113]. It is not obvious that the quark mass effects on the static $q\bar{q}$ force at distances around 0.5 fm are negligibly small. The study of the dependence of r_0 on the masses of dynamical quarks is at an early stage: in Ref. [114] a weak dependence is reported for $a \approx 0.1\,\text{fm}$ at least for some combination of gauge and fermion actions. It would certainly be advantageous to avoid the lattice scale problem completely by considering dimensionless ratios (*e.g.* ratios of the masses to the pion decay constant) and performing the whole m_π-dependence study in ChPT for these ratios. This would be possible if more data points for different observables with the same simulation parameters were available.

The Monte Carlo data that we used have been computed with different actions: the UKQCD and QCDSF collaborations work with the standard Wilson plaquette gauge action and the non-perturbatively $\mathcal{O}(a)$-improved clover action for the fermions [113]. JLQCD uses the same actions as QCDSF-UKQCD but with a slightly different value for the improvement parameter c_{SW} [112]. CP-PACS data instead are worked out with a renormalization-group improved gauge action and a mean-field clover quark action [111].

Table 3.1: Lattice data points selected for the analysis of $M_N(m_\pi)$. See text and Ref. [113] for details.

Collaboration	a [fm]	L [fm]	$m_\pi L$	m_π [GeV]	M_N [GeV]
UKQCD	0.11	1.68	6.5	0.760(11)	1.657(26)
UKQCD	0.10	1.56	6.1	0.7791(76)	1.629(20)
QCDSF	0.09	2.21	6.2	0.5570(69)	1.320(19)
QCDSF	0.09	2.16	7.8	0.7172(29)	1.5062(94)
CP-PACS	0.11	2.68	7.1	0.5214(21)	1.2751(82)
CP-PACS	0.12	2.83	10.2	0.7088(25)	1.4971(77)
CP-PACS	0.09	2.22	6.7	0.5946(52)	1.348(13)
CP-PACS	0.10	2.29	8.5	0.7345(37)	1.519(11)
JLQCD	0.11	2.16	8.0	0.7324(84)	1.509(18)
JLQCD	0.10	1.96	5.4	0.5453(90)	1.300(22)

The available data points are collected in Ref. [113]. In order to minimize artifacts from discretization and finite volume effects, we have selected the simulations with $a < 0.15\,\mathrm{fm}$ and $m_\pi L > 5$, where L is the spatial size of the lattice. In Ref. [115] a lattice regularized version of ChPT is used to determine the typical size of discretization errors. For *physical* values of m_q, baryon masses turn out to be essentially independent of lattice spacing when $\pi/a \gtrsim \Lambda_\chi$. However, as pointed out in Ref. [116], the explicit chiral symmetry breaking of Wilson-type quark actions could require a modification (due to finite lattice spacing) of the ChPT formulae used for extrapolations on a coarse lattice ($a \approx 0.2\,\mathrm{fm}$). It is a remarkable fact that the Monte Carlo data compatible with our cuts, while obtained with *different* (improved) actions, all lie close to a single curve (see Fig.3.4). This makes us confident that lattice artifacts in the selected set of points are minimized.

The authors of Ref. [113] studied finite-size effects for M_N [117] in the framework of $SU(2)$ BChPT, up to and including $\mathcal{O}(p^4)$. They computed the graphs in Fig.3.1, replacing any integral over the spatial components $\vec{p}$ of the loop momentum by a sum over the discrete set of momenta allowed by periodic boundary conditions. The parameters in the relevant formulae have been fixed according to our results in the infinite-volume limit [106] and a successful, parameter-free *prediction* of finite-size effects has been obtained [113]. We have then checked that for $m_\pi L > 5$ finite-size corrections to M_N are within error bars for the data points that we used as input. Furthermore, in Ref. [107] we performed *fits* to lattice data using the finite volume formulae in Ref. [113]. The results confirm and sharpen the outcome of our study in Ref. [106].

In the numerical analysis we restricted ourselves to simulations with $m_\pi < 600\,\mathrm{MeV}$ and equal valence and sea quark masses. For further discussion, in Table 3.1 we collect the data up to 800 MeV in pion mass. The cut at $m_\pi < 600\,\mathrm{MeV}$ represents a compromise between the smallest available pion masses and an amount of data sufficient to perform a

meaningful statistical analysis. At the time of writing there are no unquenched two-flavor data with $m_\pi \lesssim 500\,\mathrm{MeV}$. None of the recent simulations in Ref. [118] survives our cuts in a, L and m_π, see Ref. [107]. A large span is still left between physical nucleon mass and lattice results. Of course, it would be more reassuring to have a data sample with good statistics and smaller pion masses because ChPT is thought to work for *small* u- and d-quark masses, although *a priori* we do not know how small. Our work describes a *systematic* way to explore whether some inconsistencies emerge by assuming that BChPT makes contact with state-of-art full-QCD results. Future lattice simulations will allow to test and strengthen our predictions in the region of smaller quark masses and will provide the missing input for reliable extrapolations.

3.3.2 Numerical results without explicit $\Delta\,(1232)$ degrees of freedom

The statistics of our data set forces us to constrain some low-energy parameters. We have fixed $g_A^0 = g_A^{\mathrm{phys}} = 1.267$, $f_\pi^0 = f_\pi^{\mathrm{phys}} = 92.4\,\mathrm{MeV}$ and checked the sensitivity of our results to such input values. The regularization scale λ has been chosen equal to $1\,\mathrm{GeV}$, without any loss of generality since we are dealing with scale-independent relations. At order p^3 we are then left with three parameters – M_0, c_1 and $e_1^r(1\,\mathrm{GeV})$: we have determined them by fitting to the selected lattice data. At fourth order we deal with four parameters in the truncated expression, Eq. (3.29) – M_0, c_1 and the two linear combinations $e_1^r(1\,\mathrm{GeV}) + 3c_2/(128\pi^2 f_\pi^2)$ and $c_2 + 4c_3$. In the full formula, Eq.(3.27), the renormalized coupling $e_2^r(1\,\mathrm{GeV})$ enters in addition.

The results of our best-fit analysis are summarized in Table 3.2. All quoted errors are of purely statistical origin and have been determined through the MINUIT package and maximum likelihood method. In these fits we neglect the errors on m_π. If not explicitly mentioned, the physical nucleon mass has been included as input to improve the statistics without considering very large pion masses. Of course, it is not optimal to fit *both* to the physical point *and* to two-flavor lattice data: the effects of quarks heavier then u and d – encoded in the LECs – are different in the real and the lattice world. However, the results obtained by fitting to three-flavor data by the MILC collaboration [101] are statistically compatible with the outcome of our two-flavor numerical analysis [119].

We investigate whether it is possible to extract from the lattice some reliable estimate of the LECs, by looking at the m_q axis, not accessible to experiments. We look for good interpolating functions from the chiral limit, across the physical point, up to lattice data. We check the agreement of the output parameters with available information from low-energy hadron phenomenology and determine whether the formula shows an acceptable convergence pattern.

A naive, linear extrapolation in the quark mass turns out to be totally inappropriate. Indeed the $\mathcal{O}(p^2)$-fit based on the leading pion-mass dependence of M_N (Fit 0),

$$M_N = M_0 - 4\,c_1 m_\pi^2 \,, \tag{3.48}$$

leads to a value of c_1 which is about a factor 3 larger than in reality, see Sec.2.9. We must use more sophisticated extrapolation functions.

Table 3.2: Fit results for $M_N(m_\pi)$ in BChPT. The errors from the MINUIT package have been rounded to the first significant digit.

	M_0 [GeV]	c_1 [GeV^{-1}]	$e_1^r(1\,\text{GeV})$ [GeV^{-3}]	χ^2/d.o.f.
Fit 0	0.914 ± 0.001	-0.322 ± 0.006	-	1.52
Fit I	0.891 ± 0.004	-0.79 ± 0.05	0.9 ± 0.2	0.24
Fit Ia	0.891 ± 0.004	-0.80 ± 0.05	0.9 ± 0.2	0.24
Fit II	0.883 ± 0.003	-0.93 ± 0.04	0.7 ± 0.2	0.29
Fit IIa	0.872 ± 0.003	-1.11 ± 0.04	0.8 ± 0.2	0.39
Fit III	0.89 ± 0.06	-0.93 ± 0.05	0.7 ± 0.1	1.77
Fit IIIa	0.76 ± 0.06	-1.24 ± 0.05	0.4 ± 0.1	1.72

$\mathcal{O}(p^3)$ analysis

Let us consider the $\mathcal{O}(p^3)$ result, Eq.(3.21), with g_A and f_π equal to their physical values (Fit I). The corresponding best-fit curve is the solid line drawn in Fig.3.4. Remarkably, the low-energy constants come out of natural size, a non-trivial result. Furthermore, c_1, which determines the slope of $M_N(m_\pi^2)$ for small m_π^2, has the correct sign and size and the estimate of M_0 is consistent with empirical information about the pion-nucleon sigma term, see Sec.3.5 for a detailed discussion. The use of chiral limit values for g_A and f_π leads to statistically indistinguishable results, as we can see in Fit Ia where we set $g_A^0 = 1.2$ (cf. Ref. [120] and Chapter 4) and $f_\pi = 86.2\,\text{MeV}$ (cf. Sec.2.7).

We can therefore conclude that a remarkably good interpolation between the relatively large quark masses accessible in full-QCD simulations, and the small quark masses relevant for comparison with the physical M_N, can already be achieved by a leading-one-loop calculation in BChPT with infrared regularization.

The counterterm at m_π^4 turns out to be numerically crucial to get a good interpolation. This term, required for renormalization in our approach, is equivalent to that introduced in Ref. [121], in the context of one-loop HBChPT. Evaluating the loop diagrams in Fig.3.1 with the help of a radial cutoff, the authors of Ref. [121] show that the term $-4\,e_1 m_\pi^4 \bar{\Psi}\Psi$ is necessary to reduce the sensitivity to momentum modes close to Λ_χ for pion masses larger 400 MeV.

Fig.3.4 also shows how Fit I develops term by term when the NLO expression is expanded around $m_\pi = 0$, Eq.(3.23). The leading-one-loop Heavy Baryon expression is inadequate for pion masses larger than 300 MeV. Instead, truncating the expansion at m_π^5 already provides a good approximation to the full $\mathcal{O}(p^3)$ result. Higher powers in m_π do not destroy this convergence pattern, for the whole range in m_π that we consider.

In our approach, *all the terms* beyond the leading c_1-contribution in Eq.(3.23) are part of the *same* chiral order p^3. We count powers according to Eq.(2.69) while keeping the full relativistic propagator. Compared to the HBChPT result, the infrared regularization scheme resums a string of terms with increasing powers of m_π/M_0, which are of higher order in the non-relativistic framework. When higher-order counterterms are needed

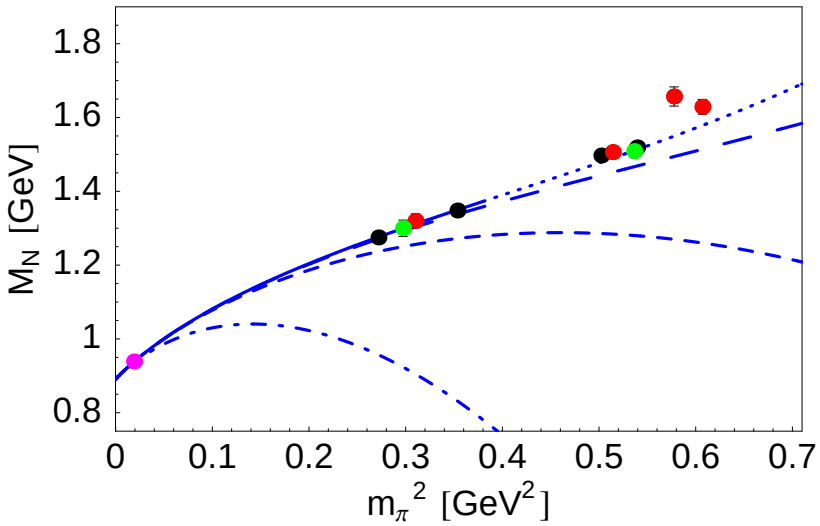

Figure 3.4: Solid line: $\mathcal{O}(p^3)$ best-fit curve based on Eq.(3.21). Input: four lowest lattice data points with $m_\pi < 600\,\mathrm{MeV}$ and physical nucleon mass (Fit I). All data points by CP-PACS, JLQCD, QCDSF-UKQCD collaborations in Table 3.1 are shown. The dot-dashed, dashed and long-dashed curves show, respectively, the contributions from the sum of the first three, four and five terms in the expansion in powers of m_π of the $\mathcal{O}(p^3)$ expression, Eq.(3.23).

for renormalization, we include them in the calculation. Fig.3.4 shows that the large fluctuations in dimensionally regularized chiral extrapolation functions reported in Ref. [122,123], arise from examining only the very first terms in Eq.(3.23), instead of keeping the full $\mathcal{O}(p^3)$ expression, Eq.(3.21).

$\mathcal{O}(p^4)$ results

At next-to-leading one-loop order, Eq.(3.29), we fixed one of the four parameters using input values for c_2 and c_3. We set $c_2 = 3.2\,\mathrm{GeV}^{-1}$ according to different low-energy pion-nucleon scattering analyses, see Sec.2.9. The dimension-two LEC c_3 is known with much less accuracy than c_2: in Fit II and Fit IIa we set $c_3 = -3.4\,\mathrm{GeV}^{-1}$ and $c_3 = -4.7\,\mathrm{GeV}^{-1}$, respectively. The former choice is consistent with empirical peripheral NN phase shifts [79][2] while the latter coincides with the central value obtained in Ref. [72], for πN scattering inside the Mandelstam triangle (see Sec.2.9 for a detailed discussion). In this section we will show that:

- our numerical analysis, both in the infinite and finite volume, supports small values in magnitude for c_3, about $-3\,\mathrm{GeV}^{-1}$;

- the truncated expression in Eq.(3.29) represents a good approximation of the full Eq.(3.27);

[2]See also Refs. [80,81].

- an amazing result can be obtained by fitting to the ten lattice data up to $m_\pi \approx 800\,\mathrm{MeV}$, *without the physical point as input*.

Remarkably, for $c_3 = -3.4\,\mathrm{GeV}^{-1}$, c_1 turns out to be in agreement with Ref. [72] and with the outcome of a (tree-level) analysis of low-energy πN scattering in $SU(2)$ Baryon ChPT with infrared regularization [70], the same framework we use. Applying the Feynman-Hellmann theorem and the Gell-Mann – Oakes – Renner relation to Eq.(3.9),

$$\sigma_N = m_q \frac{\partial M_N}{\partial m_q} \approx m_\pi^2 \frac{\partial M_N}{\partial m_\pi^2} \ , \tag{3.49}$$

see Sec.3.5 for details. Combining this result with Eq.(3.29) and the outcome of Fit II, we get $\sigma_N = 49 \pm 3\,\mathrm{MeV}$. Fit IIa with $c_3 = -4.7\,\mathrm{GeV}^{-1}$, gives $c_1 \approx -1.10\,\mathrm{GeV}^{-1}$ and $\sigma_N = 57 \pm 3\,\mathrm{MeV}$. The correlation between larger magnitudes for c_3 in input and larger magnitudes for c_1 and pion-nucleon σ-term is confirmed for other choices of c_3. A large theoretical uncertainty affects the empirical determination of σ_N and a relatively broad range of values for c_1 is consistent with πN scattering analyses: hence, in such fits, there is agreement between output and phenomenology for the extended input range $c_3 = -5.5 \cdots -3.4\,\mathrm{GeV}^{-1}$.

However, resonance exchange shows that c_3 receives an important contribution from the singularities generated by the $\Delta\,(1232)$ [52, 73]. Consider an effective Lagrangian with mesonic and baryonic resonances chirally coupled to nucleons and pions. One can generate local pion-nucleon operators of higher dimension with given LECs by letting the resonance masses become very large with fixed ratios of coupling constants to masses. This procedure amounts to decoupling the resonance degrees of freedom from the effective field theory. However the traces of these frozen particles are encoded in the numerical values of certain LECs.

The physics underlying c_3 can be sorted out as follows. Let us start from elastic πN scattering at lowest order in the theory with explicit $\Delta\,(1232)$ degrees of freedom: at tree level we have to compute the direct and crossed $\Delta\,(1232)$-pole diagrams. $\mathcal{L}^{(1)}_{\pi N \Delta}$ provides the relevant vertex. We then match the result in the non-relativistic limit with the $\pi N \to \pi N$ graph from the second-order pion-nucleon Lagrangian $\mathcal{L}^{(2)}_{\pi N}$, which involves the c_i. Equating the P-wave isospin-even non-spin-flip terms and choosing the off-shell parameter $Z = -1/2$, we obtain that c_3 corresponds to

$$-\frac{4c_A^2}{9}\,\frac{\Delta}{\Delta^2 - \omega^2} \ , \tag{3.50}$$

where ω is the pion energy in the laboratory frame, cf. [86, 124]. According to this result, the ratio between the $\Delta\,(1232)$ contributions to c_3 in the chiral (static) limit and at threshold, is about 3/4. What is relevant for our analysis is the value of c_3 in the chiral limit. For $c_A = 1.5$ and $\Delta = 293\,\mathrm{MeV}$, the expression (3.50) gives $c_3 = -3.4\,\mathrm{GeV}^{-1}$ as $\omega = 0$, while $c_3 = -4.4\,\mathrm{GeV}^{-1}$ at threshold. The fact that $\Delta \approx 2m_\pi$ plays a crucial role in the energy denominator.

We showed in Sec.2.9 that $c_3 \approx -5\,\mathrm{GeV}^{-1}$ is compatible with the isospin-even pion-nucleon scattering amplitude *at threshold*. If we multiply by the factor 3/4, c_3 comes out

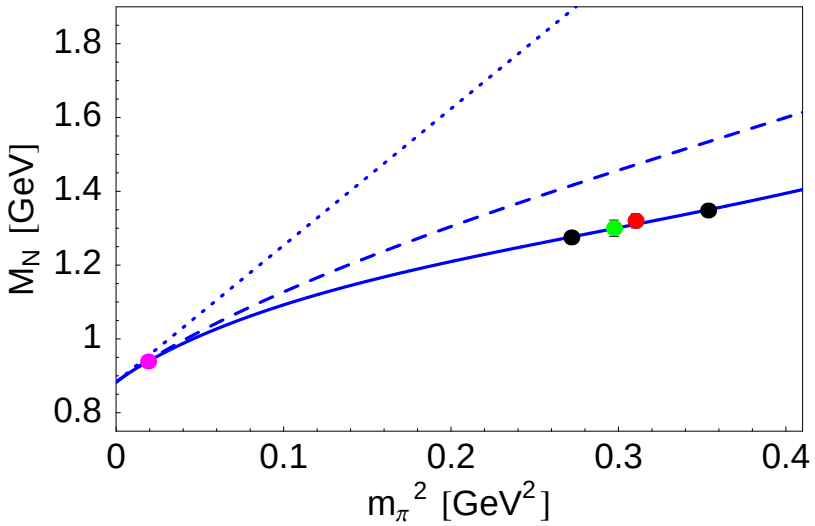

Figure 3.5: Solid curve: $\mathcal{O}(p^4)$ best fit based on Eq.(3.29), with $c_3 = -3.4\,\mathrm{GeV}^{-1}$ as input (Fit II). Dashed curve: $\mathcal{O}(p^3)$ result from Eq.(3.21), using as parameters the central values of Fit II at the matching scale $\bar{\lambda} = 1.175\,\mathrm{GeV}$. Dotted curve: $\mathcal{O}(p^2)$ result.

in agreement with peripheral NN phase shift analyses. This is not surprising. Indeed, the one-loop 2π-exchange diagrams with single $\Delta\,(1232)$ excitation (planar and crossed box graphs) give the dominant contribution to the isoscalar central component of the on-shell nucleon-nucleon scattering amplitude. In the sum of those diagrams, the energy dependence of the delta propagator disappears [125] and we would obtain the same result using a $NN\pi\pi$-contact vertex with $c_3 = -4c_A^2/(9\Delta)$ – the $\omega \to 0$ limit of the expression (3.50) from the spin-isospin averaged P-wave πN scattering volume.

Numerical analyses of present lattice data agree nicely with this picture of the physics in c_3. The input value $c_3 = -3.4\,\mathrm{GeV}^{-1}$ leads for example to a successful prediction of finite size effects for M_N [113]. The finite-volume dependence of M_N can also be exploited to gain statistics: we can indeed fit to an enlarged set of data using the $\mathcal{O}(p^4)$ expression in Ref. [113], which takes into account finite-size corrections. The parameters which enter in such an analysis are the same as for our study in the infinite volume. Thanks to the improved statistics, we can release c_3. A fit to the lattice data in Refs. [111–113, 118] with $m_\pi < 650\,\mathrm{MeV}$ and $L > 1\,\mathrm{fm}$, gives $c_3 = -2.9 \pm 0.6\,\mathrm{GeV}^{-1}$ and strongly rules out values about $-5\,\mathrm{GeV}^{-1}$ [107].

Furthermore, *only* for a c_3 small in magnitude, the $\mathcal{O}(p^4)$ correction to the $\mathcal{O}(p^3)$ result indicates a reasonable convergence pattern for relatively large quark masses. In Fig.3.5 we demonstrate that, according the central values from Fit II, higher-order chiral corrections are indeed acceptably small, even at pion masses well above the physical one. For Fit IIa, these corrections are sensibly larger, as one can appreciate from Fig.3.6. In drawing the curves for the $\mathcal{O}(p^3)$ results in Figs.3.5 and 3.6, we used the estimate of $e_1^r(\lambda)$ in the

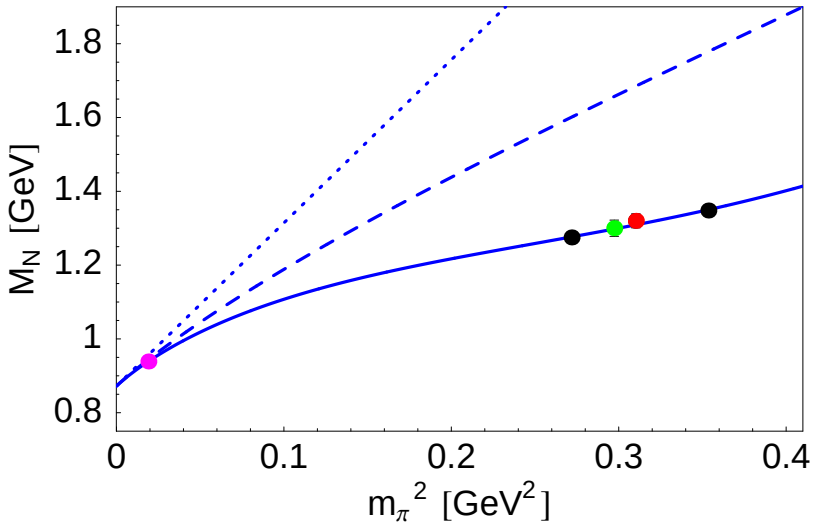

Figure 3.6: The same as in Fig.3.5, but for Fit IIa, with $c_3 = -4.7\,\mathrm{GeV}^{-1}$ as input. Here $\bar{\lambda} = 1.042\,\mathrm{GeV}$.

fit at order p^4, which we consider our best description of $M_N(m_\pi)$. Since the running of the effective coupling $e_1^r(\lambda)$ changes from $\mathcal{O}(p^3)$ to $\mathcal{O}(p^4)$, importing any information about that from fourth to third order has to take place at a specific λ. We have chosen this matching scale $\bar{\lambda}$ as the scale for which the *estimates* of $e_1^r(\bar{\lambda})$ in the *fits* at order p^3 and p^4 coincide. We get $\bar{\lambda} = 1.175\,\mathrm{GeV}$ for $c_3 = -3.4\,\mathrm{GeV}^{-1}$ and $\bar{\lambda} = 1.042\,\mathrm{GeV}$ for $c_3 = -4.7\,\mathrm{GeV}^{-1}$.

We notice that the shape of our $\mathcal{O}(p^4)$ best-fit curve is in good agreement up to $m_\pi \approx 600\,\mathrm{MeV}$ with extrapolation curves that has been worked out in different theoretical frameworks [126]. In particular, we refer both to the studies of $M_N(m_\pi)$ in the chiral quark soliton model [126] and to the approach of the Adelaide group, employing suitable vertex form factors, which are referred to as "finite range regulators" and intended to model effects of the pion cloud in the presence of a finite size of the nucleon [123].

Let us now concentrate on the full Eq.(3.27), where the term $-e_2\, m_\pi^6 \bar{\Psi}\Psi$ has been included for renormalization. Using the central values from Fit II, we are left with one free parameter, $e_2^r(1\,\mathrm{GeV})$. Fitting to the four lattice data up to 600 MeV in m_π, we obtain $e_2^r(1\,\mathrm{GeV}) = 0.090 \pm 0.003\,\mathrm{GeV}^{-5}$, with $\chi^2/\mathrm{d.o.f.} = 0.12$. The trend of the lattice data is nicely reproduced, even for pion masses larger than 600 MeV. The function is sensitive to the precise value of $e_2^r(1\,\mathrm{GeV})$: if we set it equal to zero, the resulting curve is not compatible with lattice data. Unfortunately, there is no available information on this $\mathcal{O}(p^6)$ effective coupling from low-energy hadron phenomenology. However, in view of the small size of our estimate of e_2, we can argue that the truncation at m_π^5 of the full $\mathcal{O}(p^4)$ expression looks quite natural and reliable in the range of pion masses of interest here. In order to make firmer statements, a better statistics together with an accurate determinations of the relevant dimension-two and -three LECs are mandatory.

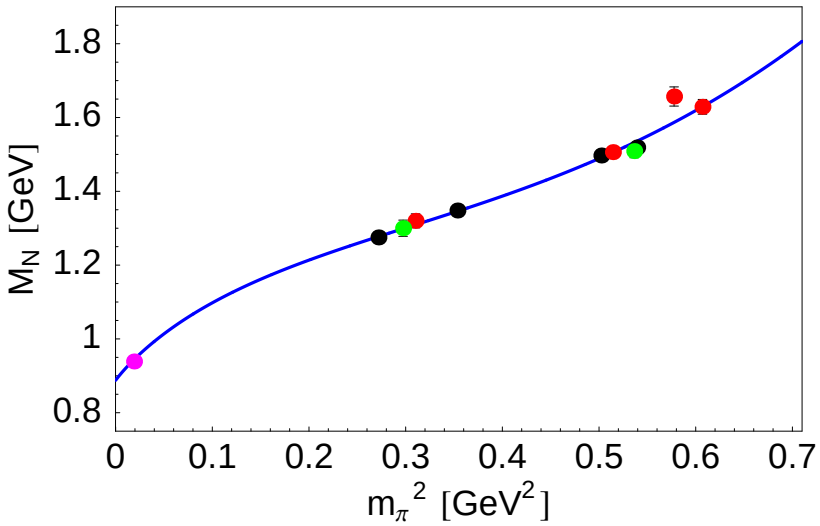

Figure 3.7: Chiral extrapolation according to the $\mathcal{O}(p^4)$ formula (3.29). All the points up to 800 MeV in pion mass are included in input, *except the physical one*. Here we show the best fit curve with three free parameters corresponding to the choice $c_3 = -3.4\,\mathrm{GeV}^{-1}$ (Fit III).

From the numerical point of view, it is sufficient to truncate at m_π^4, *i.e.* to use the HBChPT result at order p^4. The fits indeed yield results that are statistically compatible with Fit II and Fit IIa, for different c_3 as input, cf. Ref. [121].

We performed also extrapolations for the ten lattice data up to $m_\pi \approx 800\,\mathrm{MeV}$, without the physical point as input. The outcome is amazing (Fits III and IIIa, for different c_3, as before). In particular, for the choice $c_3 = -3.4\,\mathrm{GeV}^{-1}$ we get the best-fit curve shown in Fig.3.7. The $\mathcal{O}(p^4)$ Eq.(3.29) seems to work astonishingly well also for pion masses up to 800 MeV. This remarkable result deserves a thorough statistical analysis.

3.3.3 Statistical analysis

We have obtained an excellent description of the m_π-dependence of M_N shown by fully dynamical lattice simulations (at least) up to 600 MeV in pion mass. Successful interpolations between lattice data and physical point have been achieved: the low-energy parameters in output nicely agree with phenomenology and the comparison of different orders exhibits a convergent pattern. We now try to answer the following questions in order to examine the reliability and the efficiency of our approach [107, 119]:

- What is the region in the parameter space where we expect to find the "true" value for the parameter set at some confidence level?

- Our functions are evaluated at a specific order in BChPT. What is the convergence

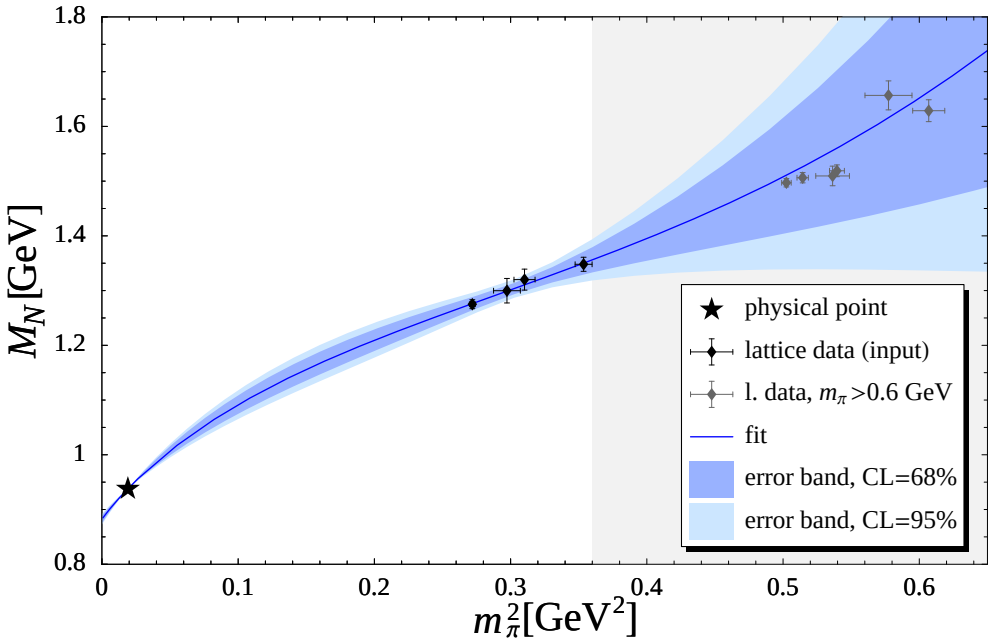

Figure 3.8: Error bands corresponding to the joint 68 and 95% confidence regions for the free parameters in Fit II. We fit to physical point and lattice data only up to 600 MeV in m_π: the light grey points have not been used for our statistical considerations [119].

radius of the perturbative expansion for $M_N(m_\pi)$? How large is the error associated to the omission of higher order effects?

The first problem concerns the statistical errors associated with the uncertainties in input parameters and lattice data. The second point raises the issue of the "theoretical", systematic error attached to a (chiral) perturbative approach for a certain range of m_π.

We have addressed the first question for Fit II at order p^4. Through a Monte Carlo routine we have explored the joint 68% and 95% confidence regions for the free parameters M_0, c_1 and $e_1^r(1\,\text{GeV})$; g_A^0 and f_π^0 are given as input. The resulting error bands, shown in Fig.3.8, refer to the case $g_A^0 = g_A^{\text{phys}} = 1.267$, $f_\pi^0 = f_\pi^{\text{phys}} = 92.4\,\text{MeV}$ and $c_3 = -3.4\,\text{GeV}^{-1}$. The errors on m_π have been taken into account. The inclusion of the physical point is crucial to shrink the band below 300 MeV in m_π. The (surprising) agreement between best-fit curve and lattice data up to $m_\pi \approx 750\,\text{MeV}$, visible already at $\mathcal{O}(p^3)$ (Fig.3.4), should be taken with the necessary caveat. Indeed, we loose predictive power about the shape of the curve for $m_\pi > 600\,\text{MeV}$: the input (in the form of lattice data and parameters), even though suitably "squeezed", constrains weakly the shape of the interpolating functions at very large pion masses.

In a second step we have studied how the 68% error bands change if we vary in input g_A^0 and f_π^0. We scanned the ranges $1.1 \ldots 1.3$ for g_A^0 (see [120] and Chapter 4) and

$86.2 \ldots 92.4\,\mathrm{MeV}$ for f_π^0, according to uniform probability distributions. No change in the error bands is visible up to $m_\pi = 600\,\mathrm{MeV}$ [107, 119].

Our fit strategy does not allow to perform a chiral extrapolation of present lattice data *with small uncertainties*. The region spanned by the statistical bands grows dramatically for $m_\pi < 350\,\mathrm{MeV}$ if the physical point is not included. However, an advantage of chiral effective field theories over "naive" polynomial fits is its ability to produce expressions for *different* observables involving a *common* subset of LECs. By fitting to data for several observables one can get redundancy for the unknown parameters. In order to gain statistics, one can make use of lattice features that can be encoded in a chiral effective field theory framework, like finite size effects and dependence on the lattice spacing. A posteriori, one should analyze convergence and check agreement with phenomenological information about the parameters. Our work is a first step in this direction: we resort to low-energy hadron phenomenology and investigate whether, within errors and up to $m_\pi \approx 600\,\mathrm{MeV}$, lattice data are compatible with one-loop BChPT.

Let us now come to the second question formulated at the beginning of this section. The best (systematic) way to evaluate the impact of higher-order effects is, of course, to work out the $\mathcal{O}(p^5)$ calculation – which involves also two-loop graphs – and repeat the procedure described in the previous sections. However, due to the increasing number of parameters not fixed by chiral symmetry, at $\mathcal{O}(p^5)$ there is no hope to extract *quantitative*, stringent results from the presently available data sample.

A simple way of reducing the weight of the operators of higher dimension is to include the $\Delta\,(1232)$ as an explicit degree of freedom.

As already pointed out, the running of g_A and f_π with the pion mass starts contributing at fifth order: the difference between results using either g_A^0, f_π^0 or $g_A(m_\pi)$, $f_\pi(m_\pi)$, is a measure of the importance of higher-order effects. It would be therefore interesting to have under control the quark mass dependence for g_A and f_π for relatively large quark masses. While this is the case for the former (see Chapter 4), present knowledge of the latter is not completely satisfactory (see Sec.2.7). In Eq.(3.29), we have replaced g_A^0 with our successful extrapolation function for $g_A(m_\pi)$: the $\mathcal{O}(\epsilon^3)$ non-relativistic SSE expression in Ref. [120]. We checked that the running of g_A can be fairly attributed to higher orders. This is not surprising: the pion mass dependence of g_A on the lattice is quite flat and the height of the typical data plateau is close the physical value $g_A = 1.267$, see Chapter 4. We already know, however, that varying g_A^0 in input between 1.1 and 1.3 does not affect the shape of the best-fit curve at order p^4. Still, one should keep in mind that this is not a systematic way to analyze the impact of higher-order effects since we do not take into account other contributions that belong to the same order.

3.3.4 Including explicit $\Delta\,(1232)$ degrees of freedom

Following the strategy outlined in Sec.3.3.2, we have analyzed the $\mathcal{O}(\epsilon^3)$ expressions for $M_N(m_\pi)$ worked out in Sec.3.2.3: the non-relativistic formula in Eq.(3.41), the $\mathcal{O}(1/M_0)$-truncated Eq.(3.44) and the "full" relativistic expression.

We have treated the nucleon-axial-delta coupling c_A and $\Delta = M_\Delta^0 - M_0$ as input values.

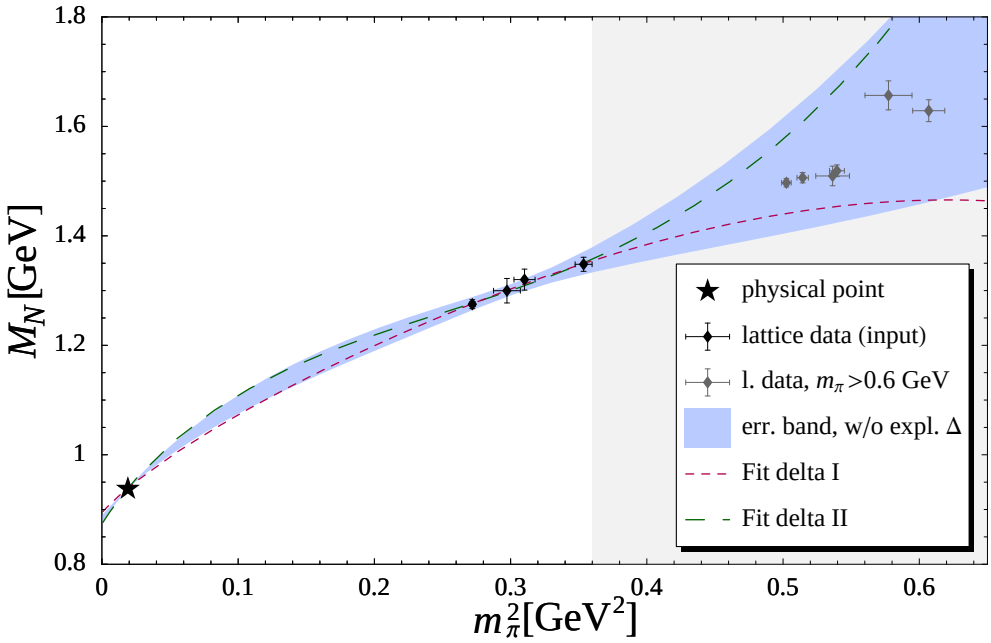

Figure 3.9: Best-fit curves based on the formula at order ϵ^3 in manifestly covariant SSE, with $c_A = 1.5$ as input parameter [107]. For comparison, we plot also the $\mathcal{O}(p^4)$ 68% error band of Fig.3.8, where the $\Delta\,(1232)$ is not an explicit degree of freedom.

For c_A, we have used phenomenological estimates at the physical value of m_π, since nothing is known about the quark mass dependence of this coupling. We have performed fits both with $c_A = 1.5$ and $c_A = 1.125$, the values extracted from the strong decay width of the $\Delta\,(1232)$ in the relativistic and non-relativistic framework, respectively, see Sec.2.10.2. We identify the parameter Δ with the *physical* delta-nucleon mass splitting and fit setting $\Delta = 271.1$ and $293\,\mathrm{MeV}$, see Sec.2.10.2. The former value corresponds to the real part of the $\Delta\,(1232)$ pole in the complex W-plane, the latter to the 90^0 πN phase-shift in the spin-3/2 isospin-3/2 channel, see Sec.2.10.2.

We fix the regularization scale $\lambda = 1\,\mathrm{GeV}$. Both Eqs.(3.41) and (3.44) are scale independent.

The $\mathcal{O}(\epsilon^3)$ non-relativistic SSE result – without an additional "improvement term" at m_π^4 [110] – cannot provide a satisfactory interpolation between lattice data and physical point. Compared to $\mathcal{O}(p^3)$ HBChPT, the inclusion of explicit $\Delta\,(1232)$ in the non-relativistic framework does not improve the situation.

Fit delta I in Table 3.3 refers to Eq.(3.44), with $c_A = 1.5$, $\Delta = 271.1\,\mathrm{MeV}$, $g_A = 1.267$ and $f_\pi = 92.4\,\mathrm{MeV}$. We fit to the four data with $m_\pi < 600\,\mathrm{MeV}$ including the physical point, see Fig.3.9. Nothing is known about the linear combination of couplings $\tilde{e}_1^r(1\,\mathrm{GeV})$ from low-energy hadron phenomenology. The input parameters c_A and Δ together with $\tilde{e}_1^r(1\,\mathrm{GeV})$ govern the behaviour of the curve in the region where the lattice data are.

Table 3.3: Fit results for $M_N(m_\pi)$ at leading-one-loop order, including explicit $\Delta\,(1232)$ degrees of freedom. Here $\lambda = 1\,\mathrm{GeV}$.

	M_0 [GeV]	c_1 [GeV^{-1}]	$\tilde{e}_1^r/\,\dot{e}_1^r(1\,\mathrm{GeV})$ [GeV^{-3}]	χ^2/d.o.f.
Fit delta I	0.894 ± 0.004	-0.76 ± 0.05	4.5 ± 0.1	0.19
Fit delta II	0.873 ± 0.004	-1.08 ± 0.05	2.8 ± 0.2	0.43
Fit delta IIa	0.881 ± 0.004	-0.95 ± 0.06	2.0 ± 0.2	0.34

As discussed in Sec.3.2.3, in the "full" relativistic formula the decoupling of the delta is implemented only up to and including m_π^3 in the chiral expansion and, at m_π^6 and m_π^8, there is a residual scale dependence due to missing counterterms. We fit with three free parameters: M_0, c_1 and the effective coupling $\dot{e}_1^r(1\,\mathrm{GeV})$, which appears in the counterterm $-4\dot{e}_1 m_\pi^4 \bar{\Psi}\Psi$ in Eq.(3.34). In Fit delta II we fix $c_A = 1.5$, $\Delta = 271.1\,\mathrm{MeV}$, $g_A^0 = 1.267$ and $f_\pi^0 = 92.4\,\mathrm{MeV}$, see Table 3.3 and Fig.3.9. For Fit delta IIa, $c_A = 1.125$. The LEC c_1 comes out larger in magnitude than in Fit delta I, and correspondingly $\sigma_N = 57 \pm 4\,\mathrm{MeV}$ since the pion-nucleon sigma-term is basically driven by c_1, see Sec.3.5. However, both of them are still compatible with present knowledge from low-energy hadron phenomenology (see Sec.2.9 and Sec.3.5). If we vary the regularization scale within a broad range around 1 GeV and keep equal to zero the finite parts of higher-order counterterms *at the scale at which we are working*, the output parameters M_0 and c_1 are pretty stable (within error bars). The residual scale dependence is basically absorbed by $\dot{e}_1^r(\lambda)$. Our analysis shows that the differences in the outcome between Fit delta I and Fit delta II can be fairly attributed to higher order effects.

In Fig.3.9 we plot the curves corresponding to Fit delta I and Fit delta II, together with 68% error band in Fig.3.8. At that confidence level, BChPT $\mathcal{O}(p^4)$ and $\mathcal{O}(\epsilon^3)$ SSE are compatible, for the whole range of pion masses under study: treating the $\Delta\,(1232)$ as a propagating field is not essential for a satisfactory description of the quark mass dependence of the nucleon mass. An equally successful interpolating function can be obtained by "freezing" the delta effects into LECs. In other words, for the nucleon mass, the graphs describing the exchange of a $\Delta\,(1232)$ are adequately represented by those terms of the chiral expansion that occur up to and including $\mathcal{O}(p^4)$. These conclusions hold for any choice of the input parameters, within phenomenologically motivated ranges for them.

3.4 Conclusions after the numerical analysis

The results of our study can be stated as follows:

- There exists a range of overlap in m_q accessible both to one-loop baryon ChPT and present full-QCD lattice calculations. Interpolations between this range and the physical region of small m_q are feasible.

- The parameters resulting from the interpolation are consistent with the constraints imposed by low-energy hadron phenomenology.

- There is a decreasing hierarchy among contributions of increasing orders.

- For a correct description of the quark mass dependence of the nucleon mass, it is not essential that the $\Delta\,(1232)$ is incorporated as a dynamical field in the effective Lagrangian. Its contribution is effectively accounted for through low-energy couplings.

3.5 The pion-nucleon sigma term

As already mentioned in Sec.3.1, the pion-nucleon sigma term σ_N is defined as the nucleon scalar form factor $\sigma_N(t)$ at zero momentum transfer,

$$\sigma_N \equiv \sigma_N(0) = \langle N_s(\vec{p}\,)\,|m_u\bar{u}u + m_d\bar{d}d|\,N_s(\vec{p}\,)\rangle\ . \tag{3.51}$$

If the nucleon (eigen)states have a continuous dependence on the parameter $m_q = m_{u,d}$, then the Feynman-Hellmann theorem leads to

$$\sigma_N = m_q\,\frac{\partial M_N}{\partial m_q} \tag{3.52}$$

where we have neglected isospin breaking effects setting $m_u = m_d = m_q$. Hence σ_N is a measure of the strength of the light quark scalar density in the nucleon and it is the response of the nucleon mass to a variation in the light quark masses which are related to the *explicit* chiral symmetry breaking in QCD. Making use of the Gell-Mann – Oakes – Renner relation (2.50), we obtain,

$$\sigma_N = m_\pi^2 \frac{\partial M_N}{\partial m_\pi^2}\ . \tag{3.53}$$

Applying Eq.(3.53) to the $\mathcal{O}(p^3)$ expression for M_N in Eq.(3.23) yields

$$\begin{aligned}\sigma_N =& -4c_1\,m_\pi^2 - \frac{9{g_A^0}^2}{64\pi f_\pi^{0\,2}}\,m_\pi^3 + 2e_1^r(\lambda)m_\pi^4 - \frac{3{g_A^0}^2}{64\pi^2 f_\pi^{0\,2}M_0}\left(3 + 4\ln\frac{m_\pi}{\lambda}\right)m_\pi^4 \\ &+ \frac{15{g_A^0}^2}{512\pi f_\pi^{0\,2}M_0^2}\,m_\pi^5 + \mathcal{O}(m_\pi^6)\ .\end{aligned} \tag{3.54}$$

The next-to-next-to-leading-order result derives from Eq.(3.29) [3]:

$$\sigma_N = -4c_1\, m_\pi^2 - \frac{9{g_A^0}^2}{64\pi f_\pi^{0\,2}}\, m_\pi^3 + \left[2e_1^r(\lambda) - \frac{1}{16\pi^2 f_\pi^{0\,2}}\left(\frac{9g_A^2}{4M_0} - 6c_1 + 3c_3\right) - \frac{3}{16\pi^2 f_\pi^{0\,2}}\left(\frac{{g_A^0}^2}{M_0} - 8c_1 + c_2 + 4c_3\right)\ln\frac{m_\pi}{\lambda}\right] m_\pi^4 + \frac{15{g_A^0}^2}{512\pi f_\pi^{0\,2} M_0^2}\, m_\pi^5 + \mathcal{O}(m_\pi^6)\ . \tag{3.55}$$

In Table 3.4 we collect values for $\sigma_N(m_\pi^{\rm phys})$ from fits to $M_N(m_\pi)$. The contribution from the term proportional to m_π^5 in Eqs.(3.54, 3.55) amounts to about 0.1 MeV. All our estimates lie within the most widely accepted range for the empirical σ_N, as we now going to discuss.

Table 3.4: πN sigma-terms deduced from Fits to $M_N(m_\pi)$, see Tables 3.2-3.3.

	σ_N [MeV]
Fit I	43 ± 4
Fit II	49 ± 3
Fit IIa	58 ± 3
Fit delta I	39 ± 4
Fit delta II	57 ± 4

To relate the pion-nucleon sigma-term to phenomenology, consider the standard representation for the πN amplitude:

$$T_{\pi N} = \bar u(p')\,[A(\nu,t) + \frac{1}{2}\gamma^\mu(q+q')_\mu\, B(\nu,t)]\, u(p)\ , \tag{3.56}$$

where q_μ and q'_μ are the four-momenta of the incoming and outgoing pion, respectively. The crossing variable ν is given by

$$\nu = \frac{s-u}{4M_N} \tag{3.57}$$

in terms of the Mandelstam variables s and u, see Sec.2.9. The amplitude D is defined as

$$D(\nu,t) = A(\nu,t) + \nu B(\nu,t)\ . \tag{3.58}$$

The isoscalar $(+)$ and the isovector $(-)$ combinations $D^\pm$ are related to the amplitudes in the physical channels,

$$D^\pm = \frac{1}{2}(D_{\pi^- p} \pm D_{\pi^+ p})\ . \tag{3.59}$$

[3] For an analogous calculation in $SU(3)$ Heavy-Baryon ChPT see Ref. [136].

Chiral symmetry connects the nucleon scalar form factor to the isoscalar πN scattering amplitude $\bar{D}^+(\nu,t)$ at the Cheng-Dashen point, $\nu = 0$ and $t = 2m_\pi^2$ [127]. The bar over D^+ indicates that the pseudovector Born term has been subtracted. In particular, we have

$$\Sigma \equiv f_\pi^2\, \bar{D}^+(\nu = 0, t = 2m_\pi^2) = \sigma_N(0) + \Delta_\sigma + \Delta_R\ . \tag{3.60}$$

Here Δ_R is the so-called remainder term. An $\mathcal{O}(p^4)$ HBChPT calculation, with pertinent LECs saturated via resonance exhange, yields the upper limit $\Delta_R \approx 2\,\mathrm{MeV}$ [128]. Δ_σ is the shift of the nucleon scalar form factor from $t = 2m_\pi^2$ to $t = 0$,

$$\Delta_\sigma = \sigma(2m_\pi^2) - \sigma(0)\ . \tag{3.61}$$

Its value, about 15 MeV, has been extracted from a $\pi\pi$ and πN dispersion relation analysis [129] and confirmed by a calculation in $SU(2)$ BChPT with infrared regularization [57].

The Cheng-Dashen point lies outside the physical πN scattering region: the experimental $\bar{D}^+$ amplitude must be extrapolated to obtain Σ. The most reliable estimates are based on dispersion relation analyses of the scattering amplitudes. The result in Ref. [130], $\Sigma = 64 \pm 8\,\mathrm{MeV}$, has been obtained using hyperbolic dispersion relations; in Ref. [131], from the subthreshold expansion of $\bar{D}^+$, $\Sigma \simeq 60\,\mathrm{MeV}$.

Using as input $\Sigma = 64 \pm 8\,\mathrm{MeV}$ Gasser, Leutwyler and Sainio, according to their estimate of Δ_σ, obtained $\sigma_N = 45 \pm 8\,\mathrm{MeV}$ [63]. In Fig.3.10 we plot the behaviour of the sigma term as a function of the pion mass in $SU(2)$ BChPT, as it comes out from the expression of the pion mass dependence of the nucleon mass at order p^4, Eq.(3.29), and from Fit IIa. Within errors, this curve is perfectly compatible with the empirical value of the pion-nucleon sigma-term in Ref. [63]. This is a non-trivial fact since no such constraint has been built into the procedure. Our result is also consistent with the broad range for σ_N quoted in Ref. [123]: by fitting finite-range regulated expressions for $M_N(m_\pi)$ to CP-PACS lattice data [111] up to 1 GeV in m_π, the Adelaide group gets $\sigma_N = 35 - 73\,\mathrm{MeV}$, depending on the choice of the regulator.

The SESAM collaboration tried to determine σ_N directly on the lattice, by evaluating $\langle N|\bar{u}u + \bar{d}d|N\rangle$. They performed a two-flavor full-QCD calculation of this matrix element, reconstructed the scale invariant quantity $m_q\,\langle N|\bar{u}u + \bar{d}d|N\rangle$ and extrapolated from the simulated large quark mass to the physical one, without resorting to any formula motivated by ChPT [132]. They obtained $\sigma_N = 18 \pm 5\,\mathrm{MeV}$. This result illustrates how difficult *this* procedure is. Our approach in extracting a value for σ_N from the lattice is indirect, but has the important advantage that one only needs to work with renormalization-group invariant quantities.

Coming back to phenomenology, we point out that the estimates of Σ quoted above refer to the KH80 solution of the relevant dispersion relations by the Karlsruhe group [133]. The VPI/GWU group has recently published the outcome of a partial wave analysis [64] which indicates that Σ could be 20-30% larger than the numbers reported above [134]: these results are currently under debate and the issue about Σ is still open. On-going

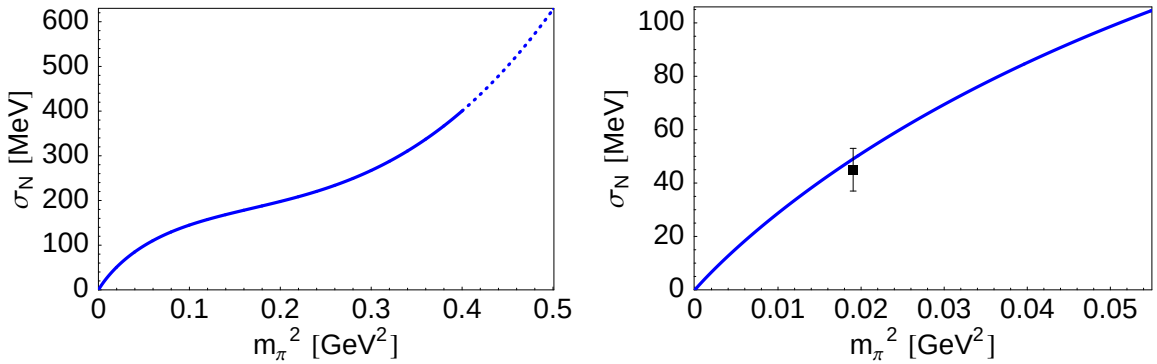

Figure 3.10: The pion-nucleon sigma-term at chiral order p^4 as a function of m_π^2 from Eq.(3.55), using as input the central values from Fit II, see Table 3.2. The small m_π region is magnified in the right panel and plotted together with the empirical value $\sigma_N = 45 \pm 8\,\mathrm{MeV}$ of Ref. [63].

novel analysis of meson-factory data should help in fixing the value of this quantity more accurately [131].

A pion-nucleon sigma-term of 60 MeV or more is disfavored by our analysis and gives puzzingly large values for the strangeness fraction y. The parameter y is defined by

$$\sigma_N = \frac{\langle N|m_q\,(\bar{u}u + \bar{d}d - 2\bar{s}s)|N\rangle}{1-y} \tag{3.62}$$

from which

$$y = \frac{2\,\langle N|\bar{s}s|N\rangle}{\langle N|\bar{u}u + \bar{d}d|N\rangle}\ . \tag{3.63}$$

The Okubo–Zweig–Iizuka (OZI) rule and any naive quark model picture of the nucleon would imply $y = 0$. This parameter is a measure of the (scalar) strange quark content of the nucleon. Under the assumption that $SU(3)$ symmetry breaking is *small*, ChPT determines the combination $(1-y)\,\sigma_N$. At first order,

$$(1-y)\,\sigma_N = \frac{m_q}{m_s - m_q}\,(M_\Xi + M_\Sigma - 2M_N)\ . \tag{3.64}$$

Including one-loop corrections in $SU(3)$ HBChPT [135, 136], together with $\sigma_N = (45 \pm 8)\,\mathrm{MeV}$, one gets $y \approx 0.2 \pm 0.2$. This result is affected by large uncertainties and has to be interpreted as a *qualitative* result: it can indicate a non-vanishing admixture of strange quark pairs in the nucleon wave-function but it is also compatible with zero. In order to shed light on this issue, an analysis of lattice data with three active flavors seems to be mandatory. In particular, from the quark mass expansion of the nucleon mass, one gets the expression

$$y = 2\,\frac{\partial M_N}{\partial m_s}\left(\frac{\partial M_N}{\partial m_q}\right)^{-1} \tag{3.65}$$

which allows for a direct determination of y from $M_N = M_N(m_u, m_d, m_s)$.

Strictly speaking there is no reason *a priori* for the matrix element $\langle N|\bar{s}s|N\rangle$ to be small, apart from the OZI rule. In spite of a large "strangeness content" y (somehow a misleading term), the *total* contribution of the strange to the nucleon mass can be small. In Ref. [137] Ji evaluated $\langle N|m_s\bar{s}s|N\rangle$ adopting two approaches. Treating the strange quark mass as small with respect to QCD scale and using ChPT to calculate $SU(3)$ symmetry breaking effects, he got about 115 MeV for the matrix element of interest. Considering instead the strange quark as heavy on the QCD scale and using heavy-quark expansion, Ji found a value about 62 MeV. These numbers do not take into account higher-order perturbative effects and errors on the sigma term and the current quark masses. However, the total effect of such errors is quantified as about 5 to 10 MeV [137]. Ji argues that the *total* strange contribution to the nucleon mass is quite small, between -45 and -30 MeV. This result has been obtained by summing up the contribution of the strange quark to the trace anomaly term, the contributions to the mass term and to the quark and antiquark kinetic and potential energies. The smallness of the result is, to a large extent, insensitive to the precise value of the matrix element $\langle N|m_s\bar{s}s|N\rangle$ [137].

Chapter 4

Quark mass dependence of g_A

In this chapter we investigate the quark mass dependence of the nucleon axial-vector coupling constant both in $SU(2)$ Baryon ChPT (BChPT) and in the Small Scale Expansion (SSE), at one-loop order.

Historically, attempts to obtain a chiral extrapolation function for g_A based on the leading-non-analytic (LNA) term in the quark-mass expansion in combination with a phenomenological (quark-mass dependent) regularization procedure did not yield satisfactory results, displaying axial couplings less than unity at the physical point [138]. We will show that the LNA quark-mass behavior dominates only for quark masses which are extremely close to the chiral limit of the theory. Such a feature has also been observed in the quark-mass expansion of the anomalous magnetic moment of the nucleon [139]. More recently, Detmold *et al.* [140], in their analysis of moments of polarized deep inelastic scattering structure functions, found an improved extrapolation formula for $g_A(m_\pi)$ using a chiral quark model which also allows for contributions from intermediate $\Delta\,(1232)$ states [141]. However, the resulting extrapolation function – which has most of the $\Delta\,(1232)$ related couplings fixed from SU(4) spin-flavor symmetry – still does not provide an enhancement of $g_A(m_\pi)$ near the physical point, which would at the same time connect lattice results with the real world. In our analysis we specify a power counting scheme plus a certain order in that scheme and then systematically evaluate all (short- and long-distance) contributions to that order. We then apply those results to chiral extrapolations of present lattice data.

4.1 g_A in QCD and in ChEFT

Let us consider the on-shell nucleon matrix element of an isovector axial-vector field $A^i_\mu(x)$. Lorentz invariance and parity conservation require this matrix element to take the form

$$\langle N(p_2)|A^i_\mu(0)|N(p_1)\rangle = \bar{u}(p_2)\left[G_A(Q^2)\gamma_\mu\gamma_5 + \frac{G_P(Q^2)}{2M_N}q_\mu\gamma_5 + i\frac{G_T(Q^2)}{2M_N}\sigma_{\mu\nu}\gamma_5 q^\nu\right]u(p_1)\,\eta^\dagger\frac{\tau^i}{2}\eta$$

where $u(p)$ is the nucleon Dirac spinor and η is a unit (two-component) isospinor. The momentum transfer is $q \equiv p_2 - p_1$ and $Q^2 \equiv -q^2$. The form factors $G_A(Q^2)$, $G_P(Q^2)$ and $G_T(Q^2)$ reflect the structure of the nucleon as seen by a probing external axial field.

According to time reversal invariance the phases are chosen so that each form factor is a real function of Q^2. The nucleon mass M_N is introduced for dimensional convenience.

Consider the specific case of the isovector axial-vector current

$$A^i_\mu = \bar{\psi}_q \gamma_\mu \gamma_5 \frac{\tau^i}{2} \psi_q \tag{4.1}$$

where ψ_q is the $(u,d)^T$ quark isospin doublet. This operator enters into strangeness conserving semileptonic weak interactions like nuclear β-decay $^{14}O \to {}^{14}N^* + e^+ + \nu_e$, muon capture $\mu^- + p \to \nu_\mu + n$, neutrino scattering $\bar{\nu}_\mu + p \to \mu^+ + n$. The charge changing currents $A^\mu_\pm = A^\mu_1 \pm i A^\mu_2$ have charge conjugation properties that make the coefficient G_T of the axial tensor term vanishing. Such term would violate G-parity invariance, but the existence of second-class currents [142] is experimentally excluded to high precision [143].

g_A is defined as the limit for vanishing momentum transfer of the nucleon axial form factor $G_A(Q^2)$. The most suitable process to determine the empirical value of g_A is the β-decay since the momentum transfer in this reaction is so small that in the nucleon matrix element of the axial current only the axial-vector piece contributes. The neutron-to-proton matrix element of the charged hadronic weak current in the zero-momentum transfer limit is

$$\cos\theta_C \, \langle p | V^\mu_+(0) - A^\mu_+(0) | n \rangle = \bar{u}_p (g_V \gamma^\mu - g_A \gamma^\mu \gamma_5) u_n \ , \tag{4.2}$$

where θ_C is the Cabibbo angle. The vector part of the hadronic weak current belongs to a triplet of conserved currents $V^\mu_{1,2,3}$ associated with the isospin symmetry of the strong interactions (Conserved Vector Current (CVC) hypothesis [144]). If isospin is an *exact* symmetry, then $g_V = 1$ in units of $\cos\theta_C$. Moreover, according to CVC, g_V is equal (in units of e and $\cos\theta_C$) to the isovector combination of proton and neutron Dirac form factors. While any deviation of g_V from unity is a signal of breakdown of the CVC hypothesis, g_A is not related to any manifestly conserved charge and in general deviates from 1 because of spontaneous and explicit chiral symmetry breaking, as we will show in Sec.4.4.3. The most accurate determination of the ratio g_A/g_V from β-decay gives [13]

$$g_A/g_V = 1.2695 \pm 0.0029 \ . \tag{4.3}$$

g_A is called the axial-vector coupling constant of the nucleon due to the form of the first order πN effective Lagrangian, see Eq.(2.64). In ChEFT g_A is calculated from the response of the nucleon to the presence of an external axial field [1]. As we will show in the next section, the leading term in the quark-mass expansion of the nucleon axial form factor for vanishing momentum transfer is precisely the coupling g^0_A appearing in $\mathcal{L}^{(1)}_{\pi N}$.

g_A is also related to the nucleon spin structure function $g_1^{p,n}(x,Q^2)$ defined in deep inelastic lepton scattering processes where both beam and target are polarized. The

[1] Cf. for example the pioneering works [47, 145].

structure functions measured in deep inelastic scattering are related to the nucleon matrix element of the correlation function of two currents

$$T_{\mu\nu} = i \int d^4z \, \langle N(P')|T\{J_\mu(z)\, J_\nu(0)\}|N(P)\rangle \ . \tag{4.4}$$

Using the Operator Product Expansion we can express the nonlocal product of currents as a series of local operators and relate moments of structure functions to matrix elements of certain operators in a twist expansion. For the polarized structure function $g_1(x, Q^2)$ we are dealing with local twist-2 operators

$$\mathcal{O}^{5,\sigma\mu_1\ldots\mu_n} = \left(\frac{i}{2}\right)^n \psi\gamma^{\{\sigma}\gamma^5 D^{\mu_1}\ldots D^{\mu_n\}}\psi - \text{traces} \tag{4.5}$$

where all the indices are symmetrized. The expression is made traceless on all pairs of indices by subtracting contractions with the metric tensor $g^{\mu_i\mu_j}$. Lorentz invariance requires

$$\langle N(\vec{p},s)|\mathcal{O}^{5,\sigma\mu_1\ldots\mu_n}|N(\vec{p},s)\rangle = \frac{2}{n+1}\, a_n(s^\sigma p_1^\mu \ldots p_n^\mu - \text{traces}) \tag{4.6}$$

where s^σ is the covariant spin vector.

The n-th moment of the structure function $g_1(x, Q^2)$ is then related both to the nucleon matrix element of the leading twist operator and to the Wilson coefficients $E^{\overline{\rm MS}}(Q^2/\mu^2, g^{\overline{\rm MS}}(\mu))$ which can be evaluated using perturbative QCD:

$$2\int_0^1 dx\, x^n g_1^{p-n}(x,Q^2) = \sum_f E_{g1;n}^{(f)\,\overline{\rm MS}}\left(\frac{Q^2}{\mu^2}, g^{\overline{\rm MS}}(\mu)\right) a_n^{(f)\,\overline{\rm MS}}(\mu) + \mathcal{O}\left(\frac{1}{Q^2}\right) \ . \tag{4.7}$$

Here we consider the flavor $f = u, d$ and non-singlet or "p−n" matrix elements. The a_n have an interpretation in the parton model. For $n = 0$ the structure of the operator in Eq.(4.5) is the same as in Eq.(4.1). g_A is therefore related to the zeroth-order moment of $g_1^{p-n}(x, Q^2)$, cf. the Bjorken sum rule [146]. In the parton model language g_A amounts to the difference between the "spin fractions" carried by quark u and quark d,

$$g_A = \Delta u - \Delta d \tag{4.8}$$

where

$$\Delta q = \int_0^1 dx\, [q_\uparrow(x,\mu) - q_\downarrow(x,\mu) + \bar{q}_\uparrow(x,\mu) - \bar{q}_\downarrow(x,\mu)] \ . \tag{4.9}$$

Δq is μ-independent according to the DGLAP [147–149] equation, cf. for example Ref. [150].

4.2 Analytic results in BChPT

In order to work out the vertices relevant for our calculation, in the effective Lagrangian we have to look at the term linear in the external axial field $a_\mu(x)$: this a hermitian color-neutral 2×2 matrix in flavor space, which can be written as

$$a_\mu(x) = a_\mu^i(x)\,\frac{\tau^i}{2} \tag{4.10}$$

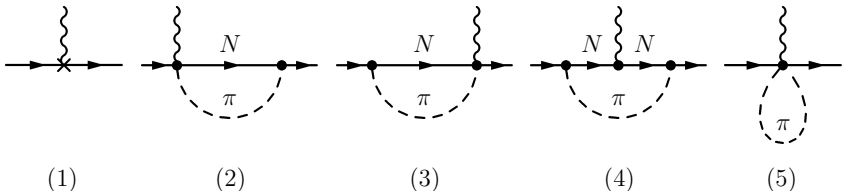

Figure 4.1: Diagrams contributing to the quark mass dependence of g_A up to order p^3. The wiggly line denotes an external isovector axial-vector field, interacting with a nucleon (solid line). In the loop graphs all the vertices belong to the leading πN Lagrangian $\mathcal{L}^{(1)}_{\pi N}$. Wave-function renormalization effects are shown in Fig.4.2. Graph (1) encodes contributions from the counterterms.

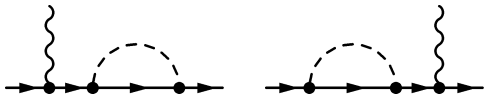

Figure 4.2: Nucleon field renormalization contributions at order p^3. All the vertices appear in $\mathcal{L}^{(1)}_{\pi N}$.

where τ^i denote the Pauli matrices acting on the isospin indices.

The leading-one-loop contribution to g_A is represented by the graphs in Fig.4.1. In order to simplify the calculation, we have made use of the gauge condition $a_\mu q^\mu = 0$, without any loss of generality. The detailed form of the relevant amplitudes can be found in Appendix D.

At order p^3, nucleon field renormalization contributes in the way shown in Fig.4.2. At this level of accuracy

$$\Sigma(\not{p} = M_N) \approx \Sigma(\not{p} = M_0) \ , \tag{4.11}$$

which implies

$$Z_N \approx 1 + \left.\frac{\partial \Sigma_a}{\partial \not{p}}\right|_{\not{p}=M_0} \ . \tag{4.12}$$

Here Σ_a is the nucleon self-energy at order p^3, according to the notation in Sec.3.2.1.

Using Eq.(3.20) and infrared regularization, we obtain

$$\begin{aligned} Z_N = 1 - \frac{1}{32\pi^2 f_\pi^2 M_0^3 \sqrt{4 - m_\pi^2/M_0^2}} \Bigg\{ 3 {g_A^0}^2 m_\pi^2 \Bigg[(2m_\pi^3 - 6M_0^2 m_\pi) \arccos\left(-\frac{m_\pi}{2M_0}\right) \\ + M_0 \sqrt{4 - \frac{m_\pi^2}{M_0^2}} \left(48 L(\lambda) \pi^2 M_0^2 + M_0^2 + (3M_0^2 - 2m_\pi^2) \ln \frac{m_\pi}{\lambda} - 32 L(\lambda) m_\pi^2 \pi^2 \right) \Bigg] \Bigg\} \\ - 8 B_{20} m_\pi^2 + 32\, F_2\, m_\pi^4 \ , \end{aligned} \tag{4.13}$$

where $L(\lambda)$ subsumes any ultraviolet divergence for $d \to 4$, Eq.(C.2). F_2 denotes a fifth-order counterterm needed to absorb the divergence proportional to m_π^4. Expanding

around the chiral limit we have

$$Z_N = 1 + \left(-\frac{9{g_A^0}^2 L(\lambda)}{2f_\pi^2} - \frac{9{g_A^0}^2}{32\pi^2 f_\pi^2} \ln\frac{m_\pi}{\lambda} - \frac{3{g_A^0}^2}{32\pi^2 f_\pi^2} \right) m_\pi^2 - 8B_{20} m_\pi^2 + \frac{9{g_A^0}^2 m_\pi^3}{64 f_\pi^2 M_0 \pi}$$
$$+ \frac{3{g_A^0}^2}{64 f_\pi^2 M_0^2 \pi^2} (64\pi^2 L(\lambda) + 3 + 4\ln\frac{m_\pi}{\lambda})\, m_\pi^4 + 32\, F_2\, m_\pi^4 + \mathcal{O}(m_\pi^5) \ , \tag{4.14}$$

which up to and including the m_π^3 term coincides with the result in the Heavy Baryon formalism [151]. For a detailed discussion on Z_N in the non-relativistic framework we refer to [152].

Projecting out the contributions to g_A from the leading-one-loop amplitudes in Fig.4.1, we obtain the following expression in terms of the basic integrals I_N and Δ_π in Appendix C:

$$g_A = g_A^0 Z_N + \Delta_\pi \left(\frac{{g_A^0}^3}{4f_\pi^2} - \frac{g_A^0}{f_\pi^2} \right) + \frac{{g_A^0}^3 m_\pi^2}{32 f_\pi^2 \pi^2} + 4\, B_9\, m_\pi^2 + \left(\frac{{g_A^0}^3}{4f_\pi^2} - \frac{2g_A^0}{f_\pi^2} \right) m_\pi^2\, I_N$$
$$- \frac{{g_A^0}^3 m_\pi^4}{64\pi^2 f_\pi^2 M_0^2} + \frac{{g_A^0}^3 m_\pi^4}{8 f_\pi^2 M_0} \left. \frac{\partial}{\partial M_0} I_N(p^2) \right|_{p^2 = M_0} + 32\, F_1\, m_\pi^4 \ . \tag{4.15}$$

B_9 is the third-order counterterm defined in Eq.(2.92) and F_1 takes care of a divergence at m_π^4.

Substituting Z_N appearing in Eq.(4.15) with Eq.(4.13), our result at order p^3 is

$$g_A = \frac{1}{16\pi^2 f_\pi^2 M_0^3 \sqrt{4 - m_\pi^2/M_0^2}} \left\{ g_A^0 m_\pi^3 (8({g_A^0}^2 + 1) M_0^2 - (3{g_A^0}^2 + 2) m_\pi^2) \arccos\left(-\frac{m_\pi}{2M_0} \right) \right.$$
$$- M_0 \sqrt{4 - \frac{m_\pi^2}{M_0^2}} \left[M_0^2 m_\pi^2 {g_A^0}^3 + (m_\pi^4 - 16 f_\pi^2 M_0^2 \pi^2) g_A^0 \right.$$
$$\left. \left. + g_A^0 ((4{g_A^0}^2 + 2) M_0^2 - (3{g_A^0}^2 + 2) m_\pi^2) m_\pi^2 \ln\frac{m_\pi}{\lambda} - 64 C^r(\lambda) f_\pi^2 M_0^2 m_\pi^2 \pi^2 \right] \right\}$$
$$+ 32 F^r(\lambda) m_\pi^4 \ . \tag{4.16}$$

$C^r(\lambda) \equiv B_9^r(\lambda) - 2g_A^0 B_{20}^r(\lambda)$ and $F^r(\lambda) = F_1^r(\lambda) + F_2^r(\lambda)$ are the renormalized, regularization scale λ dependent parts of the corresponding couplings. They encode short-distance dynamics effects and scale in such a way that the right-hand side of Eq.(4.16) is scale independent:

$$C^r(\lambda) = B_9 - 2g_A^0 B_{20} - \frac{L(\lambda)}{f_\pi^2} \left(\frac{1}{2} g_A^0 + {g_A^0}^3 \right) \tag{4.17}$$

$$F^r(\lambda) = F + \frac{L(\lambda)}{32 f_\pi^2 M_0^2}\, g_A^0 (2 + 3{g_A^0}^2) \ . \tag{4.18}$$

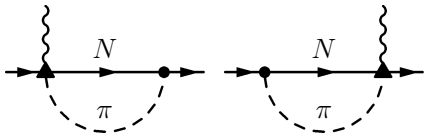

(6) (7)

Figure 4.3: One-particle-irreducible fourth order diagrams contributing to g_A at the next-to-leading one-loop level. The triangle denotes a vertex appearing in $\mathcal{L}^{(2)}_{\pi N}$.

B_{20} absorbs the divergence proportional to m_π^2 in the nucleon Z-factor. The corresponding term in the third-order Lagrangian can be eliminated through a field redefinition. Therefore the finite part of this coupling cannot be observed independently (of $B_9^r(\lambda)$ in our case).

The factor 32 in the fifth-order counterterm emphasizes that F is the LEC to which one should apply "naive" dimensional arguments, cf. [28] and Sec.2.5. The effective πN Lagrangian at order p^5 can indeed contribute via

$$\mathcal{L}_N^{(5)} = f\,\bar\Psi[\mathrm{Tr}(\chi_+)]^2\,\not{v}\gamma_5\Psi + \cdots \approx 32 f m_\pi^4\,\bar\Psi\frac{\tau^i}{2}a_\mu^i\gamma_\mu\gamma_5\Psi + \ldots \tag{4.19}$$

for which we expect $f = \mathcal{O}(1/\Lambda_\chi^4)$.

Expanding Eq.(4.16) around $m_\pi = 0$ we obtain

$$\begin{aligned} g_A = g_A^0 &+ \left[4\,C(\lambda) - \frac{{g_A^0}^3}{16\pi^2 f_\pi^2} - \frac{g_A^0 + 2{g_A^0}^3}{8\pi^2 f_\pi^2}\ln\frac{m_\pi}{\lambda}\right] m_\pi^2 + \frac{g_A^0 + {g_A^0}^3}{8\pi f_\pi^2 M_0} m_\pi^3 \\ &+ \left[32F(\lambda) + \frac{g_A^0 + 2{g_A^0}^3}{16\pi^2 f_\pi^2 M_0^2} + \frac{g_A^0(2+3{g_A^0}^2)}{16\pi^2 f_\pi^2 M_0^2}\ln\frac{m_\pi}{\lambda}\right] m_\pi^4 + \mathcal{O}(m_\pi^5)\,. \end{aligned} \tag{4.20}$$

The sum of the first two terms in this expansion coincides with the leading-one-loop expression for g_A in HBChPT, as expected in BChPT with infrared regularization. The relativistic calculation gives a full tower of "recoil corrections" in the form of increasing powers of $1/M_0$. We will test their numerical impact at the relatively large pion masses that can be presently handled in lattice QCD calculations. These recoil corrections are naturally part of the same chiral order p^3, but the terms starting with m_π^3 can be modified by higher orders, as we will show explicitly at $\mathcal{O}(p^4)$.

We include the counterterm $32\,F\,m_\pi^4$ in the third-order calculation in order to achieve renormalization without truncating the recoil corrections. Since contact terms *up to and including* $\mathcal{O}(p^3)$ cannot absorb higher-order divergences at m_π^4, their β-functions cannot compensate for scale dependence which is suppressed by two powers of $1/M_0$. By introducing the counterterm $32\,F\,m_\pi^4$, we remove this unphysical scale dependence.

Figure 4.4: c_1-insertion in a nucleon line. The diamond corresponds to the vertex $i\,4\,c_1 m_\pi^2$ from $\mathcal{L}^{(2)}_{\pi N}$.

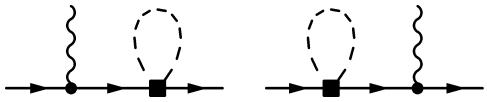

Figure 4.5: One-particle-reducible graphs contributing to g_A at order p^4. The square denotes a vertex from $\mathcal{L}^{(2)}_{\pi N}$ involving c_1, c_2 and c_3.

The next-to-leading one-loop result $\mathcal{O}(p^4)$ is obtained again through the evaluation of both one-particle irreducible and reducible graphs. The former are shown in Fig.4.3. The triangle there denotes a vertex from the second order πN Lagrangian $\mathcal{L}^{(2)}_{\pi N}$ containing the two LECs c_3 and c_4. The explicit expressions of amplitudes (6) and (7) are given in Appendix D.

The reducible graphs are evaluated through nucleon field and mass renormalization, consistently with the accuracy at which we are working. We draw as a diamond the second order insertion in the nucleon line proportional to c_1, Fig.4.4. At order p^4 we have to compute all the graphs resulting from the insertion of *at most one* c_1 vertex in *at most one* nucleon line in the diagrams (2), (3) and (4) in Fig.4.1 and in those of Fig.4.2. Since for small m_π

$$\frac{i}{\not p - M_0 - 4\,c_1 m_\pi^2} = \frac{i}{\not p - M_0} + \frac{i}{\not p - M_0}\,(i\,4\,c_1 m_\pi^2)\,\frac{i}{\not p - M_0} + \dots\ , \tag{4.21}$$

we can summarize the c_1-insertions by a simple shift of the pole of the nucleon propagator from the "bare" nucleon mass to its renormalized value at second chiral order,

$$M_N = M_0 - 4\,c_1 m_\pi^2 + \mathcal{O}(p^3)\ . \tag{4.22}$$

Since at most *one* c_1-insertion is allowed at fourth order, we have worked out the relevant amplitudes through the shift $M_0 \to M_N$ and extract the contribution to g_A looking at the expansion of the result in powers of c_1: only the terms up to and including the one linear in c_1 have been retained, cf. Appendix D.

The remaining reducible $\mathcal{O}(p^4)$ graphs are drawn in Fig.4.5. The evaluation of these amplitudes is done through nucleon wave-function renormalization, cf. Appendix D.

The pion mass dependence of g_A at order p^4 is finally given by

$$
\begin{aligned}
g_A = \frac{1}{576\pi^2 f_\pi^2 M_0^4 (4M_0^2 - m_\pi^2)\sqrt{4 - m_\pi^2/M_0^2}} \Big\{ & 12 g_A^0 (-128(c_3 - 2c_4) M_0^6 + 96({g_A^0}^2 + 1) M_0^5 \\
& + 96(c_3 - c_4 + 4c_1({g_A^0}^2 + 1)) m_\pi^2 M_0^4 - 12(5{g_A^0}^2 + 4) m_\pi^2 M_0^3 \\
& - 24(c_3 + 6c_1(3{g_A^0}^2 + 2)) m_\pi^4 M_0^2 + 3(3{g_A^0}^2 + 2) m_\pi^4 M_0 \\
& + 2(c_3 + c_4 + 12c_1(3{g_A^0}^2 + 2)) m_\pi^6) \arccos\left(-\frac{m_\pi}{2M_0}\right) m_\pi^3 + M_0 \sqrt{4 - \frac{m_\pi^2}{M_0^2}} \Big[-432 c_1 {g_A^0}^3 m_\pi^8 \\
& + 20 c_3 g_A^0 m_\pi^8 + 20 c_4 g_A^0 m_\pi^8 + 1152 c_1 {g_A^0}^3 M_0^2 m_\pi^6 - 27 c_2 g_A^0 M_0^2 m_\pi^6 - 176 c_3 g_A^0 M_0^2 m_\pi^6 \\
& - 32 c_4 g_A^0 M_0^2 m_\pi^6 + 36 g_A^0 M_0 m_\pi^6 + 108 c_2 g_A^0 M_0^4 m_\pi^4 + 384 c_3 g_A^0 M_0^4 m_\pi^4 - 192 c_4 g_A^0 M_0^4 m_\pi^4 \\
& + 36 {g_A^0}^3 M_0^3 m_\pi^4 - 144 g_A^0 M_0^3 m_\pi^4 - 2304 C^r(\lambda) f_\pi^2 M_0^3 \pi^2 m_\pi^4 - 144 {g_A^0}^3 M_0^5 m_\pi^2 \\
& - 12 g_A^0 (m_\pi^2 - 4M_0^2)(2(36 c_1 {g_A^0}^2 + 24 c_1 + c_3 + c_4) m_\pi^4 - 3(3c_2 + 4c_3 - 4c_4) M_0^2 m_\pi^2 \\
& + 3(3{g_A^0}^2 + 2) M_0 m_\pi^2 - 6(2{g_A^0}^2 + 1) M_0^3) m_\pi^2 \ln\frac{m_\pi}{\lambda} + 9216 C^r(\lambda) f_\pi^2 M_0^5 \pi^2 m_\pi^2 \\
& - 576 f_\pi^2 g_A^0 M_0^3 \pi^2 m_\pi^2 + 2304 f_\pi^2 g_A^0 M_0^5 \pi^2 \Big] \Big\} + 32 F^r(\lambda) m_\pi^4 + 128 G^r(\lambda) m_\pi^6 \ . \qquad (4.23)
\end{aligned}
$$

$G^r(\lambda)$ is a seventh-order coupling appearing in the counterterm needed to absorb the divergence at m_π^6: this compensates the unphysical scale dependence at this power in m_π. The factor 128 is motivated by the fact that the effective πN Lagrangian at order p^7 can contribute via

$$
\mathcal{L}_N^{(7)} = g\, \bar\Psi [\mathrm{Tr}(\chi_+)]^3 \not{u} \gamma_5 \Psi + \cdots \approx 128\, g\, m_\pi^6\, \bar\Psi \frac{\tau^i}{2} a_\mu^i \gamma^\mu \gamma_5 \Psi + \ldots \qquad (4.24)
$$

"Naive" dimensional arguments suggest $g \approx 1/\Lambda_\chi^6$. At order p^4 we have

$$
F^r(\lambda) = F + \frac{L(\lambda)}{32 f_\pi^2 M_0^2} (3{g_A^0}^3 + 2g_A^0 - 3c_2 g_A^0 M_0 - 4c_3 g_A^0 M_0 + 4c_4 g_A^0 M_0) \qquad (4.25)
$$

$$
G^r(\lambda) = G + \frac{L(\lambda)}{128 f_\pi^2 M_0^3} (24 c_1 {g_A^0}^3 + 16 c_1 g_A^0 + \frac{2}{3} c_3 g_A^0 + \frac{2}{3} c_4 g_A^0) \ . \qquad (4.26)
$$

The expansion of the next-to-leading one-loop expression in Eq.(4.23) around the chiral limit gives

$$
\begin{aligned}
g_A = g_A^0 + & \left[4\, C(\lambda) - \frac{{g_A^0}^3}{16\pi^2 f_\pi^2} - \frac{g_A^0 + 2{g_A^0}^3}{8\pi^2 f_\pi^2} \ln\frac{m_\pi}{\lambda} \right] m_\pi^2 \\
& + \left(\frac{g_A^0 + {g_A^0}^3}{8\pi f_\pi^2 M_0} + \frac{2c_4 - c_3}{6\pi f_\pi^2} \right) m_\pi^3 + \left[\frac{4g_A^0 + 8{g_A^0}^3 + 16 c_4 g_A^0 M_0 + 3 c_2 g_A^0 M_0}{64\pi^2 f_\pi^2 M_0^2} + 32\, F(\lambda) \right. \\
& \left. + \frac{g_A^0 (2 + 3{g_A^0}^2 - 3c_2 M_0 - 4c_3 M_0 + 4c_4 M_0)}{16\pi^2 f_\pi^2 M_0^2} \ln\frac{m_\pi}{\lambda} \right] m_\pi^4 + \mathcal{O}(m_\pi^5) \ . \qquad (4.27)
\end{aligned}
$$

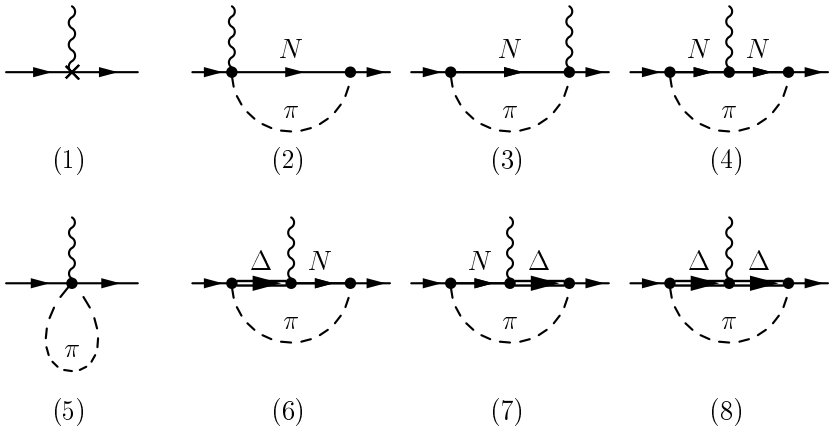

Figure 4.6: Diagrams contributing to the nucleon axial-vector coupling constant g_A at leading-one-loop order in SSE. The wiggly line denotes an external isovector axial-vector field. All the vertices shown here appear in the leading πN and $\pi N\Delta$ Lagrangians. Wave-function renormalization contributions are shown in Fig.4.7.

The sum of the first three terms coincides with the $\mathcal{O}(p^4)$ expression in HBChPT [152]. See also the results in covariant BChPT with infrared regularization for the nucleon axial form factor and g_A in Ref. [153].

4.3 Analytic results in SSE

We now turn to the result in the Small Scale Expansion approach, which includes explicit $\Delta\,(1232)$ degrees of freedom. The delta-nucleon mass difference (in the chiral limit) is treated as a small parameter and incorporated in the power counting in ϵ.

In this section we describe the $\mathcal{O}(\epsilon^3)$ formulae used for the numerical analysis, first in the manifestly covariant and then in the non-relativistic framework. For details on the formalism we refer the reader to Sec.2.10.

The bare result for the pion mass dependence of g_A at leading-one-loop order originates from diagrams 1-8 in Fig.4.6. Graphs (2) and (3) are non-vanishing when the intermediate nucleon is replaced by a spin-3/2 baryon. However, the *leading-order* $N\Delta$ transition Lagrangian in Eq.(2.120) does not include operators connecting $N\Delta$ via an even number of axial-vector fields. The corresponding diagrams are therefore of higher order than the graphs considered here.

Wave-function renormalization contributes at order ϵ^3 in the way shown in Figs.4.2 and 4.7. The resulting expressions for $g_A(m_\pi)$ and $Z_N(m_\pi)$, in manifestly Lorentz invariant SSE with infrared regularization, can be found in Appendix E, in terms of the basic loop integrals I_Δ, I_N and Δ_π in Appendix C.

Let us clarify the structure of the ultraviolet divergences in Eqs.(E.1) and (E.5) per-

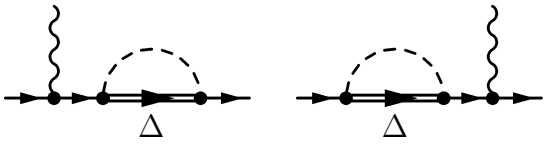

Figure 4.7: Nucleon field renormalization effects related to the propagation of the $\Delta\,(1232)$, at order ϵ^3.

forming an expansion of the terms proportional to L around the point $(0, \Delta)$ in the m_π-Δ plane. For the Z-factor we get

$$\begin{aligned} Z_N^{\rm inf} = &\left(\frac{16c_A^2\,L\Delta^2}{f_\pi^2} + \frac{344c_A^2\,L\Delta^3}{9f_\pi^2 M_0} + \frac{100c_A^2\,L\Delta^4}{3f_\pi^2 M_0^2} + \mathcal{O}(\Delta^5)\right) \\ &+ \left(-\frac{8c_A^2\,L}{f_\pi^2} - \frac{116c_A^2\,L\Delta}{3f_\pi^2 M_0} - \frac{172c_A^2\,L\Delta^2}{3f_\pi^2 M_0^2} + \mathcal{O}(\Delta^3)\right) m_\pi^2 \\ &+ \left(\frac{74c_A^2 L}{3f_\pi^2 M_0^2} + \frac{62c_A^2\,L\Delta}{3f_\pi^2 M_0^3} + \frac{18c_A^2\,L\Delta^2}{f_\pi^2 M_0^4} + \mathcal{O}(\Delta^3)\right) m_\pi^4 \\ &+ \left(-\frac{112c_A^2\,L}{9f_\pi^2 M_0^4} + \frac{28c_A^2\,L\Delta}{3f_\pi^2 M_0^5} + \mathcal{O}(\Delta^2)\right) m_\pi^6 \\ &+ \left(\frac{5c_A^2\,L}{3f_\pi^2 M_0^6} - \frac{10c_A^2\,L\Delta}{3f_\pi^2 M_0^7} + \mathcal{O}(\Delta^2)\right) m_\pi^8\ , \end{aligned} \tag{4.28}$$

while the result for g_A has the following form:

$$\begin{aligned} g_A^{\rm inf} = &\left(-\frac{16c_A^2(25g_1 + 24g_A^0)\,L\Delta^2}{81f_\pi^2} - \frac{32c_A^2(25g_1 + 12g_A^0)L\Delta^3}{81f_\pi^2 M_0} + \mathcal{O}(\Delta^4)\right) \\ &+ \left(\frac{16(25g_1 + 72g_A^0)c_A^2 L + 81g_A^0({g_A^0}^2 - 4)L}{162f_\pi^2} + \frac{8c_A^2(125g_1 + 72g_A^0)L\Delta}{81f_\pi^2 M_0} + \mathcal{O}(\Delta^2)\right) m_\pi^2 \\ &+ \left(\frac{162g_A^0 L - 25c_A^2(23g_1 + 36g_A^0)L}{81f_\pi^2 M_0^2} + \frac{20c_A^2(5g_1 + 12g_A^0)L\Delta}{27f_\pi^2 M_0^3} + \mathcal{O}(\Delta^2)\right) m_\pi^4 \\ &+ \left(\frac{20c_A^2(10g_1 + 9g_A^0)L}{81f_\pi^2 M_0^4} - \frac{4c_A^2(250g_1 + 189g_A^0)L\Delta}{243f_\pi^2 M_0^5} + \mathcal{O}(\Delta^2)\right) m_\pi^6 \\ &+ \left(-\frac{c_A^2(175g_1 + 36g_A^0)L}{486f_\pi^2 M_0^6} + \frac{2c_A^2(125g_1 + 18g_A^0)L\Delta}{243f_\pi^2 M_0^7} + \mathcal{O}(\Delta^2)\right) m_\pi^8 \\ &+ \left(\frac{5c_A^2\,g_1 L}{243f_\pi^2 M_0^8} - \frac{20c_A^2 g_1 L\Delta}{243f_\pi^2 M_0^9} + \mathcal{O}(\Delta^2)\right) m_\pi^{10}\ . \end{aligned} \tag{4.29}$$

The last two equations show that one has to include higher-order counterterms for renormalization. The situation is the same as in the $\mathcal{O}(\epsilon^3)$ calculation in covariant SSE for $M_N(m_\pi)$, see Sec.3.2.3. Looking at the πN and $\pi N\Delta$ effective Lagrangians, four counterterms are available *at third order* in ϵ: $-8\,m_\pi^2 B_{20}$, $-\Delta^2 B_{30}$ and $4\,m_\pi^2 B_9$, $\Delta^2 B_{31}$. These are sufficient to renormalize the nucleon Z-factor and g_A only *at leading order*

in the expansion in powers of $1/M_0$, *i.e.* in the non-relativistic limit. In the numerical analysis we will mainly focus on the non-relativistic expression.

Finally, Eqs.(E.1) and (E.5) are valid only for $m_\pi \leq \Delta$. Their analytic continuations to the m_π region suitable for comparison with lattice simulations are obtained through the replacements

$$\ln\left(\frac{\Delta^2+2M_0\Delta-m_\pi^2}{2M_0m_\pi}+\sqrt{\frac{(\Delta^2+2M_0\Delta-m_\pi^2)^2}{4M_0^2m_\pi^2}-1}\right)\to i\,\arccos\left(\frac{\Delta^2+2M_0\Delta-m_\pi^2}{2M_0m_\pi}\right)$$

$$\sqrt{\Delta^2-m_\pi^2}\to i\,\sqrt{m_\pi^2-\Delta^2}\;.$$

Let us now move to the non-relativistic framework. After performing the limit $M_0\to\infty$ in Eqs.(E.1, E.5), we have set $B^r_{30}(\lambda)$ and $B^r_{31}(\lambda)$ in such a way that the chiral limit values for g_A and the Z-factor are g_A^0 and 1, respectively. The resulting expression of $g_A(m_\pi)$ is non-relativistic SSE result at order ϵ^3 (cf. Refs. [95] and [120]):

$$\begin{aligned}g_A^{SSE}(m_\pi^2) &= g_A^0-\frac{(g_A^0)^3m_\pi^2}{16\pi^2f_\pi^2}+4\left[C^{SSE}(\lambda)+\frac{c_A^2}{4\pi^2f_\pi^2}\left(\frac{155}{972}\,g_1-\frac{17}{36}\,g_A^0\right)+\gamma^{SSE}\ln\frac{m_\pi}{\lambda}\right]m_\pi^2\\ &+\frac{4c_A^2g_A^0}{27\pi f_\pi^2\Delta}m_\pi^3+\frac{8}{27\pi^2f_\pi^2}\,c_A^2g_A^0m_\pi^2\sqrt{1-\frac{m_\pi^2}{\Delta^2}}\,\ln R\\ &+\frac{c_A^2\Delta^2}{81\pi^2f_\pi^2}\left(25g_1-57g_A^0\right)\left(\ln\frac{2\Delta}{m_\pi}-\sqrt{1-\frac{m_\pi^2}{\Delta^2}}\ln R\right)+\mathcal{O}(\epsilon^4)\;,\end{aligned}\tag{4.30}$$

with

$$\begin{aligned}\gamma^{SSE} &= \frac{1}{16\pi^2f_\pi^2}\left[\frac{50}{81}\,c_A^2g_1-\frac{1}{2}\,g_A^0-\frac{2}{9}\,c_A^2g_A^0-(g_A^0)^3\right]\;,\\ R &= \frac{\Delta}{m_\pi}+\sqrt{\frac{\Delta^2}{m_\pi^2}-1}\,.\end{aligned}\tag{4.31}$$

Expanding around $m_\pi=0$ we obtain

$$\begin{aligned}g_A &= g_A^0+4\,\gamma^{HB}\,m_\pi^2\ln\frac{m_\pi}{\lambda}+m_\pi^2\left\{-\frac{(g_A^0)^3}{16\pi^2f_\pi^2}+4\,C^{SSE}(\lambda)\right.\\ &\left.+\frac{c_A^2}{\pi^2f_\pi^2}\left[\left(\frac{25g_1}{162}-\frac{g_A^0}{18}\right)\ln\frac{2\Delta}{\lambda}+\frac{115}{486}\,g_1-\frac{35}{54}\,g_A^0\right]\right\}+\mathcal{O}(m_\pi^3)\;.\end{aligned}\tag{4.32}$$

with

$$\gamma^{HB}=-\frac{1}{16\pi^2f_\pi^2}\left[(g_A^0)^3+\frac{1}{2}\,g_A^0\right]\;.\tag{4.33}$$

In the non-relativistic framework $B_{30}^r(\lambda)$ and $B_{31}^r(\lambda)$ amount to

$$B_{30}^r(\lambda) = \frac{1}{\pi^2 f_\pi^2}\, c_A^2 \ln\frac{2\Delta}{\lambda}$$
$$B_{31}^r(\lambda) = \frac{c_A^2}{\pi^2 f_\pi^2}\left[\frac{40}{243}g_1 - \frac{16}{81}g_A^0 + \left(\frac{25}{81}g_1 + \frac{8}{27}g_A^0\right)\ln\frac{2\Delta}{\lambda}\right] . \qquad (4.34)$$

While the result in Eq.(4.30) is unique, the separation into B_{30}^r and B_{31}^r is not. With the choice of Eqs.(4.34) we have restored g_A^0 as the chiral limit value of $g_A(m_\pi^2)$. Furthermore, the structure of the leading non-analytic term in the quark-mass expansion, proportional to $m_\pi^2 \ln m_\pi$, is not modified by the addition of explicit $\Delta\,(1232)$ degrees of freedom, consistently with chiral symmetry [26], cf. Eq.(4.20). According to Eq.(4.34), in the limit $\Delta \to \infty$ we recover the $\mathcal{O}(p^3)$ result in HBChPT:

$$g_A = g_A^0 + \left[4\,C^r(\lambda) - \frac{{g_A^0}^3}{16\pi^2 f_\pi^2} - \frac{g_A^0 + 2{g_A^0}^3}{8\pi^2 f_\pi^2}\ln\frac{m_\pi}{\lambda}\right] m_\pi^2 . \qquad (4.35)$$

New features in the leading-one-loop non-relativistic SSE result compared to Eq.(4.35), are the terms proportional to m_π^3 as well as the logarithms depending explicitly on the delta-nucleon mass splitting.

We can link $C^r(\lambda)$ in the framework with πN degrees of freedom and $C^{\rm SSE}(\lambda)$ in the theory with *explicit* delta. Comparing the terms proportional to m_π^2 in Eq.(4.32) and Eq.(4.35), it is clear that the renormalized third order couplings in the two schemes have different λ-dependence:

$$C^r(\lambda) = C^{\rm SSE}(\lambda) + \frac{1}{4}\left[\frac{115\,c_A^2 g_1}{486 f_\pi^2\pi^2} - \frac{35\,c_A^2 g_A^0}{54 f_\pi^2\pi^2} + \left(\frac{25\,c_A^2 g_1}{162 f_\pi^2\pi^2} - \frac{c_A^2 g_A^0}{18 f_\pi^2\pi^2}\right)\ln\frac{2\Delta}{\lambda}\right] . \qquad (4.36)$$

Let us now analyze the separate contributions to Eq.(4.30) coming from the different diagrams in Fig.4.6. Graphs (1)-(5) give the pion mass dependence of g_A in HBChPT at order p^3. At the leading-one-loop level, the inclusion of $\Delta\,(1232)$ degrees of freedom brings new wave-function renormalization contributions, new counterterms and the graphs (6)-(8) with propagating deltas. The explicit $\Delta\,(1232)$ degrees of freedom leave their marks in the running of $B_{30}^r(\lambda)$, $B_{31}^r(\lambda)$ and $C^{\rm SSE}(\lambda)$. We identify the "πN contribution" with the order p^3 result in HBChPT, which can be recovered from Eq.(4.30) using Eq.(4.36) and setting $c_A = g_1 = 0$. In the difference between the left-hand sides of Eqs.(4.30) and (4.35), the term proportional to g_1 – the "$\Delta\Delta$ contribution" – stems only from graph (8). The structure of its chiral expansion is what we expect according to the decoupling theorem:

$$\left(-\frac{25 g_1\, c_A^2}{2592\Delta^2 f_\pi^2\pi^2} - \frac{25 g_1\, c_A^2}{648\Delta^2 f_\pi^2\pi^2}\ln\frac{m_\pi}{2\Delta}\right) m_\pi^4 + \mathcal{O}(m_\pi^6/\Delta^4) . \qquad (4.37)$$

Subtracting then the $\Delta\Delta$ contribution, we are left with the effects of the graphs (6) and (7). Expanding this single-delta contribution in the chiral limit, we get

$$\frac{4c_A^2 g_A^0 m_\pi^3}{27\Delta f_\pi^2\pi} + \left(-\frac{5 g_A^0 c_A^2}{96\Delta^2 f_\pi^2\pi^2} + \frac{17 g_A^0 c_A^2}{72\Delta^2 f_\pi^2\pi^2}\ln\frac{m_\pi}{2\Delta}\right) m_\pi^4 + \mathcal{O}(m_\pi^6/\Delta^4) . \qquad (4.38)$$

In the limit $\Delta \to \infty$, graphs (6) and (7) correspond to the diagrams of Fig.4.3 in BChPT: both of them start indeed contributing at m_π^3 in the chiral expansion, cf. Eq.(4.27). Comparing the term at m_π^3 in Eq.(4.38) and the term involving the LECs c_3 and c_4 in Eq.(4.27), we obtain

$$c_3^\Delta = -2c_4^\Delta = -\frac{4c_A^2}{9\Delta} \ , \tag{4.39}$$

which coincides with the prediction from resonance saturation in the chiral (static) limit, cf. the expression (3.50).

If we shrink the delta propagator to a point, graph (8) in Fig.4.6 starts contributing at order p^5 as a fifth order tadpole with an attached external axial field, which is responsible for a structure of the type $A\, m_\pi^4 + B\, m_\pi^4 \ln m_\pi/\lambda$. We exemplify this in Fig.4.8. Hence even the leading term in the m_π/Δ expansion of the $\Delta\Delta$ contribution in *leading*-one-loop in SSE is of higher order compared to our calculation in BChPT, performed up to *next-to-leading* one-loop.

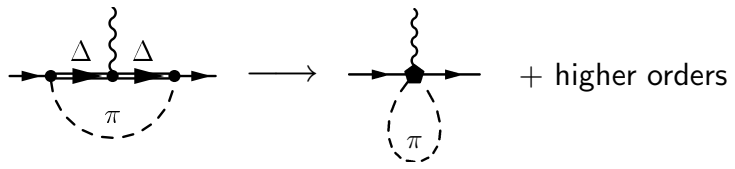

Figure 4.8: Contribution of the diagram with two delta propagators in the limit $M_\Delta \to \infty$. The pentagon indicates a vertex from the third order πN Lagrangian. The tadpole graph is of fifth order.

4.4 Numerical analysis

This section is devoted to the comparison of the expressions for $g_A(m_\pi)$ derived in the previous sections with the most recent lattice data. The strategy is the same as for the nucleon mass in Chapter 3.

After the description of the different lattice data sets used as input for our fits, we will discuss in detail the outcome of our numerical analysis of Eqs.(4.16), (4.23), (4.30). We postpone to Sec.4.4.7 the discussion of our results in the manifestly covariant framework with explicit $\Delta\,(1232)$.

4.4.1 Lattice data

The calculation of g_A on the lattice involves the computation of the nucleon matrix element of the axial-vector current operator in Eq.(4.1). Such hadronic matrix elements can be extracted from ratios of three-point functions over two-point functions. First, one has to choose interpolating fields for the particle to be studied. For a proton with

momentum $\vec{p}$ a suitable choice is:

$$B_\alpha(t,\vec{p}) = \sum_{x;x_4=t} e^{-i\vec{p}\cdot\vec{x}} \epsilon_{ijk} u^i_\alpha(x) u^j_\beta(x) (C\,\gamma_5)_{\beta\gamma} d^k_\gamma(x) \tag{4.40}$$

where the Latin (Greek) indices are color (Dirac) indices and C is the charge conjugation matrix. As the time extent of the lattice tends to infinity, the ratio R between three- and two-point functions

$$R \equiv \frac{\langle B(t)\mathcal{O}(\tau)\bar{B}(0)\rangle}{\langle B(t)\bar{B}(0)\rangle} = \langle \text{proton}|\mathcal{O}|\text{proton}\rangle + \ldots \tag{4.41}$$

will be independent of the times τ and t, if $t \gg \tau \gg 0$ so that excited states can be neglected.

The proton three-point function for a 2-quark operator contains quark-line connected as well as quark-line disconnected pieces. The latter are very hard to compute. However, in the limit of exact isospin invariance, the disconnected contributions of the u and d quarks cancel in the case of non-singlet two-quark operators, the case relevant for g_A.

In our work we focus mainly on a set of two-flavor lattice QCD data provided by the RIKEN-BNL-Columbia-KEK (RBCK) collaboration [154]. These simulations are performed with Domain Wall Fermions (DWF), a lattice formulation of the Dirac operator based on a solution of the Ginsparg-Wilson relation. Ginsparg-Wilson fermions need more computer time, but permit to work with considerably lighter quarks than most other lattice fermions. DWF preserve chiral symmetry on the lattice by introducing a fictitious fifth dimension with extent L_s: if the lattice spacing is sufficiently small, the symmetry violation is exponentially suppressed with finite L_s in quenched simulations if the gauge field is sufficiently smooth [154].

The simulations in Ref. [154] are all quenched: five points with $395\,\text{MeV} < m_\pi < 860\,\text{MeV}$. First low-statistics results by the RBCK group within full-QCD simulations show, within error bars, perfect consistency with the quenched results [154]: for the relatively large pion masses computed on the lattice, the effects of "quenching" turn out to be negligible. However, the difference between "quenched" and fully dynamical QCD simulations should become visible at lower pion masses: in quenched QCD indeed the axial coupling of the nucleon develops a singularity $g_A(m_\pi \to 0) \sim \log m_\pi$ in the chiral limit [155], in contrast to the finite value g_A^0 in full QCD.

While we are confident that (un)quenching effects are small in the presently accessible pion mass range, corrections arising from the finite (small) simulation volume turn out to be important. The data points that we take from Ref. [154] refer to simulations performed on lattices with spatial size $L = 2.4\,\text{fm}$, $m_\pi\, L \geq 4.8$ and lattice spacing $a \approx 0.15\,\text{fm}$. The latter has been determined in such a way that $m_\rho a$ reproduces the physical value of the ρ mass. In the same paper the RBCK collaboration compares simulations at $L = 1.2$ and $L = 2.4\,\text{fm}$: g_A is shown to be sensitive to finite size corrections. For small lattices g_A exhibits a strong quark mass dependence [156] while for large L it basically shows a plateau for $m_\pi \gtrsim 400\,\text{MeV}$. Among the results quoted in Ref. [154] we have restricted ourselves to $m_\pi < 665\,\text{MeV}$ and the largest available lattice size. A recent analysis of

finite volume effects for g_A at order ϵ^3 in non-relativistic Small Scale Expansion [157] shows that for $L \approx 2.5\,\mathrm{fm}$ these lattice artifacts are quite negligible for the lattice pion masses that we take as input, see also Ref. [158].

Other possible sources of systematic error in the calculation of g_A on the lattice have been discussed in Ref. [154]. They can basically be identified with: operator renormalization, nonzero lattice spacing and loss of chiral symmetry for Wilson and Kogut-Susskind fermions. The loss of chiral symmetry on the lattice is dangerous for our purposes: g_A is sensitive to both spontaneous and explicit chiral symmetry breaking. Therefore the explicit breaking of chiral symmetry at nonzero lattice spacing for Wilson fermions may induce significant errors which are removed only in the continuum limit. The determination of the renormalization factor for the axial current seems also to be important. The DWF calculation of g_A should not suffer from the systematic errors due to operator renormalization and loss of chiral symmetry: this fermion discretization scheme greatly simplifies the non-perturbative determination of renormalization factors for quark bilinear currents [159]. For example, the renormalization factors of local vector and axial-vector current operators turn out to be equal, $Z_A = Z_V$: this means that the ratio g_A/g_V calculated on the lattice directly yields the continuum value, *i.e.* it is not renormalized. By employing the DWF scheme, one eliminates the ambiguity in the renormalization of quark currents, which may be present and problematic in other fermion discretization schemes.

The RBCK data that we use for our analysis are obtained with an improved gauge action in order to meet both large volume and chiral symmetry, the latter requiring a sufficiently small lattice spacing. Such "renormalization group inspired" improved gauge actions, differently from Wilson actions, preserve with good accuracy the chiral symmetry of DWF while not demanding a very small a [160].

As already pointed out, for the largest volume considered in Ref. [154], the data exhibit very mild quark mass dependence. A simple linear extrapolation of $(g_A/g_V)^{\mathrm{ren}}$ underestimates the experimental value of 1.267 by less than 5%. For the purpose of our numerical analysis the g_A simulation data provide the constraint of specifying the location of the "data plateau". Any sensible formula for the interpolation between lattice data and the physical point must have enough structure in m_π to reproduce such a plateau, at least over a certain range in pion mass. In essence, this implies a strong constraint: different terms in the quark mass expansion of g_A must co-operate in such a way that the interpolation function is basically flat once the pion mass exceeds 400 MeV. Given that the available lattice data are still restricted to relatively large quark/pion masses, can one nevertheless make use of this information to determine the interpolating function? What can we say about the relevant physics in the region where the quark mass is much smaller than in lattice simulations? We expect that the role of the "pion cloud" sorrounding the nucleon becomes important there. Nevertheless, the values of $g_A(m_\pi)$ at the relatively large quark masses that one can presently handle on the lattice lie just a few percent below the experimental value and show little dependence on the quark mass. So, what can we conclude about the role of the "pion cloud"? We are going to shed some light on that in the next sections, where we describe the outcome of our numerical analysis.

In Ref. [120] we used as input five quenched data by the QCDSF collaboration [161–163], with Wilson fermions on small lattices, $L = 1.45 \ldots 1.60\,\mathrm{fm}$ [2]. The pion masses range from 580 to 750 MeV. The same collaboration together with UKQCD has been performing also full-QCD simulations for g_A with two active flavors, nonperturbatively improved Wilson quarks (clover fermions) and the standard plaquette action for the gauge fields [164]. Unfortunately, at the time of writing, these results are still preliminary and we could not compare them with the quenched data.

Although the status of the RBCK results is more advanced then the QCDSF simulations, we have also performed fits to the quenched data points by the latter collaboration, exploring the feasibility of a chiral extrapolation based only on the lattice data, Sec.4.4.5.

In Sec.4.4.6 we compare our formulae with full-QCD data recently released by the LHP Collaboration [165] [3]. These simulations are performed with three active flavors within a so-called "hybrid" framework, using domain-wall valence quarks and improved Kogut-Susskind sea quarks (the so-called Asqtad action by the MILC collaboration [166]). This scheme – although breaking unitarity at finite lattice spacing – will still have the same continuum limit as a fully dynamical calculation provided this limit exists. The collaboration is able to treat pion masses as light as 359 MeV in volumes with spatial size as large as 3.5 fm. At the lowest pion mass the simulations in lattice volumes of $(2.6\,\mathrm{fm})^3$ and $(3.5\,\mathrm{fm})^3$ yield statistically indistinguishable results, indicating the absence of finite volume corrections at this lattice size. The full data set consists of five points with pion masses of 359, 498, 605, 696 and 775 MeV.

The three full-QCD points by the RBCK collaboration [154] in a $(1.9\,\mathrm{fm})^3$ box are consistent with the LHP data within error bars, whereas the full QCDSF-UKQCD results in a smaller volume lie systematically lower [165]. At present the reason of that discrepancy is not clear yet. Future simulations with chirally improved actions, larger volumes and better statistics will help to solve that issue.

Since we cannot combine data by different collaborations, the statistics for our numerical study is very limited. We have therefore treated f_π^0, M_0, c_A and Δ as input parameters in our fits. All couplings and masses on the right-hand side of the relevant equations refer to their leading-order values in their quark-mass expansions: as discussed in detail in Chapter 2, only a few of those parameters are accurately determined by matching ChPT with low-energy hadron phenomenology.

Setting the regularization scale $\lambda = 1\,\mathrm{GeV}$, we are then left with the following parameters not fixed by chiral symmetry:

- g_A^0 and the third-order combination of couplings $C^r(1\,\mathrm{GeV})$ or $C^{\mathrm{SSE}}(1\,\mathrm{GeV})$,

- M_0, $F^r(1\,\mathrm{GeV})$ and $G^r(1\,\mathrm{GeV})$ in the expressions with πN degrees of freedom, Eqs.(4.16) and (4.23),

[2] The data provided have been obtained with an improved action for clover fermions on three different grids ($16^3 \times 32$, $24^3 \times 48$ and $32^3 \times 48$ points) with lattice spacings $a = 0.09$, 0.07, 0.05 fm.

[3] We are grateful to LHP Collaboration for providing us data prior publication.

- g_1 in the $\pi N\Delta$ framework.

We now first focus on the three RBCK data points with $m_\pi \leq 665\,\mathrm{MeV}$. The available statistics is too low to extract quantitative information on the unknown parameters from lattice data *alone*. We have therefore treated the physical point as input. Of course, it is somehow arbitrary to compare our formulae *simultaneously* with the empirical value of g_A and *two-flavor* lattice QCD simulations. However, our analysis of the LHP data in Sec.4.4.6 shows that the effects of the addition of one heavier flavor on the lattice are absorbed within the error bars of the output parameters.

4.4.2 BChPT: "freezing" the $\Delta\,(1232)$

Several low-energy πN scattering analyses give estimates for the dimension-two low-energy constants c_1, c_2, c_3 and c_4, see Sec.2.9. The analysis in Refs. [83,85] of $\pi N \to \pi\pi N$ scattering at leading-one-loop order in HBChPT constraints the combination of couplings B_9 and B_{20}, cf. Sec.2.9.

We have first exploited the information on the quark mass dependence of g_A contained in $\mathcal{O}(p^3, p^4)$ BChPT expressions together with this input from low-energy hadron phenomenology, *without fitting to the lattice data*. We have produced Monte Carlo bands both from the relativistic expressions in Eqs.(4.16), (4.23) and the HB formulae at order p^3 and p^4: we have eliminated g_A^0 through the physical constraint $g_A(m_\pi^{\mathrm{phys}}) = 1.267$ and chosen randomly the remaning parameters in phenomenologically motivated ranges, cf. Sec.2.9. For the couplings F and G we had to resort to naive dimensional arguments, at the regularization scale $\lambda = 1\,\mathrm{GeV}$. None of the these bands, which take into account also the uncertainties on the input parameters, comes close to the lattice data in the m_π region of interest. The recoil corrections to the non-relativistic results do not improve the situation. In the framework without propagating $\Delta\,(1232)$, up to the order at which we are working, it is not possible to obtain a satisfactory interpolation between the physical point and lattice data, as we convinced ourselves by fitting with the relevant formulae. Either we get unacceptably large values of χ^2/d.o.f. or the output parameters are not in agreement with phenomenology. This holds for any of the RBCK, QCDSF, LHP data sets. At order p^4, for example, including the physical point as input, in order to adapt the curve to the lattice data, the price we have to pay is that c_3 must be tuned to a value which is totally inconsistent with the empirical one. Freezing the delta and relegating its effects into low-energy couplings is not enough to capture the physics in the quark mass dependence of g_A. This does not come as a surprise: intermediate $\Delta\,(1232)$ contributions are known to play an important role in axial current matrix elements between nucleon states and quark spin-flip transitions [167], due to the quantum numbers of the $\Delta\,(1232)$, its near degeneracy with the nucleon and its strong coupling with the $\pi N\gamma$ system. We discuss this in the specific example of relevance here.

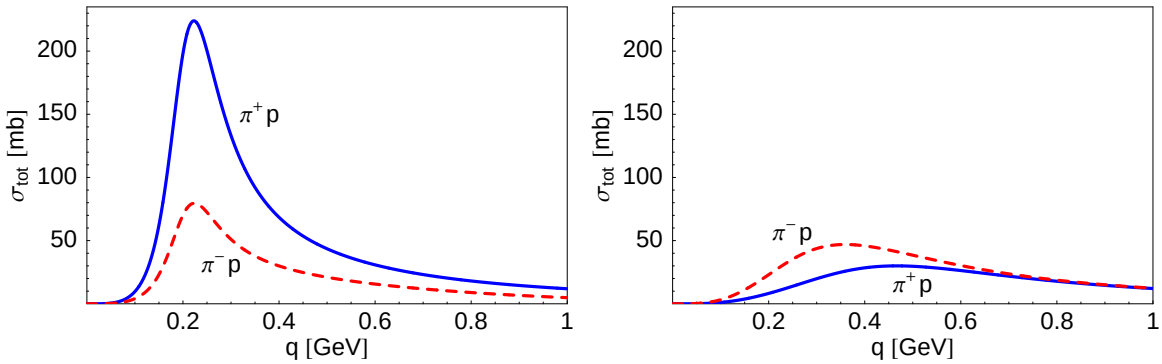

Figure 4.9: Total $\pi^+ p$ and $\pi^- p$ cross sections plotted against the pion momentum in the laboratory frame. In the left panel the direct and crossed $\Delta(1232)$-pole graphs are included, in the right panel not.

4.4.3 The Adler-Weisberger sum rule

The Adler-Weisberger sum rule [168] connects low-energy parameters of the πN system (f_π and g_A) with an integral over the difference of the $\pi^+ p$ and $\pi^- p$ total cross-sections. Let us choose the laboratory frame where the nucleon is at rest and ω is the pion energy. Consider $T^-(\omega)$, the isospin-odd πN T-matrix for forward scattering. Regge pole theory suggests that this amplitude should behave at asymptotically high energies as $T^- \sim \sqrt{\omega}$, see for example [169]. Consequently, $T^-(\omega)/\omega$ satisfies an unsubtracted dispersion relation:

$$\frac{T^-(\omega)}{\omega} = \frac{2g_A^2}{f_\pi^2}\frac{m_\pi^2 M_N^2}{4M_N^2\omega^2 - m_\pi^4} + \frac{2}{\pi}\int_{m_\pi}^{\infty} d\omega' \frac{\mathrm{Im}\, T^-(\omega')}{\omega'^2 - \omega^2 - i\epsilon} \,, \tag{4.42}$$

where the first term on the right-hand side is the contribution from the nucleon-pole piece of the πN amplitude.

Let us now go to threshold ($\omega = m_\pi$) and use the Weinberg-Tomozawa low-energy result [170]

$$T^-(\omega) = \frac{\omega}{2f_\pi^2} \,. \tag{4.43}$$

Neglecting the corrections of order $m_\pi^2/(4M_N^2) \ll 1$ in the denominator of the nucleon-pole piece, we get

$$\frac{1}{2f_\pi^2} = \frac{g_A^2}{2f_\pi^2} + \frac{2}{\pi}\int_{m_\pi}^{\infty} d\omega \frac{\mathrm{Im}\, T^-(\omega)}{\omega^2 - m_\pi^2} \,. \tag{4.44}$$

Using the optical theorem to connect $\mathrm{Im}\, T^-$ with the $\pi^\pm p$ total cross-sections, we obtain the Adler-Weisberger sum rule

$$g_A^2 = 1 + \frac{2f_\pi^2}{\pi}\int_0^{\infty} \frac{dq}{\omega}\left[\sigma_{\pi^+ p}(\omega) - \sigma_{\pi^- p}(\omega)\right] + \mathcal{O}\left(\frac{m_\pi^2}{M_N^2}\right) \,, \tag{4.45}$$

where the integral is taken over the pion laboratory momentum, $q = |\vec{q}| = \sqrt{\omega^2 - m_\pi^2}$. The deviation of g_A from 1 is tied to pion-nucleon dynamics and spontaneous (and explicit) chiral symmetry breaking. The left- and right-hand sides of the sum rule turn out

to be consistent at the percent level using $f_\pi = 92.4\,\mathrm{MeV}$ and an accurate parameterization of the measured $\pi^\pm p$ cross-sections [78].

According to the optical theorem, for any spin – isospin channel $\alpha = (2I, 2J)$,

$$\sigma_\alpha(\omega) = \frac{4\pi}{|\vec{q}|}\,\mathrm{Im} f_\alpha(\omega) \tag{4.46}$$

where σ_α and f_α are total cross-section and partial wave amplitude in that channel, respectively; the amplitude $f(\omega)$ for forward scattering in the laboratory frame is defined so that the laboratory frame differential cross-section in the forward direction is $|f(\omega)|^2$. In terms of the K-matrix, or "reaction matrix" [171],

$$f_\alpha(\omega) = \frac{K_\alpha(\omega)}{1 - i|\vec{q}|K_\alpha(\omega)}\ . \tag{4.47}$$

K_α has poles on the real axis for each intermediate state in the scattering amplitude and each pole is located at the physical mass of the corresponding state. In the present case, there are poles representing the nucleon and the $\Delta\,(1232)$ intermediate state, for example. Identifying the direct and crossed nucleon- and $\Delta\,(1232)$-pole terms with the corresponding pieces of the K-matrix, we find in the extreme non-relativistic (static) limit and *at threshold*,

$$K_{13} = K_{31} = \frac{1}{4}\,K_{11} = \frac{\vec{q}^{\,2}}{12\pi m_\pi^2}\left[-\frac{2f^2}{m_\pi} + \frac{4f_\Delta^2}{9(\Delta + m_\pi)}\right]$$

$$K_{33} = \frac{\vec{q}^{\,2}}{12\pi m_\pi^2}\left[\frac{4f^2}{m_\pi} + \frac{f_\Delta^2}{\Delta - m_\pi} + \frac{f_\Delta^2}{9(\Delta + m_\pi)}\right]\ , \tag{4.48}$$

cf. Ref. [124]. Here

$$f^2 = \frac{g_A^2 m_\pi^2}{4f_\pi^2}\ , \qquad f_\Delta^2 = \frac{c_A^2 m_\pi^2}{f_\pi^2}\ . \tag{4.49}$$

Using physical values on the right-hand sides of these last two equalities — and crucially $c_A = 1.5$ —, the P-wave πN scattering volumes agree very well with experiments, see also Ref. [124]. Eq.(4.47) and the optical theorem lead to the total $\pi^+ p$ and $\pi^- p$ cross-sections in the left panel of Fig.4.9. The curves are in good agreement with the empirical ones from near threshold up to $q \approx 0.5\,\mathrm{GeV}$ [78,124]: the region between 0.5 and 2 GeV is partly dominated by higher resonances. Using these cross-sections to evaluate Eq.(4.45), we obtain $g_A = 1.24$ for the physical m_π and f_π. If the calculation includes only the P-wave Born terms for static nucleons, $\sigma_{\pi^\pm p}$ change as in the right panel of Fig.4.9. "Switching off" the $\pi N\Delta$ coupling, the contribution from the dispersion integral in the Adler-Weisberger sum rule changes sign and g_A is reduced to 0.94.

4.4.4 Non-relativistic SSE

In the framework with explicit $\Delta\,(1232)$, we first analyze the non-relativistic expression for $g_A(m_\pi)$, Eq.(4.30), where renormalization and decoupling do not give rise to any ambiguities.

Table 4.1: Input parameters in the fits to the RBCK data [154].

Fit	c_A	f_π [MeV]	Δ [MeV]
1	1.5	92.4	271.1
2	1.125	92.4	271.1
3	1.5	86.2	271.1
4	1.125	86.2	271.1
5	1.5	92.4	293
6	1.125	92.4	293
7	1.5	86.2	293
8	1.125	86.2	293

With three free parameters and three RBCK data points, we cannot afford a meaningful chiral *extrapolation* with small single-parameter errors in output. We have therefore performed several fits including the physical constraint, in order to quantify the sensitivity to the input parameters, cf. Table 4.1. The outcome is summarized in Table 4.2. Only the precise value of c_A turns out to be crucial: in the fits with $c_A = 1.125$ the $SU(4)$ quark model prediction for g_1 is badly broken. Moreover, both for Fit 2 and Fit 4, $C^r(1\,\mathrm{GeV})$ from Eq.(4.36) is not compatible with $\pi N \to \pi\pi N$ scattering. The fit results are also insensitive, within error bars, to a 15% larger value of the delta-nucleon mass difference in the chiral limit [93].

The best fit curve in Fit 1 is the solid line in Fig.4.10, with $\chi^2/\mathrm{d.o.f.} = 0.2$. For illustrative purpose we also plot its dotted extension for pion masses larger than 665 MeV and the RBCK data points with the same simulation parameters that we did not include in the fit [154]. The $\mathcal{O}(\epsilon^3)$ non-relativistic SSE expression represents a good inter-

Table 4.2: Fit results for $g_A(m_\pi)$ at order ϵ^3. The physical point is included as input. Central values and errors have been obtained using the MINUIT package and have been rounded to the first significant digit.

Fit	g_A^0	$C^{\mathrm{SSE}}(\lambda = 1\,\mathrm{GeV})$ $[\mathrm{GeV}^{-2}]$	g_1	$\chi^2/\mathrm{d.o.f.}$
1	1.223 ± 0.007	-1.7 ± 0.4	2.8 ± 0.3	0.2
2	1.207 ± 0.007	-3.5 ± 0.4	5.8 ± 0.5	0.4
3	1.217 ± 0.007	-1.8 ± 0.4	2.8 ± 0.2	0.2
4	1.198 ± 0.007	-3.9 ± 0.4	5.7 ± 0.4	0.4
5	1.221 ± 0.007	-1.8 ± 0.4	2.9 ± 0.3	0.2
6	1.205 ± 0.007	-3.8 ± 0.4	6.0 ± 0.5	0.4
7	1.214 ± 0.007	-2.0 ± 0.4	2.8 ± 0.4	0.2
8	1.196 ± 0.007	-4.2 ± 0.4	5.8 ± 0.4	0.5

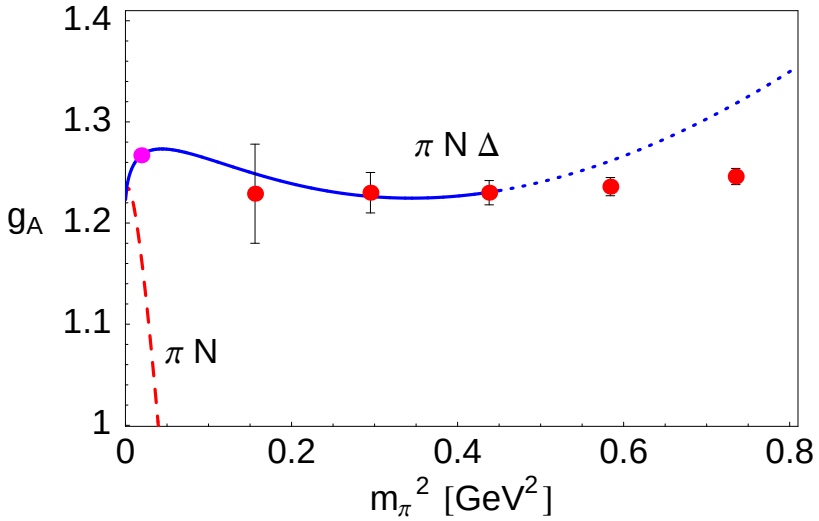

Figure 4.10: Solid/dotted curve: $\mathcal{O}(\epsilon^3)$ SSE best fit to the three RBCK lattice data [154] with m_π up to 665 MeV including the physical point in input, Fit 1. Dashed curve: corresponding leading-one-loop result in HBChPT.

polating function between physical point and lattice data with parameters compatible with phenomenology. The estimate of g_1 is not far from the $SU(4)$ quark model prediction, $9/5\, g_A^0 \simeq 2.2$. However, *imposing* $g_1 = 9/5\, g_A^0$ in the fit, the χ^2 comes out unacceptably large. The value of $C^{\rm SSE}(1\,{\rm GeV})$ in Fit 1 is consistent with $\pi N \to \pi\pi N$ scattering. Indeed, using the central values of g_A^0 and g_1 in Fit 1, Eq. (4.36) gives $C^r(1\,{\rm GeV}) = -4\,{\rm GeV}^{-2}$, in perfect agreement with the (broad) range derived from Ref. [85]:

$$C^r(\lambda = 1\,{\rm GeV}) = -6.2 \cdots - 3.8\,{\rm GeV}^{-2}\ . \tag{4.50}$$

In order to obtain the last result, we set g_A^0 and f_π^0 as in Fit 1 in the HBChPT β-functions used to run the couplings $B_9^r(\lambda)$ and $B_{20}^r(\lambda)$ from $\lambda = m_\pi^{\rm phys}$, the scale in Ref. [85].

Treating the physical point on the same level as data from lattice calculations is, of course, not optimal. The error bar of the former is also one order in magnitude smaller than for the lattice data. Therefore the quoted errors on the output parameters have to be taken *cum granu salis*.

The dashed curve in Fig.4.10 corresponds to the leading-one-loop HBChPT result, where $C^r(1\,{\rm GeV})$ has been extracted from the central values in Fit 1 via Eq.(4.36). By construction of the SSE expression, we have required that the chiral limit value of g_A^0 is the same in both EFT schemes. Moreover, the identification of the terms proportional to m_π^2 through Eq.(4.36) is expected to be valid for sufficiently small pion masses: HBChPT and SSE can indeed build up the contributions to a particular term in the chiral expansion more or less effectively in their respective perturbative series. Fig.4.10 clearly shows that the leading-non-analytic term does not describe correctly the quark mass dependence of g_A outside a quark-mass region which is *extremely* close to the chiral

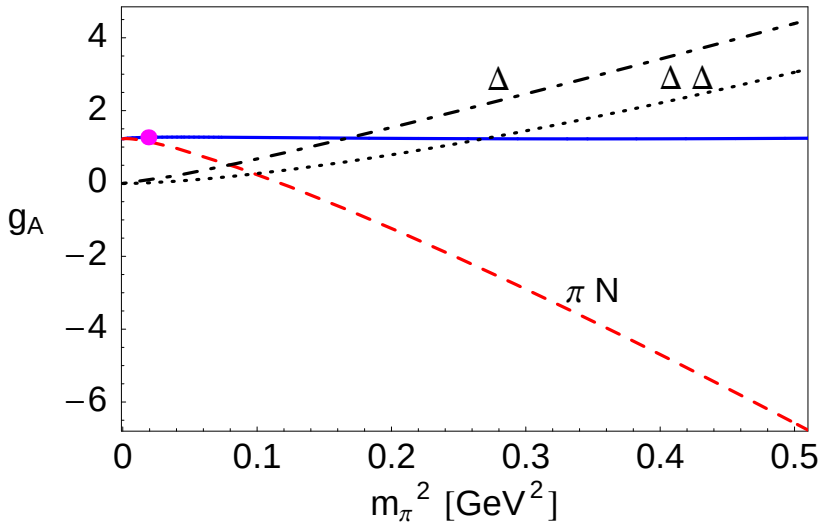

Figure 4.11: Solid curve: $\mathcal{O}(\epsilon^3)$ non-relativistic SSE fit to the RBCK data [154], Fit 1. Dashed, dot-dashed, dotted curves: contributions from the diagrams without, with one and with two Δ propagators in Fig.4.6, respectively.

limit.

It is instructive to look at the separate contributions to the best-fit curve coming from the different diagrams in Fig.4.6, as explained in Sec.4.3. These contributions are drawn in Fig.4.11 and are based on Fit 1. The inclusion of the explicit $\Delta\,(1232)$ degrees of freedom is crucial to compensate the downward bending of the πN contribution, at this order [4]. In what we call "πN contribution" we include also the effects of graphs with propagating deltas which are absorbed by g_A^0 and $C^r(\lambda)$. Therefore the chiral expansion of graphs (6) and (7) in Fig.4.6 starts at m_π^3/Δ and for graph (8) at m_π^4/Δ, cf. Sec.4.3.

Fig.4.11 explicitly shows that the graph with two delta propagators plays an important numerical role in order to compensate the πN trend at the pion masses presently manageable on the lattice. Since graph (8) encodes higher-order effects with respect to our BChPT calculations, SSE seems to be effective in resumming powers of m_π/Δ. In the region of present lattice data, m_π/Δ is *not* a good expansion parameter. We show, "empirically", that in SSE important effects due to the $\Delta\,(1232)$ are moved to low chiral orders. However, before any firm conclusion can be drawn it is mandatory to study g_A at order ϵ^4. It is needless to say that for a numerical study of the fourth-order formula, we must wait for an improvement of the statistics for the lattice data.

[4]Such a cancellation of individually large πN and $\pi\Delta$ loop effects in g_A was already observed in Ref. [100].

Table 4.3: Fits to the QCDSF data [161].

Fit	g_A^0	$C^{r/\mathrm{SSE}}(1\,\mathrm{GeV})\ \left[\mathrm{GeV}^{-2}\right]$	g_1	χ^2/d.o.f.
Ia	0.71 ± 0.04	$+0.12 \pm 0.03$	-	0.4
Ib	≈ 0.78	$\approx +1.06$	≈ 0.0	0.55
IIa	0.94 ± 0.04	-0.25 ± 0.04	$9/5\ g_A^0$	0.4
IIb	1.14 ± 0.03	-0.66 ± 0.04	$9/5\ g_A^0$	0.45
III	1.19, 1.25, 1.31	$-1.2,\ -2.0,\ -2.8$	2.47, 3.05, 3.63	0.48, 0.53, 0.58
IVa	1.21 ± 0.01	-3.4 ± 0.4	5.6 ± 0.5	0.5
IVb	1.22 ± 0.01	-1.7 ± 0.4	2.8 ± 0.3	0.5

4.4.5 Comparison with QCDSF data

We now compare the quark mass dependence of g_A at leading-one-loop level in non-relativistic SSE and HBChPT [120] by analyzing the quenched data provided by the QCDSF Collaboration in the range between 580 and 752 MeV, see Refs. [162, 163]. The scale is set through the Sommer parameter $r_0 \approx 0.5\,\mathrm{fm}$, see Sec.3.3.1 for details. We assume that lattice artifacts are negligible.

In the first round of fits we have explored whether the five available lattice data are sufficient to constrain the unknown parameters in Eq.(4.30) and Eq.(4.35). The results are summarized in Table 4.3 under the labels Fit Ia, Fit Ib for HBChPT and SSE, respectively. The χ^2/d.o.f. for either curve is small, but both extrapolation functions miss the physical point by a wide margin. Such a strong downward bending in the region of small m_π has also been reported in Ref. [138].

We refrain from quoting errors for the free parameters in FitIb, because the MINUIT routine is not able to give reliable estimates for them: the lattice data analyzed here are not sufficiently accurate yet, the statistics of our data sample is too low to properly constrain the parameters in the SSE formula. Additional physical constraints have to be invoked to sharpen our analysis.

In a second step we have fixed the axial-Δ-Δ coupling $g_1 = 9/5\, g_A^0$, leaving free g_A^0 and $C^{\mathrm{SSE}}(1\,\mathrm{GeV})$ in Eq.(4.30). The outcome for $c_A = 1.125$ and $c_A = 1.5$ as input is shown in Table 4.3 under the label Fit IIa and IIb, respectively.

With $c_A = 1.125$ as input, the constraint on g_1 does not allow for the correct enhancement of the chiral extrapolation curve around the physical pion mass. Similar conclusions can be drawn from the calculation by Detmold et al. [140], which also includes – not systematically though – explicit $\Delta\,(1232)$ contributions and makes use of $SU(4)$ symmetry assumptions to reduce the number of unknown couplings.

Fit IIb, with $c_A = 1.5$, represents a bigger improvement compared to the unconstrained fits.

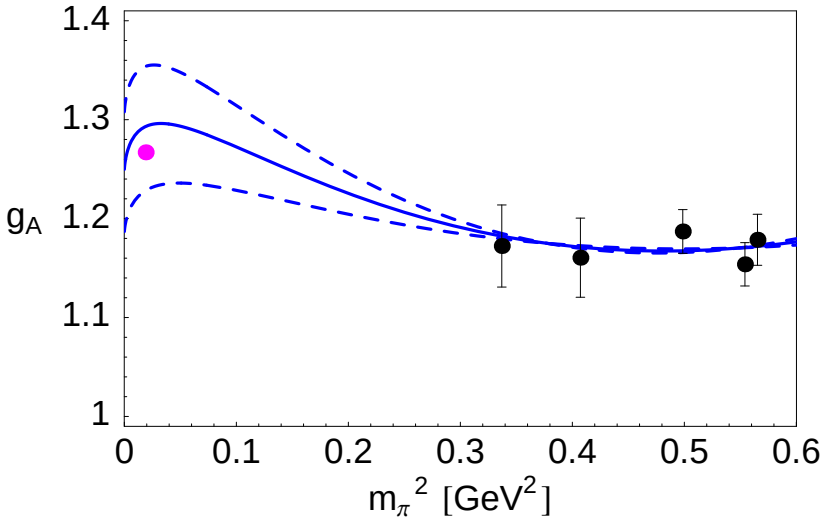

Figure 4.12: Analysis of QCDSF data [161], incorporating information from $\pi N \to \pi\pi N$ into the leading-one-loop SSE result (Fit III). In input $c_A = 1.5$. The dashed curves correspond to the upper and lower boundaries for the parameter $C^r(\lambda)$ from Ref. [85].

When varying g_A^0, $C^{\rm SSE}(\lambda = 1\,{\rm GeV})$ and g_1 in such a way that the resulting curve fits to the lattice data, the parameter $C^{\rm SSE}(\lambda)$ is crucial for an enhancement of $g_A(m_\pi)$ at small pion masses, close to the physical point. We profit by the Heavy Baryon analysis of $\pi N \to \pi\pi N$ in Refs. [83, 85] to constrain $C^r(\lambda)$ in the fits. While we can directly use the outcome of such a study in the BChPT framework, there is no unique procedure to import this information into the scheme with explicit $\Delta\,(1232)$ degrees of freedom: $B_9^r(\lambda)$, $B_{20}^r(\lambda)$ indeed have different β-functions in HBChPT and SSE. We have determined a "matching scale" $\bar\lambda$ as follows. Starting from the result of Ref. [85],

$$B_9^r(\lambda = m_\pi^{phys}) = (-1.4 \pm 1.2)\,{\rm GeV}^{-2}\ , \quad B_{20}^r(\lambda = m_\pi^{phys}) \equiv 0\ , \tag{4.51}$$

we run these couplings up to $\bar\lambda$ according to their HB β-functions [60] with $g_A^0 = 1.267$ and $f_\pi^0 = 92.4\,{\rm MeV}$. We then fix $\lambda = \bar\lambda$ and $C^{\rm SSE}(\bar\lambda) \equiv C^r(\bar\lambda)$. Several input values of $C^{\rm SSE}(\bar\lambda)$, inside the range corresponding to Eq.(4.51), have been used in the fits. We have then obtained a set of best-fit curves and checked whether the physical point is inside the envelope of those curves. As a self-consistency test, we have required that, using the fit results and Eq.(4.36), the HBChPT and SSE expressions for $g_A(m_\pi)$ agree within error bars up to and including the term proportional to m_π^2 in the chiral expansion. It turns out that a suitable matching scale is $\bar\lambda = 300\,{\rm MeV}$. The outcome of this analysis is labelled as Fit III in Table 4.3: for an easier comparison with other fits we run $C^{\rm SSE}(\lambda)$ from $\bar\lambda$ up to $\lambda = 1\,{\rm GeV}$, according to the relevant SSE β-function. Fig.4.12 shows the resulting SSE chiral extrapolation curves for $g_A(m_\pi)$, with $c_A = 1.5$ as input. The solid line in Fig.4.12 refers to the central value for $C^{\rm SSE}(\lambda = 300\,{\rm MeV})$ given by the matching condition, whereas the two dashed curves show the effects of the uncertainty on $B_9^r(\lambda)$

Table 4.4: Numerical results for the fits to the $2+1$ – flavor data provided by the LHP Collaboration based on the non-relativistic $SU(2)$ leading one-loop formula in the Small Scale Expansion. For the input parameters see Table 4.1. In Fit 9 $c_A = 1.5$, $f_\pi = 92.4\,\mathrm{MeV}$ and $\Delta = 271.1\,\mathrm{MeV}$.

Fit	g_A^0	$C^{\mathrm{SSE}}(\lambda = 1\,\mathrm{GeV})$ $\left[\mathrm{GeV}^{-2}\right]$	g_1	χ^2/d.o.f.
1	1.226 ± 0.004	-1.8 ± 0.1	2.86 ± 0.09	1.2
2	1.208 ± 0.004	-3.5 ± 0.1	5.7 ± 0.2	1.6
3	1.220 ± 0.004	-1.9 ± 0.1	2.79 ± 0.08	1.25
4	1.200 ± 0.004	-3.9 ± 0.1	5.5 ± 0.1	1.7
5	1.224 ± 0.004	-1.9 ± 0.1	2.9 ± 0.1	1.2
6	1.205 ± 0.004	-3.7 ± 0.1	5.9 ± 0.2	1.6
7	1.217 ± 0.004	-2.0 ± 0.1	2.83 ± 0.09	1.3
8	1.196 ± 0.003	-4.1 ± 0.2	5.7 ± 0.2	1.8
9	1.18, 1.24, 1.30	-1.2, -2.0, -2.8	2.45, 3.03, 3.61	0.9, 1.4, 2.3

in Eq.(4.51).

While the χ^2/d.o.f. values are comparable with Fits I and II, only Fit III gives a successful extrapolation. We can therefore conclude that SSE at the leading-one-loop level *together with information from $\pi N \to \pi\pi N$ scattering* can provide a meaningful chiral extrapolation of the present lattice data, consistent with the experimentally known value for g_A.

Taking the physical point as an additional input, we performed two fits with different values for the axial-N-Δ coupling: $c_A = 1.125$ (Fit IVa) and $c_A = 1.5$ (Fit IVb). Fit III is stable for the inclusion of the physical constraint.

The outcome of the analysis of the QCDSF data agrees with the results for the RBCK set. The choice $c_A = 1.5$ allows for g_1 to be close to the $SU(4)$ quark model prediction, cf. also [157]. Moreover, $C^r(1\,\mathrm{GeV})$ turns out to be compatible with $\pi N \to \pi\pi N$ phenomenology, according to Eq.(4.36) and the outcome of Fit IVb. We have checked the sensitivity to the other input parameters, f_π^0 and Δ: in both cases the induced variations in the output are not decisive.

4.4.6 LHP data

We have also fitted to the five full-QCD data provided by the LHP Collaboration with $359\,\mathrm{MeV} \leq m_\pi \leq 775\,\mathrm{MeV}$ [165]. We have remarkably found that the basic features emerged from the analyses of the other data sets remain unaltered if we take as input simulations with 2 (light) + 1 (heavy) flavors. Our numerical results are summarized in Table 4.4: Fits 1-8 differ for c_A, f_π^0 and Δ as input and include the physical g_A. We have followed the same nomenclature as in Table 4.1. The best fit curve for Fit 1 is plotted in Fig.4.13. As reported before, choosing $c_A = 1.5$, g_1 comes out in qualitative

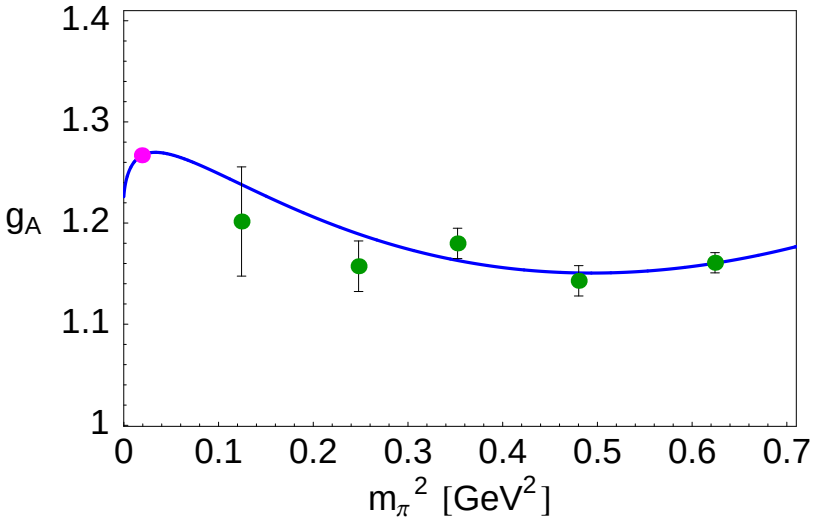

Figure 4.13: Leading-one-loop best-fit curve to the physical point and the three-flavor LHP data [165], with *explicit* $\Delta\,(1232)$ degrees of freedom (Fit 1).

agreement with the $SU(4)$ quark model prediction. In Fits 1-8 the values of $C^r(\lambda)$ extracted from both Eq.(4.36), are compatible within error bars with the range from $\pi N \to \pi\pi N$ analysis. The leading-one-loop Heavy Baryon expression has been confirmed to be totally inadequate for a correct description of the data.

Fig.4.14 shows the band of SSE fits obtained through the matching prescription, in Sec.4.4.5 at $\bar{\lambda} = 300\,\mathrm{MeV}$ (Fit 9 in Table 4.4). Comparing Tables 4.2, 4.3 and 4.4 we can conclude that the effects of the heavier flavor (together with possible systematic discrepancies due to the use of different fermion actions) are absorbed by the error bars of the output parameters.

4.4.7 Relativistic case

As explained in Sec.4.3, in manifestly covariant SSE the inclusion of the third order counterterms is not sufficient to get a renormalized result at order ϵ^3. The "tail" of recoil corrections carries an infinite string of divergent terms that can be absorbed only by an infinite number of higher-order counterterms.

The expression that we have analyzed has been worked out as follows. The starting point is the combination of Eqs.(E.1) and (E.5). We then introduce suitable combination of counterterms for Z_N,

$$-8m_\pi^2 B_{20} - \Delta^2 \tilde{B}_{30} \tag{4.52}$$

and for g_A itself,

$$4m_\pi^2 B_9 - \Delta^2 \tilde{B}_{31}\ . \tag{4.53}$$

We determine $\tilde{B}^r_{30}(\lambda)$ imposing $Z_N = 1$ as $m_\pi = 0$. Here the term $\Delta^2\tilde{B}_{30}$ is *the sum* of the whole string of counterterms able to absorb the divergences proportional to m_π^0 in the Z-factor, cf. Eq.(4.28). We then substitute the resulting Z_N in Eq.(E.1) and calculate

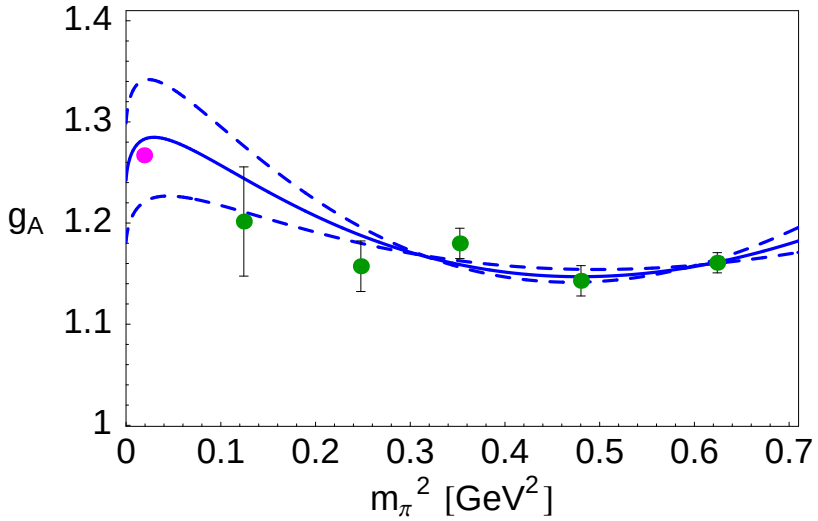

Figure 4.14: Leading-one-loop SSE fits to LHP data [165], with input from $\pi N \to \pi\pi N$ (Fit 9). The dashed curves correspond to the upper and lower boundaries for the parameter $C^r(\lambda)$ from Ref. [85].

$\tilde{B}^r_{31}(\lambda)$ imposing that $g_A = g_A^0$ as $m_\pi = 0$. Again, the term $\Delta^2\tilde{B}_{31}$ is the sum of an infinite string of counterterms. The resulting formula is still affected by (higher-order) residual regularization scale dependence and violation of decoupling [5].

We have then performed fits to the lattice data and the physical point with three free parameters, g_A^0, $C^{\rm SSE}(\lambda)$ and g_1. In the fit formulae we have chosen a specific value for the regularization scale and set equal to zero all higher-order counterterms *at this scale*.

It turns out that the output parameter g_1 is strongly affected by the choice of the scale λ. The term proportional to m_π^4, which is crucial to get a "flat" quark-mass behavior, is plagued by the uncompensated scale dependence: in our relativistic fits g_1 simply mimics the effects of neglected higher-order couplings. Therefore the inclusion of higher-order counterterms and the $\mathcal{O}(\epsilon^4)$ calculation seem to be crucial to shed light on a possible comparison of covariant SSE expression for g_A with existing lattice data. However, the available statistics is too low to permit the introduction of other free parameters in the fit function.

4.5 Summary

To conclude, we summarize the main results of our analysis of g_A:

- Up to and including next-to-next-to-leading order, it is not possible to obtain sensible interpolations between physical point and present lattice data in the framework of chiral perturbation theory restricted to pion and nucleon degrees of freedom only.

[5] Cf. the analogous case of the "full formula" for the nucleon mass in manifestiy covariant SSE, Sec.3.2.3.

- At the one-loop level, the inclusion of explicit $\Delta\,(1232)$ is crucial to get a satisfactory description of the quark mass dependence from the chiral limit across the physical point up to the lattice data. This does not come as a surprise in view of the Adler-Weisberger sum rule.

- The "chiral log" in the leading non-analytic quark-mass term is only visible for pion masses *well below* the physical point.

- Present lattice simulations *alone* cannot determine all the parameters in our extrapolation formula. Additional input from $\pi N \to \pi\pi N$ dynamics has to be invoked. $SU(4)$ spin-flavor symmetry arguments are not sufficient to generate the required form of $g_A(m_\pi)$.

- The inclusion of one heavier flavor in lattice simulations yields results that are statistically compatible with the two-flavor case.

Chapter 5

Summary and outlook

Lattice QCD is developing both on the theoretical and computational side as a major tool to quantitatively investigate the non-perturbative nature of low-energy QCD and in particular the nucleon structure. At present, however, such calculations are affected by sizeable systematic errors like discretization and finite-size effects, violation of chiral symmetry on the lattice, large quark masses in full-QCD simulations. While we are confident that all of them will be reduced by future improved algorithms and computing resources, we are still many years away from a satisfactory, quantitative, description of all non-perturbative facets of nucleon structure directly from the QCD Lagrangian, without any intermediate model-dependent assumptions. In the meantime, we are interested to explore the feasibility of systematic effective field theory approaches to provide a bridge between the lattice and the real world.

In our work we focus on the quark (pion) mass dependence of two nucleon observables, mass M_N and axial-vector coupling g_A. Both lattice QCD and chiral perturbation theory can provide such a functional dependence, in a complementary way: Green functions of QCD are computed on the lattice in terms of short-distance degrees of freedom, while their low-energy/low-mass expansions can be worked out rigorously, order by order, in terms of an effective field theory with low-energy degrees of freedom, the asymptotically observed hadrons. In Chiral Perturbation Theory, short-distance dynamics is encoded in low-energy couplings that can be determined by fits to data.

In Refs. [106, 107] we have studied intepolations of $M_N(m_\pi)$ between its physical value and a selected set of two-flavor full-QCD results, up to $m_\pi \approx 600\,\mathrm{MeV}$, with degenerate valence and sea quark masses. A remarkably good intepolation function is found already at leading-one-loop level (chiral order p^3) in the framework of manifestly covariant Baryon Chiral Perturbation Theory with infrared regularization, in the continuum and infinite volume limit. We also show that next-to-leading one-loop corrections are small, for the whole range of pion masses that we analyze. We have checked that fitting to present, large quark mass lattice data, we find remarkable consistency with information from low-energy hadron phenomenology for the low-energy couplings relevant for our analysis. These non-trivial results indicate that for the nucleon mass there exists a range of overlap in the quark masses accessible to both one-loop Baryon Chiral Perturbation Theory and present unquenched simulations. From the $\mathcal{O}(p^4)$ numerical analysis we determine the nucleon mass in the $SU(2)$ chiral limit, $M_0 \approx 0.88\,\mathrm{GeV}$ and the pion-nucleon sigma-term $\sigma_N = (49 \pm 3)\,\mathrm{MeV}$, at the physical value of the pion mass. Fits to an enlarged set of

lattice data taking into proper account finite-size corrections to M_N nicely confirm and sharpen our analysis in the infinite volume.

In the framework of leading-one-loop non-relativistic and manifestly covariant Small Scale Expansion, we have shown that for a satisfactory description of the quark mass dependence of the nucleon mass, it is not essential that the $\Delta(1232)$ is treated as a dynamical field in the effective Lagrangian. Its contribution is effectively accounted for by the low-energy couplings, whose numerical values are understood in terms of resonance exchange.

We have compared two versions of chiral effective field theory, namely Baryon Chiral Perturbation Theory and Small Scale Expansion (with and without explicit $\Delta(1232)$ degrees of freedom, respectively), also in the case of the axial-vector coupling g_A. Our analysis clearly shows that up to and including next-to-next-to-leading chiral order, it is not possible to obtain sensible interpolations between the physical point and present lattice data, if the $\Delta(1232)$ is "frozen" and its effects are encoded in contact interactions. This is not surprising in view of the Adler-Weisberger sum rule. The inclusion of *explicit* $\Delta(1232)$ degrees of freedom permits a successful interpolation already at leading-one-loop level in non-relativistic Small Scale Expansion [120]. According to our numerical study the leading "chiral log" is only visible for pion masses well below the physical one. Our results are pretty stable for different sets of lattice data as input, which are affected by different systematic errors. Remarkably, we found that the inclusion of one heavier flavor in the simulations yields statistically indistinguishable fit results compared to the two-flavor case.

The ultimate goal is to perform chiral *extrapolations*, enabling us to make *predictions* in the small quark mass region, with controlled errors, keeping the full systematics of Chiral Perturbation Theory, without any model dependence. Our statistical analysis [107] shows that in order to extract information from present, large quark mass lattice data, one must either incorporate phenomenological input or perform simultaneous fits to different observables characterized by a common subset of low-energy constants. We should make use of the property of Chiral Perturbation Theory of linking different observables via the same low-energy couplings, and get redundancy for the free parameters. Furthermore, as shown in the case of M_N, the systematic inclusion of lattice artifacts in the expressions used for the fits helps substantially to gain vital statistics.

Our work represents a first step. The joint analysis of energy and quark mass dependences of many nucleon observables, based both on empirical and lattice data at smaller quark masses, smaller lattice spacings and larger lattice volumes, will provide stringent bounds for the low-energy couplings and the chance to reliably test the convergence pattern of the low-energy/low-mass expansions. Such a fruitful synergy of numerical computation and analytic techniques will be extremely useful to make fundamental progress in understanding non-perturbative aspects of nucleon structure, one of the great and most fascinating open problems in physics.

Appendix A

The $\Delta(1232)$ Formalism

The free spin-3/2 field of mass M_Δ, represented by the vector-spinor field $\Psi_\mu(x)$, satisfies the equation of motion

$$(i\gamma_\nu\partial^\nu - M_\Delta)\Psi_\mu(x) = 0 \tag{A.1}$$

with the subsidiary condition

$$\gamma_\mu\Psi^\mu(x) = 0\ . \tag{A.2}$$

Expanding the spin-3/2 field into plane wave states of definite spin $s_\Delta = -\frac{3}{2}...+\frac{3}{2}$ and momentum p, we obtain an explicit representation of $\Psi_\mu(x)$ in terms of (anti)-particle creation and annihilation operators $b, b^\dagger$ $(d, d^\dagger)$, respectively:

$$\Psi_\mu(x) = \sum_{s_\Delta}\int\frac{d^3p}{J_F}\left(b(\mathbf{p},s_\Delta)\ u_\mu(\mathbf{p},s_\Delta)e^{-ip\cdot x} + d^\dagger(\mathbf{p},s_\Delta)\ v_\mu(\mathbf{p},s_\Delta)e^{ip\cdot x}\right)\ , \tag{A.3}$$

where $u_\mu(\mathbf{p},s_\Delta)$ is a Rarita-Schwinger spinor. For the energy dependent normalization constant J_F we choose

$$J_F = (2\pi)^3\frac{E}{M_\Delta}\ . \tag{A.4}$$

The Rarita-Schwinger spinor for the spin-3/2 field is constructed by coupling a spin-1 vector $e_\mu(\mathbf{p},\lambda)$ to a spin-1/2 Dirac spinor $u(\mathbf{p},s)$ via Clebsch-Gordan coefficients and then boosting to a velocity $\mathbf{v} = \mathbf{p}/M_\Delta$:

$$u_\mu(\mathbf{p},s_\Delta) = \sum_{\lambda,s}(1\lambda\frac{1}{2}s|\frac{3}{2}s_\Delta)\ e_\mu(\mathbf{p},\lambda)\ u(\mathbf{p},s)\ , \tag{A.5}$$

where

$$e^\mu(\mathbf{p},\lambda) = \left(\frac{\hat{\mathbf{e}}_\lambda\cdot\mathbf{p}}{M_\Delta}\ ,\ \hat{\mathbf{e}}_\lambda + \frac{\mathbf{p}(\hat{\mathbf{e}}_\lambda\cdot\mathbf{p})}{M_\Delta(p_0+M_\Delta)}\right) \tag{A.6}$$

$$u(\mathbf{p},s) = \sqrt{\frac{E+M_\Delta}{2M_\Delta}}\begin{pmatrix}\chi_s\\ \frac{\sigma\cdot\mathbf{p}}{E+M_\Delta}\chi_s\end{pmatrix}\ . \tag{A.7}$$

For the unit vectors $\hat{\mathbf{e}}_\lambda\ , \lambda = 0, \pm1$ appearing in Eq.(A.6) we use a spherical representation

$$\hat{\mathbf{e}}_+ = -\frac{1}{\sqrt{2}}\begin{pmatrix}1\\ i\\ 0\end{pmatrix}\quad \hat{\mathbf{e}}_0 = \begin{pmatrix}0\\ 0\\ 1\end{pmatrix}\quad \hat{\mathbf{e}}_- = \frac{1}{\sqrt{2}}\begin{pmatrix}1\\ -i\\ 0\end{pmatrix}\ . \tag{A.8}$$

The anti-particle spinors $v_\mu(\mathbf{p}, s_\Delta)$ can be constructed analogously.

The spin-3/2 field, due to its construction via a direct spin-1 – spin-1/2 coupling, always contains spurious spin-1/2 degrees of freedom. The following complete set of orthonormal spin projection operators enables the separation of the spin-3/2 and spin-1/2 components:

$$\left(P^{3/2}\right)_{\mu\nu} + \left(P_{11}^{1/2}\right)_{\mu\nu} + \left(P_{22}^{1/2}\right)_{\mu\nu} = g_{\mu\nu} \tag{A.9}$$

$$\left(P_{ij}^{I}\right)_{\mu\delta}\left(P_{kl}^{J}\right)^{\delta}{}_{\nu} = \delta^{IJ}\delta_{jk}\left(P_{il}^{J}\right)_{\mu\nu} \tag{A.10}$$

with

$$\begin{aligned}
\left(P^{3/2}\right)_{\mu\nu} &= g_{\mu\nu} - \frac{1}{3}\gamma_\mu\gamma_\nu - \frac{1}{3\,p^2}\left(\gamma\cdot p\;\gamma_\mu p_\nu + p_\mu\gamma_\nu\gamma\cdot p\;\right)\\
\left(P_{11}^{1/2}\right)_{\mu\nu} &= \frac{1}{3}\gamma_\mu\gamma_\nu - \frac{p_\mu p_\nu}{p^2} + \frac{1}{3\,p^2}\left(\gamma\cdot p\;\gamma_\mu p_\nu + p_\mu\gamma_\nu\gamma\cdot p\;\right)\\
\left(P_{22}^{1/2}\right)_{\mu\nu} &= \frac{p_\mu p_\nu}{p^2}\\
\left(P_{12}^{1/2}\right)_{\mu\nu} &= \frac{1}{\sqrt{3}p^2}\left(p_\mu p_\nu - \gamma\cdot p\;p_\nu\gamma_\mu\right)\\
\left(P_{21}^{1/2}\right)_{\mu\nu} &= \frac{1}{\sqrt{3}p^2}\left(\gamma\cdot p\;p_\mu\gamma_\nu - p_\mu p_\nu\right)\;.
\end{aligned} \tag{A.11}$$

$\Delta\,(1232)$ is an isospin-3/2 system. The four physical states $\Delta^{++}, \Delta^{+}, \Delta^{0}, \Delta^{-}$ can be described by treating the spin-3/2 field $\Psi_\mu(x)$ as an isospin-doublet and attaching an additional isovector index $i = 1, 2, 3$ to it. The resulting field, $\Psi_\mu^i(x)$, is therefore a vector-spinor field both in spin and in isospin space. The vector-spinor construction in isospin space would allow for six states. We therefore introduce a subsidiary condition, analogously to Eq.(A.2), to eliminate two degrees of freedom:

$$\tau^i\;\Psi_\mu^i(x) = 0\;, \tag{A.12}$$

where τ^i are the three Pauli matrices.

For the three isospin doublets we use the representation

$$\begin{aligned}
\Psi_\mu^1 &= \frac{1}{\sqrt{2}}\begin{bmatrix} \Delta^{++} - \frac{1}{\sqrt{3}}\Delta^0 \\ \frac{1}{\sqrt{3}}\Delta^+ - \Delta^- \end{bmatrix}_\mu\\
\Psi_\mu^2 &= \frac{i}{\sqrt{2}}\begin{bmatrix} \Delta^{++} + \frac{1}{\sqrt{3}}\Delta^0 \\ \frac{1}{\sqrt{3}}\Delta^+ + \Delta^- \end{bmatrix}_\mu\\
\Psi_\mu^3 &= -\sqrt{\frac{2}{3}}\begin{bmatrix} \Delta^+ \\ \Delta^0 \end{bmatrix}_\mu
\end{aligned} \tag{A.13}$$

One can construct a complete set of orthonormal isospin projection operators to separate the isospin-3/2 from the isospin-1/2 components:

$$\xi_{ij}^{3/2} + \xi_{ij}^{1/2} = \delta^{ij} \tag{A.14}$$

$$\xi_{ij}^{I}\xi_{jk}^{J} = \delta^{IJ}\xi_{ik}^{J} \tag{A.15}$$

with

$$\xi_{ij}^{3/2} = \delta^{ij} - \frac{1}{3}\tau^i\tau^j = \frac{2}{3}\delta^{ij} - \frac{i}{3}\epsilon_{ijk}\tau^k \tag{A.16}$$

$$\xi_{ij}^{1/2} = \frac{1}{3}\tau^i\tau^j = \frac{1}{3}\delta^{ij} + \frac{i}{3}\epsilon_{ijk}\tau^k \ . \tag{A.17}$$

Appendix B

Feynman rules

Here we collect the expressions of propagators and vertices relevant for our calculations.

Notation

q^μ four-momentum of an external pion

p^μ nucleon four-momentum

$a_\mu = \sum_{i=1}^{3} a_\mu^i \frac{\tau^i}{2}$ external axial field

τ^i are the Pauli matrices and isospin indices are written as Latin letters.

From $\mathcal{L}_\pi^{(2)}$

pion propagator:

$$\frac{i\delta^{ab}}{k^2 - m_\pi^2 + i\epsilon} \tag{B.1}$$

From $\mathcal{L}_{\pi N}^{(1)}$

nucleon propagator:

$$\frac{i}{\not{p} - M_0 + i\epsilon} \tag{B.2}$$

nucleon – 1 pion (q out):

$$\frac{g_A^0}{2f_\pi^0}\, q^\mu \gamma_\mu \gamma_5 \tau^a \tag{B.3}$$

nucleon – axial:

$$i\frac{g_A^0}{2} a_\mu^i \gamma^\mu \gamma_5 \tau^i \tag{B.4}$$

nucleon – 1 pion – axial:

$$\frac{i}{2f_\pi^0}\, a_\mu^b \gamma^\mu \epsilon^{abc} \tau^c \tag{B.5}$$

nucleon – 2 pions – axial:

$$i\frac{g_A^0}{4f_\pi^{0\,2}}\,a_\mu^c\gamma^\mu\gamma_5(\delta^{ac}\tau^b+\delta^{bc}\tau^a-2\delta^{ab}\tau^c) \tag{B.6}$$

From $\mathcal{L}_{\pi N}^{(2)}$

nucleon – 2 pions (q_1 in, q_2 out):

$$\frac{i\delta^{ab}}{f_\pi^{0\,2}}\left(-4c_1m_\pi^2+\frac{2c_2}{M_0^2}\,p_\mu q_1^\mu\,p_\nu q_2^\nu+2c_3\,q_1^\mu q_{2,\mu}\right)+\ldots \tag{B.7}$$

nucleon – 1 pion – axial (q out):

$$\frac{2c_3}{f_\pi^0}\,a_\mu^b q^\mu\delta^{ab}-i\frac{c_4}{2f_\pi^0}\,[\gamma^\mu,\gamma^\nu]\,q_\mu a_\nu^b\,\epsilon^{abc}\tau^c+\ldots \tag{B.8}$$

The dots indicate terms which are not needed here.

From $\mathcal{L}_{\pi N\Delta}^{(1)}$

nucleon – delta – 1 pion (q out), $Z=-1/2$:

$$\frac{c_A}{f_\pi^0}\,q^\mu\delta^{ab}g_{\mu\nu} \tag{B.9}$$

nucleon – delta – axial, $Z=-1/2$:

$$ic_A\,a_\mu^b\delta^{ab} \tag{B.10}$$

From $\mathcal{L}_{\pi\Delta}^{(1)}$

delta – delta – axial:

$$-i\frac{g_1}{2}\,a_\mu^b\gamma^\mu\gamma_5\,\xi_{3/2}^{ik}\tau^b\xi_{3/2}^{kj}\,g_{\mu\nu} \tag{B.11}$$

Furthermore, the delta propagator:

$$-i\,\frac{1}{\not{p}-M_\Delta^0+i\epsilon}\,\frac{p^2}{(M_\Delta^0)^2}\,P_{\mu\nu}^{3/2}\,\xi_{3/2}^{ij} \tag{B.12}$$

Appendix C

Loop integrals

A basic d-dimensional loop integral used at several places in the text is:

$$\Delta_\pi(m_\pi^2) = \frac{1}{i}\int \frac{d^dk}{(2\pi)^d}\frac{1}{m_\pi^2 - k^2 - i\epsilon} = m_\pi^{d-2}\,(4\pi)^{-d/2}\,\Gamma\left(1-\frac{d}{2}\right)\ . \tag{C.1}$$

Throughout this work we subtract the $1/(d-4)$ pole terms via

$$L(\lambda) = \frac{\lambda^{d-4}}{16\pi^2}\left\{\frac{1}{d-4} - \frac{1}{2}\left[\ln(4\pi) + \Gamma'(1) + 1\right]\right\}\ , \tag{C.2}$$

where λ is the dimensional regularization scale. Therefore

$$\Delta_\pi(m_\pi^2) = 2m_\pi^2\left[L(\lambda) + \frac{1}{16\pi^2}\ln\frac{m_\pi}{\lambda}\right]\ . \tag{C.3}$$

For loop integrals involving a nucleon propagator, the subscript I denotes the infrared singular part, as specified in Sec.2.8.2.

$$I_N(p^2, m_\pi^2) = \frac{1}{i}\int_I \frac{d^dk}{(2\pi)^d}\frac{1}{(m_\pi^2 - k^2 - i\epsilon)[M_0^2 - (p-k)^2 - i\epsilon]} \tag{C.4}$$

$$I_N(p^2, m_\pi^2) = -\frac{p^2 - M_0^2 + m_\pi^2}{p^2}\,L(\lambda) + \bar{I}_N(p^2, m_\pi) \tag{C.5}$$

$$\begin{aligned}\bar{I}_N(p^2, m_\pi^2) = &-\frac{1}{8\pi^2}\frac{\alpha\sqrt{1-\Omega^2}}{1+2\alpha\Omega+\alpha^2}\arccos\left(-\frac{\Omega+\alpha}{\sqrt{1+2\alpha\Omega+\alpha^2}}\right)\\ &-\frac{1}{16\pi^2}\frac{\alpha(\alpha+\Omega)}{1+2\alpha\Omega+\alpha^2}\left(2\ln\frac{m_\pi}{\lambda} - 1\right)\end{aligned} \tag{C.6}$$

$$\alpha = \frac{m_\pi}{M_0}\,, \qquad \Omega = \frac{p^2 - m_\pi^2 - M_0^2}{2m_\pi M_0}\ . \tag{C.7}$$

$$p^\mu I_N^{(1)}(p^2, m_\pi^2) = \frac{1}{i}\int_I \frac{d^dk}{(2\pi)^d}\frac{k^\mu}{(m_\pi^2 - k^2 - i\epsilon)[M_0^2 - (p-k)^2 - i\epsilon]} \ . \tag{C.8}$$

Using

$$p\cdot k = \frac{1}{2}(p^2 - M_0^2 + m_\pi^2) + \frac{1}{2}(k^2 - m_\pi^2) - \frac{1}{2}\left[(p-k)^2 - M_0^2\right] \ , \tag{C.9}$$

we obtain

$$I_N^{(1)}(p^2, m_\pi^2) = \frac{1}{2}\left[(p^2 - M_0^2 + m_\pi^2) I_N(p^2, m_\pi^2) + \Delta_\pi(m_\pi^2)\right] \ . \tag{C.10}$$

Throughout our work we use the notation

$$I_N \equiv I_N(p^2 = M_0^2, m_\pi^2), \qquad I_N^{(1)} \equiv I_N^{(1)}(p^2 = M_0^2, m_\pi^2), \tag{C.11}$$

$$I_\Delta(p^2) \equiv I_N(p^2, M_0 \to M_\Delta^0), \qquad I_\Delta \equiv I_\Delta(p^2 = M_0^2, m_\pi^2) \ . \tag{C.12}$$

Appendix D

g_A to $\mathcal{O}(p^3)$ and $\mathcal{O}(p^4)$ in BChPT

We show the contributions to the axial coupling g_A from both the leading- and next-to-leading one-loop Feynman diagrams ($\mathrm{Amp_i}$) in Baryon Chiral Perturbation Theory. To simplify the calculation we have made use of the gauge condition $a_\mu q^\mu = 0$, without any loss of generality. According to Fig.4.1, at order p^3,

$$\mathrm{Amp}_1 = i\,\eta^\dagger \frac{\tau^i}{2}\eta\;\bar{u}(p) a_\mu^i \gamma^\mu\gamma_5 u(p)\left(g_A^0 Z_N + 4m_\pi^2 B_9 + 32 m_\pi^4 F_1\right) \tag{D.1}$$

$$\mathrm{Amp}_2 = \mathrm{Amp}_3 = i\frac{g_A^0}{f_\pi^{0\,2}}\,\eta^\dagger \frac{\tau^i}{2}\eta\;\bar{u}(p) a_\mu^i \gamma^\mu\gamma_5 u(p)\left(\Delta_\pi - 2M_0^2\, I_N^{(1)}\right) \tag{D.2}$$

$$\begin{aligned}\mathrm{Amp}_4 = &-i\frac{{g_A^0}^3}{4f_\pi^2}\,\eta^\dagger \frac{\tau^i}{2}\eta\;\bar{u}(p) a_\mu^i \gamma^\mu\gamma_5 u(p)\left\{\Delta_\pi - 4M_0^2\, I_N^{(1)} - 2M_0 m_\pi^2 \frac{\partial}{\partial M_0} I_N\right.\\ &\left. -\frac{8M_0^2}{d-1}\left[\left(\frac{m_\pi^4}{8M_0^3} - \frac{m_\pi^2}{2M_0}\right)\frac{\partial}{\partial M_0} I_N - \frac{m_\pi^2}{4M_0^2} I_N - \frac{1}{2}\, I_N^{(1)}\right]\right\}\end{aligned} \tag{D.3}$$

$$\mathrm{Amp}_5 = -\,i\frac{g_A^0}{f_\pi^{0\,2}}\,\eta^\dagger \frac{\tau^i}{2}\eta\;\bar{u}(p) a_\mu^i \gamma^\mu\gamma_5 u(p)\,\Delta_\pi\ . \tag{D.4}$$

Here we use the notation

$$\frac{\partial}{\partial M_0} I_N = \left.\frac{\partial}{\partial M_0} I_N(p^2)\right|_{p^2 = M_0^2}\ . \tag{D.5}$$

The nucleon field Ψ is represented in terms of the Dirac spinor u and the isospinor η.

In the $\mathcal{O}(p^4)$ calculation, we need to evaluate the c_1-insertions to Amp_2, Amp_3 and Amp_4 in Fig.4.1. We replace M_0 with $M_0 - 4c_1 m_\pi^2$ and extract the contribution to g_A at this order by keeping the terms in the expansion in powers of c_1 up to and including the linear one.

The c_1-insertions to the graphs of Figs.4.2 and 4.5 contribute to wave-function renormalization:

$$i\, g_A^0\, \bar{u}(p)\eta^\dagger \frac{\tau^i}{2}\eta\; a_\mu^{(i)}\gamma^\mu\gamma_5\left(1 + \Sigma_a(\not{p} = M_0 - 4\,c_1 m_\pi^2) + \Sigma_b(\not{p} = M_0)\right) u(p)\ , \tag{D.6}$$

where Σ_a and Σ_b are the nucleon self-energies in Secs.3.2.1, 3.2.2. Again, what is relevant at our accuracy is the linear term in the expansion of (D.6) in powers of c_1.

The graphs shown in Fig.4.3 contribute as follows:

$$\begin{aligned}\mathrm{Amp}_6 = \mathrm{Amp}_7 = &- i\frac{g_A^0}{(d-1)f_\pi^2 M_0}\,\eta^\dagger\frac{\tau^i}{2}\eta\;\bar{u}(p)a_\mu^i\gamma^\mu\gamma_5 u(p)\,m_\pi^2\left[c_3\left(\Delta_\pi + I_N(m_\pi^2 - 4M_0^2)\right)\right.\\ &\left. + c_4\left(\Delta_\pi + 4I_N(d-2)M_0^2 + I_N\,m_\pi^2)\right)\right]\ . \qquad \text{(D.7)}\end{aligned}$$

Appendix E

g_A to $\mathcal{O}(\epsilon^3)$ in relativistic SSE

The leading-one-loop graphs 1-8 of Fig.4.6 in manifestly covariant SSE give the following expression:

$$
\begin{aligned}
g_A \;=\; & -\frac{1}{72\,d\,(d-2)(d-1)^3\,f_\pi^2\,M_0^2(M_0-M_\Delta^0){M_\Delta^0}^4}\times \\
& \Big\{10c_A^2 d g_1(M_0-M_\Delta^0)(M_0^2+2M_\Delta^0 M_0+{M_\Delta^0}^2-m_\pi^2)\left[(d-2)M_0^6+2(d^2-3d-1)M_\Delta^0 M_0^5\right. \\
& +((2d^2-9d+8){M_\Delta^0}^2-3(d-2)m_\pi^2)M_0^4-2M_\Delta^0((5d^2-16d+1){M_\Delta^0}^2 \\
& +2(d^2-3d-1)m_\pi^2)M_0^3+((-2d^2+3d+8){M_\Delta^0}^4+2(-d^2+d+5)m_\pi^2{M_\Delta^0}^2 \\
& +3(d-2)m_\pi^4)M_0^2+2M_\Delta^0({M_\Delta^0}^2-m_\pi^2)((4d^2-13d+2){M_\Delta^0}^2+(-d^2+3d+1)m_\pi^2)M_0 \\
& \left.+({M_\Delta^0}^2-m_\pi^2)^2((5d-14){M_\Delta^0}^2-(d-2)m_\pi^2)\right](d-2)^2\,\mathbf{I_\Delta}+5c_A^2(d-3)d\,g_1(M_0-M_\Delta^0) \\
& \times M_\Delta^0(M_0^2-2M_\Delta^0 M_0+{M_\Delta^0}^2-m_\pi^2)(M_0^2+2M_\Delta^0 M_0+{M_\Delta^0}^2-m_\pi^2)^2 \\
& \times(M_0^2+2dM_\Delta^0 M_0+{M_\Delta^0}^2-m_\pi^2)(d-2)^2\,\frac{\partial}{\partial M_\Delta^0}\mathbf{I_\Delta} \\
& +2c_A^2(d-2)^2\Big[\boldsymbol{\Delta}_\pi\,10g_1M_0(M_0-M_\Delta^0)(-3{M_\Delta^0}^5-5M_0{M_\Delta^0}^4+4m_\pi^2{M_\Delta^0}^3 \\
& +3M_0^3{M_\Delta^0}^2+3M_0m_\pi^2{M_\Delta^0}^2+M_0^4M_\Delta^0-m_\pi^4M_\Delta^0+4M_0^2m_\pi^2M_\Delta^0+4M_0^3m_\pi^2)d^3 \\
& +d^2\boldsymbol{\Delta}_\pi(M_0-M_\Delta^0)\Big(5g_1(M_0^6-4M_\Delta^0M_0^5-(18{M_\Delta^0}^2+29m_\pi^2)M_0^4-24M_\Delta^0m_\pi^2M_0^3 \\
& +(29{M_\Delta^0}^4-8m_\pi^2{M_\Delta^0}^2-5m_\pi^4)M_0^2+4M_\Delta^0(3{M_\Delta^0}^4-4m_\pi^2{M_\Delta^0}^2+m_\pi^4)M_0 \\
& -({M_\Delta^0}^2-m_\pi^2)^2(4{M_\Delta^0}^2-m_\pi^2))-12g_A^0{M_\Delta^0}^2(M_0^4+4M_\Delta^0M_0^3+6({M_\Delta^0}^2-2m_\pi^2)M_0^2 \\
& +(4{M_\Delta^0}^3-6M_\Delta^0m_\pi^2)M_0+({M_\Delta^0}^2-m_\pi^2)^2)\Big)-d(d-1)\,12g_A^0{M_\Delta^0}^2\Big(\mathbf{I_\Delta}(M_0+M_\Delta^0) \\
& \times(M_0^2-2M_\Delta^0M_0+{M_\Delta^0}^2-m_\pi^2)(M_0^2+2M_\Delta^0M_0+{M_\Delta^0}^2-m_\pi^2)^2 \\
& +2\mathbf{I_N}M_0(M_\pi^3-4M_0^2m_\pi)^2\Big)
\end{aligned}
$$

$$
\begin{aligned}
&-\mathbf{\Delta}_\pi\, d\,(M_0 - M_\Delta^0)\,\Big(5g_1(2M_0^6 + 6M_\Delta^0 M_0^5 + 3({M_\Delta^0}^2 - 2m_\pi^2)M_0^4 \\
&+8M_\Delta^0 m_\pi^2 M_0^3 - 2(3{M_\Delta^0}^4 - 18m_\pi^2{M_\Delta^0}^2 + 7m_\pi^4)M_0^2 \\
&-6M_\Delta^0(3{M_\Delta^0}^4 - 4m_\pi^2{M_\Delta^0}^2 + m_\pi^4)M_0 - (11{M_\Delta^0}^2 - 2m_\pi^2)({M_\Delta^0}^2 - m_\pi^2)^2) \\
&-12g_A^0{M_\Delta^0}^2(M_0^4 + 4M_\Delta^0 M_0^3 + 2(3{M_\Delta^0}^2 - 8m_\pi^2)M_0^2 + (4{M_\Delta^0}^3 - 6M_\Delta^0 m_\pi^2)M_0 \\
&+({M_\Delta^0}^2 - m_\pi^2)^2)\Big) + \mathbf{\Delta}_\pi\, 4m_\pi^2 M_0^2(M_0 - M_\Delta^0)(12g_A^0{M_\Delta^0}^2 \\
&+5g_1(4M_0^2 + 6M_\Delta^0 M_0 + 5{M_\Delta^0}^2 - 2m_\pi^2))\Big] - 18(d-1)^3 d M_0(M_0 - M_\Delta^0){M_\Delta^0}^4 \times \\
&\Big(\frac{\partial}{\partial M_0}\mathbf{I_N}\, {g_A^0}^3(m_\pi^4 + 2dM_0^2 m_\pi^2 - 8M_0^2 m_\pi^2) + \mathbf{I_N}\, 2M_0 m_\pi^2 g_A^0(d{g_A^0}^2 - 3{g_A^0}^2 - 4d + 8) \\
&+16(d-2)B_9 f_\pi^2 M_0 m_\pi^2 + 4(d-2)B_{31}(M_\Delta^0 - M_0)^2 f_\pi^2 M_0 \\
&+(d-2)\mathbf{\Delta}_\pi g_A^0({g_A^0}^2 - 4)M_0 + 4(d-2)f_\pi^2 g_A^0 M_0 Z_N\Big)\Big\}\ , \qquad \text{(E.1)}
\end{aligned}
$$

where d is the space-time dimension, M_Δ^0 is the delta mass in the $SU(2)$ chiral limit and

$$
\frac{\partial}{\partial M_0} I_N = \frac{\partial}{\partial M_0} I_N(p^2)\Big|_{p^2 = M_0^2} \qquad \frac{\partial}{\partial M_\Delta^0} I_\Delta = \frac{\partial}{\partial M_\Delta^0} I_\Delta(p^2)\Big|_{p^2 = {M_0}^2}\ . \qquad \text{(E.2)}
$$

Z_N is the wave-function renormalization factor defined as the residue at the pole of the nucleon two-point function

$$
Z_N^{-1} \;=\; 1 - \frac{\partial \Sigma_N}{\partial \not{p}}\Big|_{\not{p} = M_N}\ . \qquad \text{(E.3)}
$$

At order ϵ^3

$$
Z_N \approx 1 + \frac{\partial \Sigma_N^{(3)}}{\partial \not{p}}\Big|_{\not{p} = M_0} \qquad \text{(E.4)}
$$

where $\Sigma_N^{(3)}$ is the $\mathcal{O}(\epsilon^3)$ nucleon self-energy which includes the contribution of the explicit $\Delta\,(1232)$ degrees of freedom (see Fig.4.7 and Sec.3.2.3). Explicitly,

$$
\begin{aligned}
Z_N \;=\;& 1 + \frac{c_A^2 L}{9 f_\pi^2 M_0^4(\Delta + M_0)^2}\,\Big(15\Delta^8 + 140M_0\Delta^7 + (532M_0^2 - 60m_\pi^2)\Delta^6 \\
&+210(5M_0^3 - 2M_0 m_\pi^2)\Delta^5 + 2(566M_0^4 - 588m_\pi^2 M_0^2 + 45m_\pi^4)\Delta^4 \\
&+4(158M_0^5 - 420m_\pi^2 M_0^3 + 105m_\pi^4 M_0)\Delta^3 + 12(12M_0^6 - 107m_\pi^2 M_0^4 \\
&+63m_\pi^4 M_0^2 - 5m_\pi^6)\Delta^2 - 2(70M_0 m_\pi^6 - 315M_0^3 m_\pi^4 + 246M_0^5 m_\pi^2)\Delta \\
&+15m_\pi^8 - 112M_0^2 m_\pi^6 + 222M_0^4 m_\pi^4 - 72M_0^6 m_\pi^2\Big) \\
&+L\left(\frac{3{g_A^0}^2 m_\pi^4}{f_\pi^2 M_0^2} - \frac{9{g_A^0}^2 m_\pi^2}{2f_\pi^2}\right)
\end{aligned}
$$

$$
\begin{aligned}
&+\frac{1}{3456 f_\pi^2 M_0^4 \pi^2}\left\{\frac{4c_A^2}{(\Delta+M_0)^2}(9\Delta^8+88M_0\Delta^7+4(89M_0^2-9m_\pi^2)\Delta^6\right.\\
&+6(127M_0^3-44M_0m_\pi^2)\Delta^5+(908M_0^4-780m_\pi^2M_0^2+54m_\pi^4)\Delta^4\\
&+8(71M_0^5-147m_\pi^2M_0^3+33m_\pi^4M_0)\Delta^3+12(12M_0^6-79m_\pi^2M_0^4+41m_\pi^4M_0^2-3m_\pi^6)\Delta^2\\
&+(-88M_0m_\pi^6+414M_0^3m_\pi^4-396M_0^5m_\pi^2)\Delta+9m_\pi^8-68M_0^2m_\pi^6+165M_0^4m_\pi^4\\
&-72M_0^6m_\pi^2)+\frac{24c_A^2}{(\Delta+M_0)^2}\left(15\Delta^8+140M_0\Delta^7+(532M_0^2-60m_\pi^2)\Delta^6\right.\\
&+210(5M_0^3-2M_0m_\pi^2)\Delta^5+2(566M_0^4-588m_\pi^2M_0^2+45m_\pi^4)\Delta^4+4(158M_0^5\\
&-420m_\pi^2M_0^3+105m_\pi^4M_0)\Delta^3+12(12M_0^6-107m_\pi^2M_0^4+63m_\pi^4M_0^2-5m_\pi^6)\Delta^2\\
&-2(70M_0m_\pi^6-315M_0^3m_\pi^4+246M_0^5m_\pi^2)\Delta+15m_\pi^8-112M_0^2m_\pi^6+222M_0^4m_\pi^4\\
&\left.-72M_0^6m_\pi^2\right)\ln\frac{m_\pi}{\lambda}-8(\Delta^2+4M_0\Delta+4M_0^2-m_\pi^2)\left[6\Delta^6+31M_0\Delta^5\right.\\
&+55M_0^2\Delta^4-18m_\pi^2\Delta^4+37M_0^3\Delta^3-62M_0m_\pi^2\Delta^3+6M_0^4\Delta^2+18m_\pi^4\Delta^2\\
&-60M_0^2m_\pi^2\Delta^2+31M_0m_\pi^4\Delta-13M_0^3m_\pi^2\Delta-6m_\pi^6+5M_0^2m_\pi^4+6M_0^4m_\pi^2\\
&-\sqrt{\Delta^2-m_\pi^2}\sqrt{\Delta^2+4M_0\Delta+4M_0^2-m_\pi^2}(15\Delta^4+50M_0\Delta^3+(52M_0^2-30m_\pi^2)\Delta^2\\
&+2(9M_0^3-25M_0m_\pi^2)\Delta+15m_\pi^4-22M_0^2m_\pi^2)\\
&\left.\left.\times\ln\left(\frac{\Delta^2+2M_0\Delta-m_\pi^2}{2M_0m_\pi}+\sqrt{\frac{(\Delta^2+2M_0\Delta-m_\pi^2)^2}{4M_0^2m_\pi^2}-1}\right)\right]\right.\\
&-\frac{324{g_A^0}^2M_0m_\pi^2}{\sqrt{4-m_\pi^2/M_0^2}}\left[(2m_\pi^3-6M_0^2m_\pi)\arccos\left(-\frac{m_\pi}{2M_0}\right)\right.\\
&\left.\left.+M_0\sqrt{4-\frac{m_\pi^2}{M_0^2}}\left(M_0^2+(3M_0^2-2m_\pi^2)\ln\frac{m_\pi}{\lambda}\right)\right]\right\}\ ,
\end{aligned}
\tag{E.5}
$$

where Δ is the delta-nucleon mass splitting in the $SU(2)$ chiral limit.

List of figures

Bibliography

[1] D. J. Gross and F. Wilczek, Phys. Rev. Lett. **30**, 1343 (1973); D. J. Gross and F. Wilczek, Phys. Rev. **D8**, 3633 (1973); H. D. Politzer, Phys. Rev. Lett. **30**, 1346 (1973).

[2] K. G. Wilson, Phys. Rev. **D10**, 2445 (1974).

[3] See for example: H. J. Rothe, *Lattice Gauge Theories - An Introduction*, World Scientific, Singapore (1992); I. Montvay and G. Münster, *Quantum Fields on a Lattice*, Cambridge University Press, Cambridge (1994); J. Smit, *Introduction to Quantum Fields on a Lattice*, Cambridge University Press, Cambridge (2002).

[4] W. Schroers, Ph.D. thesis, University of Wuppertal (2001), `hep-lat/0304016`.

[5] A. S. Kronfeld, "Uses of Effective Field Theory in Lattice QCD" in: *At the Frontiers of Particle Physics*, Handbook of QCD, ed. M. Shifman, **4**, Chapter 39, World Scientific, Singapore (2002).

[6] A. Ukawa (CP-PACS & JLQCD collaborations), Nucl. Phys. B (Proc. Suppl.) **106**, 195 (2002).

[7] K. Symanzik, in *Recent Developments in Gauge Theories*, edited by G. 't Hooft *et al.*, Plenum, New York (1980); K. Symanzik, Nucl. Phys. **B226**, 187, 205 (1983).

[8] M. Lüscher, Commun. Math. Phys. **104**, 177 (1986); *Ibid.* **105**, 153 (1986).

[9] S. Weinberg, Physica **A96**, 327 (1979).

[10] J. Gasser and H. Leutwyler, Ann. Phys. **158**, 142 (1984).

[11] J. Gasser and H. Leutwyler, Nucl. Phys. **B250**, 465 (1985).

[12] D. J. Gross and F. Wilczek, Phys. Rev. Lett. **30**, 1343 (1973); S. Weinberg, Phys. Rev. Lett. **31**, 494 (1973); H. Fritzsch, M. Gell-Mann and H. Leutwyler, Phys. Lett. **B47**, 365 (1973).

[13] The Review of Particle Physics, S. Eidelman *et al.*, Phys. Lett. **B592**, 1 (2004).

[14] V. Baluni, Phys. Rev. **D19**, 2227 (1978); R. J. Crewther, P. Di Vecchia, G. Veneziano and E. Witten, Phys. Lett. **88B**, 123 (1979); *Erratum ibid.* **9B**, 187 (1980).

[15] A. Pich and E. de Rafael, Nucl. Phys. **B367**, 313 (1991); B. Borasoy, Phys. Rev. **D61**, 114017 (2000).

[16] G. 't Hooft and M. Veltman, Nucl. Phys. **B44**, 189 (1972).

[17] W. A. Bardeen, A. J. Buras, D. W. Duke and T. Muta, Phys. Rev. **D18**, 3998 (1978).

[18] T. Muta, *Foundations of Quantum Chromodynamics*, World Scientific, Singapore (1987).

[19] S. L. Adler, Phys. Rev. **177**, 2426 (1969); S. L. Adler and W. A. Bardeen, Phys. Rev. **182**, 1517 (1969); W. A. Bardeen, Phys. Rev. **184**, 1848 (1969); J. S. Bell and R. Jackiw, Nuovo Cimento, **A60**, 47 (1969).

[20] F. Karsch, Lect. Notes Phys. **583**, 109 (2002).

[21] J. Goldstone, Nuovo Cimento **19**, 154 (1961).

[22] H. Leutwyler, Ann. Phys. **235**, 165 (1994).

[23] J. Bernstein, S. Fubini, M. Gell-Mann and W. Thirring, Nuovo Cimento **17**, 757 (1960); M. Gell-Mann and M. Lévy, Nuovo Cimento **16**, 705 (1960); K.-C. Chou, Soviet Physics JETP **12**, 492 (1961).

[24] H. Leutwyler, Lecture Notes, ITP Bern (2001).

[25] M. Gell-Mann, R. J. Oakes and B. Renner, Phys. Rev. **175**, 2195 (1968).

[26] J. Gasser and A. Zepeda, Nucl. Phys. **B174**, 445 (1980).

[27] J. Gasser, Ann. Phys. **136**, 62 (1981).

[28] A. Manohar and H. Georgi, Nucl. Phys. **B234**, 189 (1984).

[29] A. V. Manohar, Lectures given at the 35th International University School of Nuclear and Particle Physics, Schladming, Austria (1996), `hep-ph/9606222`.

[30] M. Soldate and R. Sundrum, Nucl. Phys. **B340**, 1 (1990).

[31] R. S. Chivukula, M. J. Dugan and M. Golden, Phys. Rev. **D47**, 2930 (1993).

[32] M. Knecht, B. Moussallam, J. Stern and N. H. Fuchs, Nucl. Phys. **B457**, 513 (1995); *ibid.* **B471**, 445 (1996).

[33] G. Colangelo, J. Gasser and H. Leutwyler, Phys. Rev. Lett. **86**, 5008 (2001).

[34] S. Dürr, Eur. Phys. J. **C29**, 383 (2003).

[35] M. Lüscher, Talk given at the XXIIIrd International Symposium on Lattice Field Theory, Dublin, 25-30 July 2005, `hep-lat/0509152`.

[36] R. Sommer, Nucl. Phys. **B411**, 839 (1994).

[37] G. Colangelo and S. Dürr, Eur. Phys. J. **C33**, 543 (2004).

[38] M. Göckeler *et al.*, `hep-lat/0409312`.

[39] S. Weinberg, Phys. Rev. **166**, 1568 (1968).

[40] S. Coleman, J. Wess and B. Zumino, Phys. Rev. **177**, 2239 (1969); C. G. Callan, S. Coleman, J. Wess and B. Zumino, Phys. Rev. **177**, 2247 (1969).

[41] P. Langacker and H. Pagels, Phys. Rev. **D8**, 4595 (1971).

[42] H. Pagels, Phys. Rep. **16** 219 (1975).

[43] J. Gasser, M. E. Sainio and A. Švarc, Nucl. Phys. **B307**, 779 (1988).

[44] A. Krause, Helv. Phys. Acta **63**, 3 (1990).

[45] H. Georgi, *Weak Interactions and Modern Particle Theory*, Benjamin/Cummings, Menlo Park (1984).

[46] J. F. Donoghue and B. R. Holstein, Phys. Lett. **B436**, 331 (1998); J. F. Donoghue, B. R. Holstein and B. Borasoy, Phys. Rev. **D59**, 036002 (1999).

[47] E. Jenkins and A. V. Manohar, Phys. Lett. **B255**, 558 (1991).

[48] E. Jenkins and A.V. Manohar, in: *Effective Field Theories of the Standard Model*, ed. by U.-G. Meißner, World Scientific, Singapore (1992).

[49] V. Bernard, N. Kaiser, J. Kambor and U.-G. Meißner, Nucl. Phys. **B388**, 315 (1992).

[50] L. L. Foldy and S. A. Wouthuysen, Phys. Rev. **78**, 29 (1950).

[51] C. Itzykson and J. B. Zuber, *Quantum Field Theory*, McGraw-Hill, New York (1980).

[52] V. Bernard, N. Kaiser and U.-G. Meißner, Int. J. Mod. Phys. **E4**, 193 (1995).

[53] S. Weinberg, Nucl. Phys. **B363**, 3 (1991).

[54] G. Ecker, Czech. J. Phys. **44**, 405 (1994); G. Ecker, Prog. Part. Nucl. Phys. **35**, 1 (1995).

[55] V. Bernard, N. Kaiser and U.-G. Meißner, Nucl. Phys. **A611**, 429 (1996).

[56] P. J. Ellis and H.-B. Tang, Phys. Rev. **C57**, 3356 (1998).

[57] T. Becher and H. Leutwyler, Eur. Phys. J. **C9**, 643 (1999).

[58] T. Fuchs, J. Gegelia, G. Japaridze and S. Scherer, Phys. Rev. **D68**, 056005 (2003).

[59] J. Gasser and H. Leutwyler, Phys. Rep. **87C**, 77 (1982).

[60] G. Ecker, Phys. Lett. **B336**, 508 (1994).

[61] N. Fettes, U.-G. Meißner, M. Mojžiš and S. Steininger, Annals Phys. **283**, 273 (2000); *Erratum ibid.* **288**, 249 (2001).

[62] *e. g.* G. Ecker and M. Mojžiš, Phys. Lett. **B365**, 312 (1995).

[63] J. Gasser, H. Leutwyler and M. E. Sainio, Phys. Lett. **B253**, 252 (1991).

[64] R. A. Arndt, W. J. Briscoe, I. I. Strakovsky, R. L. Workman and M. M. Pavan, Phys. Rev. **C69**, 035213 (2004).

[65] N. Fettes, U.-G. Meißner and S. Steininger, Nucl. Phys. **A640**, 199 (1998).

[66] N. Fettes and U.-G. Meißner, Nucl. Phys. **A676**, 311 (2000).

[67] R. Koch, Nucl. Phys. **A448**, 707 (1986).

[68] E. Matsinos, Phys. Rev. **C56**, 3014 (1997).

[69] SAID on-line program, R.A. Arndt *et al.*

[70] T. Becher and H. Leutwyler, JHEP **0106**, 017 (2001).

[71] G. Höhler, in Landolt-Börnstein, Vol. **9b2**, ed. H. Schopper, Springer, Berlin (1983).

[72] P. Büttiker and U.-G. Meißner, Nucl. Phys. **A668**, 97 (2000).

[73] V. Bernard, N. Kaiser and U.-G. Meißner, Nucl. Phys. **A615**, 483 (1997).

[74] M. Mojžiš, Eur. Phys. J. **C2**, 181 (1998).

[75] H.-Ch. Schröder *et al.*, Phys. Lett. **B469**, 25 (1999).

[76] U.-G. Meißner, U. Raha and A. Rusetsky, Eur. Phys. J. **C41**, 213 (2005).

[77] H.-Ch. Schröder et al., Eur. Phys. J. **C21**, 473 (2001).

[78] T. E. O. Ericson, B. Loiseau and A. W. Thomas, Phys. Rev. **C66**, 014005 (2002).

[79] D. R. Entem and R. Machleidt, Phys. Rev. **C 66**, 014002 (2002).

[80] E. Epelbaum, W. Glöckle and U.-G. Meißner, Nucl. Phys. **A747**, 362 (2005).

[81] E. Epelbaum, `nucl-th/0509032`.

[82] *e.g.* see M. Kermani *et al.*, Phys. Rev. **C58**, 3419 (1998); J. B. Lange *et al.*, Phys. Rev. Lett. **80**, 1597 (1998) and references therein to earlier experiments.

[83] N. Fettes, V. Bernard, U.-G. Meißner, Nucl. Phys. **A669**, 269 (2000).

[84] J. Zhang, N. Mobed and M. Benmerrouche, `nucl-th/9806063`.

[85] N. Fettes, Berichte des Forschungszentrums Jülich Nr. 3814 (2000).

[86] G. E. Brown and W. Weise, Phys. Rep. **22**, 279 (1975).

[87] T. R. Hemmert, B. R. Holstein and J. Kambor, J. Phys. **G24**, 1831 (1998).

[88] R. F. Dashen, E. Jenkins and A. V. Manohar, Phys. Rev. **D49**, 4713 (1994); *Erratum ibid.* **D51**, 2489 (1995).

[89] V. Pascalutsa and D. R. Phillips, Phys. Rev. **C67**, 055202 (2003).

[90] P. A. Moldauer and K. M. Case, Phys. Rev. **102**, 279 (1956).

[91] L. M. Nath, B. Etemadi and J. D. Kimel, Phys. Rev. **D3**, 2153 (1971).

[92] S. Kamefuchi, L. O'Raifeartaigh and A. Salam, Nucl. Phys. **28**, 529 (1961).

[93] V. Bernard, T. R. Hemmert and U.-G. Meißner, Phys. Lett. **B622**, 141 (2005).

[94] H.-B. Tang and P. J. Ellis, Phys. Lett. **B387**, 9 (1996).

[95] V. Bernard, H. W. Fearing, T. R. Hemmert and U.-G. Meißner, Nucl. Phys. **A635**, 121 (1998); *Erratum ibid.* **A642**, 563 (1998).

[96] T. Appelquist and J. Carazzone, Phys. Rev. **D11**, 2856 (1975).

[97] B. A. Ovrut and H. J. Schnitzer, Phys. Rev. **D22**, 2518 (1980).

[98] V. Bernard, T.R. Hemmert and U.-G. Meißner, Phys. Lett. **B565**, 137 (2003).

[99] K. Johnson and E. C. G. Sudarshan, Ann. Phys. **13**, 126 (1961).

[100] E. Jenkins and A. V. Manohar, Phys. Lett. **B259**, 353 (1991).

[101] C. W. Bernard *et al.*, Phys. Rev. **D64**, 054506 (2001).

[102] O. Hanstein, D. Drechsel and L. Tiator, Phys. Lett. **B385**, 45 (1996).

[103] T.R. Hemmert, Ph.D. thesis, University of Massachussets at Amherst (1997).

[104] N. Fettes and U.-G. Meißner, Nucl. Phys. **A679**, 629 (2001).

[105] D. Jido, T. Hatsuda and T. Kunihiro, Phys. Rev. Lett. **84**, 3252 (2000).

[106] M. Procura, T. R. Hemmert and W. Weise, Phys. Rev. **D69**, 034505 (2004).

[107] M. Procura, B. U. Musch, T. R. Hemmert, T. Wollenweber and W. Weise, *forthcoming*.

[108] X.-D. Ji, Phys. Rev. **D52**, 271 (1995).

[109] J. A. McGovern and M. C. Birse, Phys Lett. **B446**, 300 (1999).

[110] M. Göckeler et al., Phys. Rev. **D71**, 034508 (2005).

[111] CP-PACS Collaboration, A. Ali Khan *et al.*, Phys. Rev. **D65**, 054505 (2002); *Erratum ibid.* **D67**, 059901 (2003).

[112] JLQCD Collaboration, S. Aoki *et al.*, Phys. Rev. **D68**, 054502 (2003).

[113] QCDSF-UKQCD Collaboration, A. Ali Khan *et al.*, Nucl. Phys. **B689**, 175 (2004).

[114] R. Sommer *et al.*, Nucl. Phys. Proc. Suppl. **129**, 405 (2004).

[115] R. Lewis and P.-P. A. Ouimet, Phys. Rev. **D64**, 034005 (2001).

[116] CP-PACS Collaboration, Y. Namekawa *et al.*, Phys. Rev. **D70**, 074503 (2004).

[117] M. Lüscher, in: *Progress in gauge field theory*, eds. G. 't Hooft *et al.*, Cargèse 1983, Plenum Press, New York (1984).

[118] B. Orth, T. Lippert and K. Schilling, Phys. Rev. **D72**, 014503 (2005).

[119] B. U. Musch, Diploma thesis, Technical University Munich, *in preparation*.

[120] T. R. Hemmert, M. Procura and W. Weise, Phys. Rev. **D68**, 075009 (2003).

[121] V. Bernard, T. R. Hemmert and U.-G. Meißner, Nucl. Phys. **A732**, 149 (2004).

[122] R. D. Young, D. B. Leinweber and A. W. Thomas, Prog. Part. Nucl. Phys. **50**, 399 (2003).

[123] D. B. Leinweber, A. W. Thomas and R. D. Young, Phys. Rev. Lett. **92**, 242002 (2004).

[124] T. E. O. Ericson and W. Weise, *Pions and Nuclei*, Clarendon, Oxford (1988).

[125] N. Kaiser, S. Gerstendörfer and W. Weise, Nucl. Phys. **A637**, 395 (1998).

[126] K. Goeke, J. Ossmann, P. Schweitzer and A. Silva, `hep-lat/0505010`.

[127] L. S. Brown, W. J. Pardee and R. D. Peccei, Phys. Rev. **D4**, 2801 (1971).

[128] V. Bernard, N. Kaiser and U.-G. Meißner, Phys. Lett. **B389**, 144 (1996).

[129] J. Gasser, H. Leutwyler, M. P. Locher, M. E. Sainio, Phys. Lett. **B213**, 85 (1988); J. Gasser, H. Leutwyler, M. E. Sainio, Phys. Lett. **B253**, 252 (1991); *ibid.*, **B253**, 260 (1991).

[130] R. Koch, Z. Phys. **C15**, 161 (1982).

[131] M. E. Sainio, Eur. Phys. J. **A24**, s2, 89 (2005).

[132] SESAM Collaboration, S. Gusken *et al.*, Phys. Rev. **D54**, 5496 (1999).

[133] R. Koch and E. Pietarinen, Nucl. Phys. **A336**, 331 (1980).

[134] M. M. Pavan, I. I. Strakovsky, R. L. Workman and R. A. Arndt, PiN Newslett. **16**, 110 (2002).

[135] I. Jameson, A. W. Thomas and G. Chanfray, Austr. J. Phys. **47**, 45 (1994) and J. Phys. **G 18**, L159 (1992).

[136] B. Borasoy and U.-G. Meißner, Ann. Phys. (N.Y.) **254**, 192 (1997).

[137] X.-D. Ji, Phys. Rev. Lett. **74**, 1071 (1995).

[138] W. Detmold, W. Melnitchouk and A. W. Thomas, Int. J. Mod. Phys. **A 18**, 1343 (2003).

[139] T. R. Hemmert and W. Weise, Eur. Phys. J. **A15**, 487 (2002).

[140] W. Detmold, W. Melnitchouk and A. W. Thomas, Phys. Rev. **D66**, 054501 (2002).

[141] A. W. Thomas, Adv. in Nucl. Phys. **13** 1 (1984).

[142] S. Weinberg, Phys. Rev. **112**, 1375 (1958).

[143] D. H. Wilkinson, Eur. Phys. J. **A 7**, 307 (2000).

[144] R. P. Feynman and M. Gell-Mann, Phys. Rev. **109**, 193 (1958).

[145] J. Bijnens, J. Sonoda and M. B. Wise, Nucl. Phys. **B261**, 185 (1985).

[146] J. D. Bjorken, Phys. Rev. **148**, 1476 (1966).

[147] V. N. Gribov and L. N. Lipatov, Sov. J. Nucl. Phys. **15**, 438 (1972).

[148] Yu. L. Dokshitzer, Sov. Phys. JETP **46**, 641 (1977).

[149] G. Altarelli and G. Parisi, Nucl. Phys. **B126**, 298 (1977).

[150] P. Hägler and A. Schäfer, Phys. Lett. **B430**, 179 (1998).

[151] S. Steininger, U.-G. Meißner and N. Fettes, JHEP **9809**, 008 (1998).

[152] J. Kambor and M. Mojžiš, JHEP **9904**, 031 (1999).

[153] J. Schweizer, Diploma Thesis, University of Bern (2000).

[154] S. Sasaki *et al.*, Phys. Rev. **D68**, 054509 (2003); S. Ohta *et al.*, Nucl. Phys. Proc. Suppl. **129**, 296 (2004) and Nucl. Phys. Proc. Suppl. **140**, 396 (2005).

[155] M. Kim and S. Kim, Phys. Rev. **D58**, 074509 (1998).

[156] T. Blum, S. Ohta and S. Sasaki, Nucl. Phys. B Proc. Suppl. **94**, 295 (2001).

[157] T. Wollenweber, Diploma thesis, Technical University Munich (2005).

[158] A. Ali Khan *et al.*, Talk given at the XXIIIrd International Symposium on Lattice Field Theory, Dublin, 25-30 July 2005, `hep-lat/0510061`.

[159] T. Blum *et al.*, Phys. Rev. **D 66**, 014504 (2002).

[160] CP-PACS Collaboration, A. Ali Khan *et al.*, Phys. Rev. **D63**, 114504 (2001); RBC Collaboration, Y. Aoki *et al.*, Phys. Rev. **D69**, 074504 (2004).

[161] G. Schierholz, private communication.

[162] S. Capitani *et al.*, Nucl. Phys. Proc. Suppl. **79**, 548 (1999).

[163] M. Göckeler *et al.*, Nucl. Phys. Proc. Suppl. **119**, 32 (2003).

[164] A. Ali Khan *et al.*, Nucl. Phys. Proc. Suppl. **140**, 408 (2005).

[165] LHP collaboration, J. W. Negele *et al.*, `hep-lat/0509101`; R. G. Edwards *et al.*, `hep-lat/0510062`; D. Richards, private communication.

[166] K. Orginos, D. Toussaint and R. L. Sugar, Phys. Rev. **D60**, 054503 (1999); K. Orginos and D. Toussaint, Phys. Rev. **D59**, 014501 (1999).

[167] A. W. Thomas and W. Weise, *The Structure of the Nucleon*, Wiley-VCH, Berlin (2001).

[168] S. L. Adler, Phys. Rev. Lett. **14**, 1051 (1965); S. Adler, Phys. Rev. **140**, B736 (1965) and *Erratum ibid.* 175, 2224 (1968); W. I. Weisberger, Phys. Rev. Lett. **14**, 1047 (1965).

[169] S. Weinberg, *The Quantum Theory of Fields*, Cambridge University Press (1996).

[170] S. Weinberg, Phys. Rev. Lett. **17**, 616 (1966); Y. Tomozawa, Nuovo Cimento **46A**, 707 (1966).

[171] M. L. Goldberger and K. M. Watson, *Collision Theory*, Wiley, New York (1967).

Acknowledgments

Many people have been supporting me during my Ph.D. studies in Munich. I gratefully thank them all. Especially,

- Prof. Dr. Wolfram Weise for the opportunity to graduate under his supervision, for his valuable guidance through many inspiring discussions at any time and place and for his unique ability to keep me highly motivated;

- Dr. Thomas Hemmert for collaboration, help and useful advice;

- all the people at ECT* in Trento;

- Dr. Norbert Kaiser for valuable help;

- Bernhard Musch for many stimulating questions and fruitful exchange of ideas;

- Prof. Dr. Gerrit Schierholz, Dr. Meinulf Göckeler, Prof. Dr. Heinrich Leutwyler, Prof. Dr. Ulf-G. Meißner for discussions and support;

- my wonderful parents and all my friends in Italy;

- Claudia for her patience and warm support;

- all members of T39 for the nice working climate, in particular my friends Alberto, Bugra, Edisher, Robin and Robert.

- all the friends I have met thanks to my Ph.D. activities, like François, Dolores, Barbara, Laura, Andi, Paolo and Daniele.